



DTIC
SELECTED
JAN 05 1995
B

FATIGUE BEHAVIOR OF A CROSS-PLY
METAL MATRIX COMPOSITE AT ELEVATED
TEMPERATURE UNDER STRAIN CONTROLLED
MODE

THESIS

Leon B. Dennis, Captain, USAF

AFIT/GAE/ENY/94D-7

DISTRIBUTION STATEMENT A
Approved for public release;
Distribution Unlimited

DEPARTMENT OF THE AIR FORCE
AIR UNIVERSITY
AIR FORCE INSTITUTE OF TECHNOLOGY

19950103 062

Wright-Patterson Air Force Base, Ohio

AFIT/GAE/ENY/94D-7

**FATIGUE BEHAVIOR OF A CROSS-PLY
METAL MATRIX COMPOSITE AT ELEVATED
TEMPERATURE UNDER STRAIN CONTROLLED
MODE**

THESIS

Leon B. Dennis, Captain, USAF

AFIT/GAE/ENY/94D-7

DTIC QUALITY INSPECTED 3

Approved for public release; distribution unlimited

REPORT DOCUMENTATION PAGE			Form Approved OMB No. 0704-0188	
Public reporting burden for this collection of information is estimated to average 1 hour per response, including the time for reviewing instructions, searching existing data sources, gathering and maintaining the data needed, and completing and reviewing the collection of information. Send comments regarding this burden estimate or any other aspect of this collection of information, including suggestions for reducing this burden, to Washington Headquarters Services, Directorate for Information Operations and Reports, 1215 Jefferson Davis Highway, Suite 1204, Arlington, VA 22202-4302, and to the Office of Management and Budget, Paperwork Reduction Project (0704-0188), Washington, DC 20503.				
1. AGENCY USE ONLY (Leave blank)	2. REPORT DATE December 1994	3. REPORT TYPE AND DATES COVERED Master's Thesis		
4. TITLE AND SUBTITLE FATIGUE BEHAVIOR OF A CROSS-PLY METAL MATRIX COMPOSITE AT ELEVATED TEMPERATURE UNDER STRAIN CONTROL MODE			5. FUNDING NUMBERS	
6. AUTHOR(S) Leon B. Dennis, Captain, USAF				
7. PERFORMING ORGANIZATION NAME(S) AND ADDRESS(ES) Air Force Institute of Technology, WPAFB, OH 45433			8. PERFORMING ORGANIZATION REPORT NUMBER AFIT/GAE/ENY/94D-7	
9. SPONSORING/MONITORING AGENCY NAME(S) AND ADDRESS(ES) Dr. Walter Jones AFOSR/NA Bolling AFB, DC 20322-6448			10. SPONSORING/MONITORING AGENCY REPORT NUMBER	
11. SUPPLEMENTARY NOTES Approved for public release; distribution unlimited				
12a. DISTRIBUTION/AVAILABILITY STATEMENT			12b. DISTRIBUTION CODE	
13. ABSTRACT (Maximum 200 words) This research extends the existing knowledge of cross-ply metal matrix composites (MMC) to include fatigue behavior under strain-controlled fully reversed loading. This study investigated fatigue life, failure modes and damage mechanisms of the SCS-6/Ti-15-3, [0/90] _{2s} MMC. The laminate was subjected to fully reversed fatigue at elevated temperature (427° C) at various strain levels. Stress, strain and modulus data were analyzed to characterize the macro-mechanical behavior of the composite. Microscopy and fractography were accomplished to identify and characterize the damage mechanisms at the microscopic level. Failure modes varied according to the maximum applied strain level showing either mixed mode (i.e. combination of both fiber and matrix dominated modes) or matrix dominated fatigue failures. As expected, higher strain loadings resulted in more ductility of the matrix at failure, evidenced by fracture surface features. For testing of the same composite laminate, the fatigue life under strain controlled mode slightly increased, compared to its load-controlled mode counterpart, using the effective strain range comparison basis. However, the respective fatigue life curves converged in the high cycle region, suggesting that the matrix dominated failure mode produces equivalent predicted fatigue lives for both control modes.				
14. SUBJECT TERMS Metal Matrix Composite, Elevated Temperature, Fatigue Testing, Compression, Fully-reversed, Titanium, Silicon Carbide, Strain Control Mode			15. NUMBER OF PAGES 125	
			16. PRICE CODE	
17. SECURITY CLASSIFICATION OF REPORT Unclassified	18. SECURITY CLASSIFICATION OF THIS PAGE Unclassified	19. SECURITY CLASSIFICATION OF ABSTRACT Unclassified	20. LIMITATION OF ABSTRACT UL	

FATIGUE BEHAVIOR OF A CROSS-PLY METAL MATRIX COMPOSITE
AT ELEVATED TEMPERATURE UNDER STRAIN CONTROLLED MODE

THESIS

Presented to the Faculty of the Graduate School of
Engineering

of the Air Force Institute of Technology

Air University

In Partial Fulfillment of the

Requirements for the Degree of

Master of Science in Aeronautical Engineering

Leon B. Dennis, B.S.M.E.

Captain, USAF

December 1994

Accession For	
NTIS GRA&I	<input checked="" type="checkbox"/>
DTIC TAB	<input type="checkbox"/>
Unannounced	<input type="checkbox"/>
Justification	
By	
Distribution/	
Availability Codes	
Dist	Avail and/or Special
A-1	

Acknowledgments

This research could not have been accomplished without the assistance of many individuals, to whom I wish to thank. To Capt Brian Sanders, thanks for your suggestions, guidance, software (STRAIN TEST), and many discussions and reviews with myself. Mark Derriso, thank you for your numerous hours of both demonstrating test equipment procedures and fine tuning the loadcell to actually accomplish tension-compression, strain-controlled loading, and for your consistent patience and assistance with us. Jay Anderson, Dan, Andy and the other lab technicians, you were of invaluable assistance and information. To Joe, Jan and the others at the AFIT Model Shop, thanks for the short lead time support for the specimen manufacture and the buckling guide. The Metlab folks, Bob, Eric and Mark, thanks for the assistance, demonstrations and training for processing the specimens. Thanks also goes to Dr. Walter Jones, AFOSR/NA, for sponsoring this research. And Dr. Mall, thank you very much for your time, patience, and guidance. And to my wife Nicole, thanks for your assistance, your understanding during my writing sessions and your love and support in general.

Table of Contents

Acknowledgments	ii
Table of Contents	iii
List of Figures	v
List of Tables.	vii
Abstract.	viii
I. Introduction.	1
II. Background and Literature Review.	6
Experimental Terminology and Techniques	6
Data Analysis and Fatigue Damage.	9
Literature Review	13
Summary	22
III. Test Equipment and Procedures	24
Composite Material and Specimen Description	24
Experimental Equipment.	32
Experimental Procedures	34
Post-Test Procedures.	38
IV. Experimental Results and Discussion	42
Monotonic Tension Test - Strain Controlled.	42
Fatigue Testing Results and Discussion - Strain Controlled	44
Mechanical Responses.	44
Region I - Fiber Dominated Failure Mode	45
Region IIa - Mixed Fiber & Matrix Failure Mode.	46
0.73% Mechanical Responses	46
0.6% Mechanical Responses.	50
Region IIb - Matrix Dominated Failure Mode.	54
0.4% Mechanical Responses.	54
Summary - Mechanical (Macromechanical) Responses.	57
Fractography, Microscopy, and Damage Mechanisms	58
Fractography	58
Fiber and Matrix Damage - Microscopy	60
Region I - Fiber Dominated Failure Mode.	69
(Static Test)	
Region IIa - Mixed Fiber and Matrix Failure Modes.	69
Region IIb - Matrix Dominated Failure Mode.	70
Summary - Fractography and Micromechanical Results.	75
V. Fatigue Life Analysis and Comparisons	79
Fatigue Life Curves - Current Work.	81
Discussion of Dominant Failure Modes.	84
Comparisons to Previous MMC Fatigue Work.	87

VI. Conclusions and Recommendations95
Appendix.A - Additional Data. 100
Appendix.B - Additional Photography 109
Bibliography. 113
Vita. 116

List of Figures

<u>Figure</u>	<u>Page</u>
2.1 Typical MMC Crack Growth10
3.1 Dogbone Specimen Geometry.27
3.2 Buckling Guide Geometry.29
3.3 Fatigue Testing Apparatus.33
3.4 Specimen Test Setup.33
3.5 Typical Failed Specimen Sectioning39
4.1 Monotonic Tension Test43
4.2 Monotonic Plot/Fatigue Failure Mode Region Overlay	.45
4.3 Modulus History, 0.73% Test.47
4.4 Maximum/Minimum Stress History, 0.73%.48
4.5 Stress-Strain Plots, 0.73% (Offset).49
4.6 Modulus History, 0.6%.51
4.7 Maximum/Minimum Stress History, 0.6%51
4.8 Fiber and Matrix Cracking, 0.6%.52
4.9 Stress-Strain Plots, 0.6% (Offset)53
4.10 Modulus History, 0.4%.55
4.11 Maximum/Minimum Stress History, 0.4%56
4.12 Stress-Strain Plots, 0.4% (Offset)57
4.13 Fracture Surface, 0.8%61
4.14 Fracture Surface, 0.73%.62
4.15 Fracture Surface Close-Up, Mixed Mode (0.73%)63
4.16 Fracture Surface, 0.6%64
4.17 Fracture Surface, 0.5%65
4.18 Fracture Surface, 0.4%66
4.19 Fracture Surface, 0.3%67
4.20 Fracture Surface, 0.25%.68
4.21 Longitudinal Fiber Cracks, 0.8% (200X)71
4.22 90 deg Radial Crack, View #2, 0.73% (1000X).71
4.23 0 deg Fibers, View #3, 0.73% (500X).72
4.24 0 deg Fibers, View #3, 0.6% (200X)72
4.25 Fiber and Matrix Cracks Close-Up, View #2, 0.6% (200X)73
4.26 Fiber and Matrix Cracks, View #2, 0.6% (50X)73
4.27 Striations, Fracture Surface Close-Up, 0.4%.76
4.28 Numerous Cracks, View #2, 0.4% (50X)76
4.29 Numerous Cracks, View #3, 0.4% (100X).77
4.30 Matrix Cracks, View #2, 0.4%I (200X)77
4.31 0 deg Fibers, View #3, 0.4%I (100X).78
4.32 0 deg Fibers, View #3, 0.4%I (200X).78
5.1 Fatigue Life Curve - Max Strain.81
5.2 Fatigue Life Curve - Max Stress.82
5.3 Fatigue Life Curve - Strain Range.83
5.4 Fatigue Life Curve - Stress Range.83
5.5 Partitioned Maximum Strain Fatigue Curve85
5.6 Partitioned Maximum Stress Fatigue Curve86
5.7 Maximum Strain Fatigue Curve - Load Control Comparison.88
5.8 Effective Strain Range Fatigue Curve - Load Control Comparison.89

5.9	Effective Strain Range Fatigue Curve - Strain Control Comparison.94
5.10	Effective Strain Range Fatigue Curve - Overall Comparison.94
A.1	Modulus History, 0.5% Test	101
A.2	Maximum/Minimum Stress History, 0.5%	101
A.3	Stress - Strain Plots, 0.5% (Offset)	102
A.4	Modulus History, 0.3% Test	103
A.5	Maximum/Minimum Stress History, 0.3%	103
A.6	Stress - Strain Plots, 0.3% (Offset)	104
A.7	Modulus History, 0.25% Test.	105
A.8	Maximum/Minimum Stress History, 0.25%.	105
A.9	Stress - Strain Plots, 0.25% (Offset).	106
A.10	Modulus History, 0.2% Test	107
A.11	Maximum/Minimum Stress History, 0.2%	107
A.12	Stress - Strain Plots, 0.2% (Offset)	108
B.1	Ductile Void Coalescence, 0.8% (Static).	109
B.2	Ductility and Fatigue Straitions, 0.73%.	110
B.3	Fracture Surface, 0.4%	110
B.4	Molyweave, Fracture Surface, 0.4%.	111
B.5	Extensive Fatigue Straitions, 0.25%.	111
B.6	Post-Fracture Specimen Comparison.	112
B.7	0 deg Fibers, View #3, 0.73% (500X).	112

List of Tables

<u>Table</u>	<u>Page</u>
3.1 Key Properties of Fibers and Matrix.25
4.1 Summary of Failure Modes44
A.1 Stress-Strain Plot Offset Data	108

Abstract

This research extends the existing knowledge of cross-ply metal matrix composites (MMC) to include fatigue behavior under strain-controlled fully reversed loading. This study investigated fatigue life, failure modes and damage mechanisms of the SCS-6/Ti-15-3, $[0/90]_{2s}$, MMC. The laminate was subjected to fully reversed fatigue at elevated temperature (427° C) at various strain levels. Stress, strain and modulus data were analyzed to characterize the macro-mechanical behavior of the composite. Microscopy and fractography were accomplished to identify and characterize the damage mechanisms at the microscopic level. Failure modes varied according to the maximum applied strain level showing either mixed mode (i.e. combination of both fiber and matrix dominated modes) or matrix dominated fatigue failures. As expected, higher strain loadings resulted in more ductility of the matrix at failure, evidenced by fracture surface features. For testing of the same composite laminate, the fatigue life under strain controlled mode slightly increased, compared to its load-controlled mode counterpart, using the effective strain range comparison basis. However, the respective fatigue life curves converged in the high cycle region, suggesting that the matrix dominated failure mode produces equivalent predicted fatigue lives for both control modes.

**FATIGUE BEHAVIOR OF A CROSS-PLY METAL MATRIX COMPOSITE
AT ELEVATED TEMPERATURE UNDER STRAIN CONTROLLED MODE**

I. Introduction

Historically, the USAF, and the aerospace industry in general, have made their greatest leaps of progress when an advance in technology has permitted engineers to test and apply their advanced concepts. These improvements have helped to improve performance, capability, reliability, and safety to the present high levels. One technological problem is that current alloys have reached their limits of both high stiffness and high strength to weight ratios, but aerospace requirements for improving these properties are ever present. Obviously these limits hamper our ability to increase capabilities and to provide next generation of aerospace systems. Examples of these new requirements are the National Aerospace Space Plane (NASP) and advanced gas turbine engine design. Both of these will be operating at much higher temperatures than current aerospace systems. One promising class of materials for meeting the increasing requirements of high specific strength and stiffness is metal matrix composites (MMC's) [12].

MMC's are metal alloys reinforced with continuous, high stiffness, high strength, light-weight ceramic fibers. This material class possesses both high specific strength and

high specific stiffness at elevated temperature. MMC's also have a low sensitivity to temperature changes, thermal shock, and surface durability [26]. One particular MMC, the SCS-6/Ti-15-3 [0/90]_{2s} titanium composite system, is a good model material in this class of materials and it is the material used for this research. The Ti-15-3 composite has a high strength to weight ratio (specific strength) and the coefficients of thermal expansion differ by a approximately a factor of two. The expanded form of annotating the matrix alloy and fiber is:

Matrix alloy: Ti-15V-3Al-3Sn-3Cr,

Fibers: SCS-6 ceramic fibers.

However, the more common reference name for the system is the SCS-6/Ti-15-3 MMC.

However, accurately predicting the performance of MMC's is difficult because of unique damage mechanisms. Some of the unique conditions of these composite include fiber-matrix thermal expansion mismatch and brittle reaction zones between the fiber and matrix. Since a large difference in coefficient of thermal expansion exists between the fiber and matrix in this material, as with most MMC's, large residual stresses result after consolidation (at 1000°C). The brittle reaction zones result from a chemical interaction between the Ti-15-3 matrix and the outer layer of the fiber[12]. These unique mechanisms of MMC's can

produce a wide range of mechanical responses especially if compared under different environmental factors.

A new material must be tested under idealized environmental and loading conditions before being used in a real world structural application. Such testing characterizes the deformation and failure modes and provides designers with material limitations. Thus far, researchers have conducted both monotonic tension and compression tests [12,13,25], and tension-tension tests [10,12], but only a few tension-compression investigations (load controlled mode) have been performed [3]. Because materials in most engineering applications are primarily under strain controlled mode, and since only a few investigations have been performed using this loading condition, more strain controlled characterization is needed. Thus, additional investigation into the strain controlled behavior of MMC's will help to better understand the behavior of these materials in actual aerospace applications.

Compression testing of MMC's has proved difficult since the material is typically manufactured in thin plates due to the high costs of MMC's. These thin specimens present a buckling problem. A fatigue buckling guide, developed for similar testing at AFIT, solved this problem and tension compression testing is progressing.

The tension-compression (fully reversed) testing environment is representative of actual loadings foreseen in many applications. For example, the wing skins for aircraft

are often bending and vibrating, providing a tension compression loading environment[23]. Additionally, most published fatigue data of metals is based on fully reversed loading [3]. Thus tension compression loading fatigue data of MMC's is desirable for both standardization and compatibility.

The objective of the current research was to investigate the fully reversed fatigue behavior and damage mechanisms in a cross-ply, $[0/90]_{2s}$, metal matrix composite (SCS-6/Ti-15-3) at elevated temperature (427° C). This was accomplished by using a tension-compression, strain-controlled loading mode. All the tests were performed at a strain rate of 0.2%/sec, compatible with other strain controlled tests [23].

Nine specimens were tested: seven strain-controlled mode fully reversed fatigue tests, one interrupted fatigue test, and one monotonic tension test. The interrupted test was run to determine the initiation of damage. The monotonic test was performed to measure the upper limit of the strain level at 427° C for the $[0/90]_{2s}$, cross-ply, since none was found in the literature. During testing, edge damage was monitored via the edge replica technique. Also stress-strain data was recorded at periodic intervals with the data acquisition system for mechanical response analysis.

After failure, the specimens were sectioned, and mounted for post-mortem examination. Fractography and micrography were performed to identify the initiation and progression of damage mechanisms. The mechanical response data (stress-strain (σ - ϵ), maximum and minimum stress (σ), and modulus (E)) was used along with the micrography to determine deformation mechanisms. These mechanisms were identified as well as their approximate starting points and progression rates. Additionally a fatigue life curve was plotted against maximum applied strain. The fatigue curve was partitioned into three regions using the observations from the macroscopic response and damage mechanisms. Conclusions were then made on the dominant damage mechanisms for the strain levels.

The details, results and conclusions of this work are in the following chapters of this thesis. First, previous MMC research is reviewed. Second, a complete description of the test equipment and techniques used in this work is provided. Third, the macromechanical results and microscopic evaluations are discussed. Fourth, a fatigue life analysis, using the results from this work and previous investigations is discussed. Finally, the conclusions and recommendations resulting from this work are presented.

II. Background and Literature Review

This chapter reviews some of the terminology, procedures and recent work accomplished regarding the characterization of Metal Matrix Composites (MMC's). First, some of the experimental techniques and terminology are discussed. Second, methods to analyze the data gathered during fatigue testing are discussed. Third, a literature review of some recent work on MMC's is presented.

Experimental Terminology and Techniques

Thermomechanical MMC Testing

Understanding the fatigue environment to which an MMC is anticipated to be exposed is a vital first step in characterizing the material. Typical load and temperature profiles are foreseen for MMC's to be somewhat complex. Before attempting to simulate these conditions, testing a MMC in a simpler fatigue environment needs to be investigated. The simplified conditions allow for the isolation of fatigue variables and characteristics. This approach also allows a researcher to analyze data obtained from simplified test conditions in order to estimate fatigue response under a more complex loading condition.

Control Modes

Typically MMC's are fatigue tested using one of two control methods: load control mode, or strain control mode. Both terms are used found throughout this document, and are

defined as follows. For load control mode, the load is controlled (independent variable) while the resultant strain is measured (dependent variable). Contrasting this is the strain control mode, where the strain is controlled (independent variable), while the load required to accomplish this is recorded (dependent variable). As previously mentioned, many aerospace material applications will be subjected to a strain-controlled environment, thus studies using this control mode are desirable.

Another parameter associated with the control mode is the loading range or strain range. The load range, or R ratio, is defined by the ratio of minimum stress to maximum stress:

$$R = \sigma_{\min} / \sigma_{\max}. \quad (1)$$

Similarly, the strain range (used for this work) is defined by the ratio of minimum strain to maximum strain:

$$R = \epsilon_{\min} / \epsilon_{\max}. \quad (2)$$

Typically R is greater than zero so that no compressive stresses are introduced, but in the current work an R=-1 was used.

Fatigue Testing

Characterizing the fatigue response of a MMC requires a foundation for documenting the material behavior. Various fatigue testing environments will be discussed, including thermal fatigue, isothermal fatigue, and thermomechanical fatigue. These techniques help to isolate a particular

fatigue condition to better understand the contributions made to the fatigue response due to damage.

Thermal fatigue (TF) is the cycling of the temperature while a constant stress is applied to the specimen. This fatigue mode isolates damage mechanisms related to a changing thermal environment. This information can help to identify evidence of TF when observing the results of a more complicated fatigue environment. Typically a triangular wave thermal ramping function is used to apply the thermal stresses. As previously mentioned, the coefficient of thermal expansion (CTE) is larger in the matrix than in the fibers. This results in a fluctuating stress at the fiber-matrix interface.

A second method of isolating fatigue damage of a MMC is the isothermal fatigue (IF) test. This type of test holds a constant temperature on the specimen while cycling the mechanical stress. Since the thermal stresses are constant, this testing environment provides an opportunity to isolate damage mechanisms caused only by the mechanical loading.

A third type of fatigue test is thermomechanical fatigue (TMF). This type of testing includes a combination of the two above discussed cases, simultaneous thermal and mechanical fatigue testing. Since the tests described in the previous two paragraphs are informative but not approaching the actual environment, the thermomechanical test attempts to come closer to the actual working conditions. The two variables can be cycled in-phase or

out-of-phase. Additionally, the cyclic profiles may be made more complex by placing hold times on one or both of the variables during the cycle. The combined loading provides an opportunity to see if the combined environment is the superposition of the separate fatigue conditions and identify what significant differences may exist.

Data Analysis and Fatigue Damage

MMC damage due to fatigue is complex as compared to most monolithic metals, which usually has a critical crack propagate along a single path. Experimental techniques are established for measuring both the crack length and predicting the crack growth rate [2]. This information allows a fatigue life to be predicted for the monolithic metal. Since in composites many cracks may develop simultaneously in the matrix, fibers, and/or the fiber-matrix interfaces, fatigue life prediction may be much more complex. Depending on the loading level, the cracks may develop and propagate primarily in the fibers, matrix, or both[10]. Figure 2.1 illustrates these typical type of crack locations. Because many simultaneous cracks may exist and/or be growing at a given time, specimen failure may not be caused by a single crack, but by the coalescence of the many cracks. Thus, the single crack growth criteria used for monolithic materials is not enough.

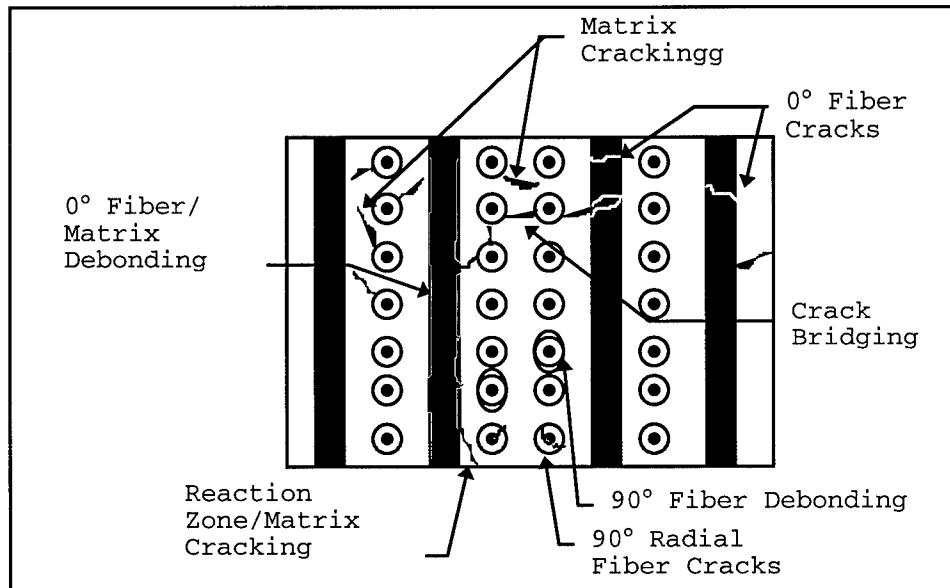


Figure 2.1: Typical MMC Crack Growth

Therefore, to help determine the damage progression in a MMC, the mechanical response data from the tests is recorded and analyzed for trends in material response. Studying these trends over the specimen fatigue life provides a better understanding of the initiation and progression of damage. Some methods for examining this data will be discussed next.

Mechanical Responses

One primary source of data analysis is the history of the stress-strain responses over the fatigue life of the specimen. Any hysteresis in the stress-strain curves are an indication that damage or deformation has occurred in the material. Thus, this type of analysis can help record and

quantify the initiation and growth of damage and deformation in a MMC [23].

Studying the mechanical response as a function of fatigue cycles is another common analysis tool. A second method of mechanical response analysis is to look at maximum and minimum values of stress (dependent variable for strain control mode) vs. the number of fatigue cycles (N). Contrasting, the load control mode would monitor maximum and minimum strain values vs. the number of cycles. Any changes usually indicate damage or deformation is occurring. The third primary method of estimating material damage is to measure the material modulus (E) vs. fatigue cycles for the specimen. A decrease in modulus is an indication of material damage.

Fatigue Life Curves

A typical fatigue life curve of a specimen is a valuable tool for determining how long a material will last when cycled at a particular stress or strain level or range. For composites, subdividing a typical fatigue life curve into regions of dominant failure modes is not uncommon[23]. The fatigue curve is divided into three regions that correspond to the dominant failure modes. Figures 5.5 and 5.6 are examples of typical subdivided graphs. These particular graphs divide Region II into subregions, for reasons discussed later. Region I represents longitudinal fiber breakage and resulting fiber-matrix interface debonding and catastrophic matrix failure. The scatter band

in this region is due to variations in both fiber strength and matrix ductility. This catastrophic damage is characterized as non-progressive damage, defined as damage resulting from a rapid failure of the specimen without prior degradation in material response. Conversely, progressive damage is defined as damage growing from an early stage of fatigue life to final failure of the specimen. The next region, Region II, indicates a dominant fatigue failure mode of matrix cracking and fiber-matrix interface failure. The last region, Region III, indicates the matrix fatigue limit. For Region III, any matrix cracking occurring does not propagate. Basically the specimen does not fail when loaded below the indicated level. Thus, the three region fatigue graph provides a useful method for relating fatigue life, applied loading and dominant damage mechanisms at the particular loading[27].

Summary - Experimental Terminology and Techniques

The previous sections of this chapter have presented and explained several of the common terms and testing techniques used for MMC fatigue testing. Some of the more common fatigue testing environments were explained. Also some data analysis techniques were presented. Finally, the typical MMC dominant fatigue failure modes were discussed.

The goal of this discussion was to provide an initial background of MMC testing. Next a literature review of recent studies of MMC related testing is presented.

Literature Review

Several experimental studies pertaining to MMC material characterization were found in the literature review. Some of the more pertinent studies relating to the present research are discussed below. The general categories are as follows: 1) Non Fatigue Tests, 2) Load Controlled Fatigue Tests, and 3) Strain Controlled Fatigue Tests. It may be noted that some of the research discussed overlap categories, but fatigue testing, if accomplished, was the primary category of concern.

Non Fatigue Tests

Inelastic tensile deformation of unidirectional SCS-6/Ti-15-3 was studied by Majumdar and Newaz [19]. The tests were monotonic tension tests to failure. The examination of the deformation mechanisms presented two categories of inelastic deformation, plasticity and damage. Plasticity was a matrix phenomenon characterized by slip band formation and a change in dislocation densities. Damage included the fibers, matrix, and interface. This category was characterized by any type of cracking (fiber, matrix, or interface), or debonding at the fiber-matrix interface.

Inelastic deformation of the 0° MMC was dominated by plasticity, while of the 90° layup had a characteristic three stage deformation behavior: Stage I - elastic; Stage II- damage (interfacial debonding); and Stage III - matrix plasticity.

Lerch and Saltsman examined the damage mechanisms of the SiC-6/Ti-15-3 composite loaded in uniaxial tension [13]. Many layups, unidirectional, as well as cross-ply laminates, were tested to failure at room temperature and 427° C, and examined microscopically afterwards. Some tests were interrupted at various strain increments and examined to document the development of damage. The [0/90]_{2s} lamina was tested at room temperature, but not elevated temperature. Debonding in the 90° plies of the [0/90]_{2s} laminates led to nonlinearities in the stress-strain curves at lower strains. At the higher strains, matrix plasticity was predicted, but could not be experimentally confirmed. A large scatter in the elastic moduli for the 0/90 crossply was found due to the partially debonded interfaces in pretested specimens as a result of the high residual radial stresses acting on the fiber-matrix interface.

Newaz and Majumdar studied the mechanical response of SCS-6/Ti-15-3 at room temperature, 538° C, and 650° C, with the goal of developing a comprehensive argument explaining the composites' response as compared to the actual

deformation mechanisms [21]. Monotonic tension tests were run on both unidirectional and cross-ply laminates. The unidirectional layup analysis provided some useful findings. The [0]_s micrographic evaluation revealed that inelastic deformation is dominated by matrix plasticity at both room and elevated temperature. The plasticity was evident as diffused slip (no distinct slip bands) at elevated temperatures. The equivalent tests at room temperature showed slip bands that were distinct. The [90]_s inelastic deformation was found to have both damage, evidenced by fiber-matrix debonding, and plasticity, evidenced by the slip band formation. Also, the 90° layup tests illustrated the same increased diffused slip band trend at elevated temperatures.

The fatigue behavior under thermal cycling of a unidirectional SCS-6/Ti-15-3 composite was examined by Mall and Ermer [16]. Damage mechanisms were investigated for two cycling ranges: 149° C to 427° C and 149° C to 649° C. The first damage observed was reaction zone degradation, starting at 500 cycles. Young's modulus, Poisson's ratio, and residual tensile strength did not change up to 15,000 cycles for either temperature range. The observed stress-strain relationship was comparatively closer to linearity for thermal cycled specimens than for untested specimens.

Mall and Schubbe introduced another variable by examining thermo-mechanical fatigue (TMF) behavior of a

cross-ply SCS-6/Ti-15-3 composite[18]. Two sets of tests, in-phase and out-of-phase TMF, from 149° C to 427° C, at various stress levels, were performed. Fatigue damage was noted to initiate at the fiber/matrix interface of 90° fibers, and progressed as transverse cracking in the matrix. Both fatigue lives and final damage modes were found to be dependent on both test conditions and stress levels.

Load Controlled Testing

Jeng et al. examined the low cycle fatigue behavior and mechanisms of fatigue damage initiation and progression in a SiC/Ti composite system [9]. The testing, at room temperature, was performed on unidirectional, heat treated specimens at a loading of R=0.1 and 10 Hz frequency. Depending on the maximum stress level applied, the fatigue damage was classified into three regions: 1) fiber failure dominated, 2) interfacial and matrix cracking and fiber breakage dominated (mixed mode), and 3) matrix cracking dominated.

Johnson investigated load controlled tension fatigue of SCS-6/Ti-15-3 (various layups) at room temperature, with an R=0.1 [10]. Dominant failure modes were found to be either matrix dominated, fiber dominated, or fiber-matrix interfacial failures. The maximum stress range varied from 800 to 500 MPa, providing a relatively low cycle fatigue curve (maximum fatigue life of 40,000 cycles).

In another study, Johnson, et al. tested five different layups of the SiC/Ti composite system at room temperature in continuing the above mentioned work[12]. They sought to determine the fatigue lives, mechanical properties, and the static strengths. The specimens were heat treated to 482° C for 16 hours before testing. The heat treatment increased the yield strength, ultimate strength, and stiffness of the matrix material. The experimental results and predicted values correlated well. Off-axis plies showed fiber-matrix interfacial failure at relatively low loading. Microscopic examination revealed that the fiber-matrix failures occurred in the chemical reaction layer between the fiber and matrix. This brittle layer was a nucleation site of matrix cracking.

The fatigue testing provided an interesting relation. Fatigue tests showed that the 0° fiber stress could be used to correlated the fatigue life of laminates containing 0° plies. This suggested that the 0° plies could be controlling the fatigue life.

Gabb, et al. studied the effect of matrix mechanical properties on unidirectional [0]_z SiC/Ti composite fatigue resistance[7]. The objective of the study was to determine the effect of matrix mechanical properties on the low cycle fatigue resistance of a unidirectional MMC. Three types of pretest vacuum heat treatments were used: 1) weak strength, ductile (WD) treatment of 700° C for 24 hours; 2) strong,

medium ductility (SM) specimens were aged at 700° C for 24 hours and then 427° C for 24 hours; and 3) the strong, brittle (SB) specimens were treated at 788° C for 15 minutes, water quenched, and aged again at 300° C for 24 hours. All fatigue tests were performed under a zero-tension triangular control waveform at room temperature. MMC tests were under load control mode while matrix alloy tests were run at a constant strain amplitude under a strain control mode. The results from the testing revealed that the fatigue resistance of the unidirectional MMC is only slightly influenced by the matrix mechanical properties resulting from various heat treatments. Also, the differences between the MMC and the matrix alloy crack starting and growth process may be a factor in the respective differences of fatigue lives of the MMC and the matrix alone.

Castelli investigated the thermomechanical and isothermal (427° C) fatigue behavior and damage mechanisms of a [90]_θ SCS-6/Ti-15-3 under load control with a R=0 [6]. The results showed that the [90]_θ TMF fatigue life trends was not found to be a limiting factor of the fatigue life, as compared to maximum temperature isothermal conditions. Out-of-phase loadings produced TMF lives approximately ten times more than fatigue lives determined under isothermal and in-phase fatigue loadings. Two items were identified

and appeared to dominate the fatigue damage of the MMC: 1) the weak fiber-matrix interface; and 2) oxidation-environmental attack of the fiber-matrix interface via the exposed 90° fiber ends.

Boyum was the first to examine fully reversed ($R=-1$) fatigue of a titanium composite under the load control mode, at both room and elevated temperature (427° C) [3]. Some room temperature tension-tension ($R=0.1$) tests were performed as well. The $[0/90]_{2s}$ laminate was examined, with mechanical responses (stress-strain data, maximum and minimum strain vs. cycles, and modulus vs. cycles) analyzed, as well as micrographic examination for damage mechanisms. With respect to maximum applied stress, the room temperature tension-tension had longer fatigue lives than the tension-compression specimens. In the fiber dominated failure region, the room and elevated temperature had similar fatigue lives. A higher temperature induced increase in matrix ductility extended the elevated temperature fatigue lives of the specimens in the matrix dominated failure region. It was reported that, in all cases, matrix damage initiated in reaction zone cracks which nucleated both matrix plasticity and matrix cracking. Also of note was the development of a fatigue test buckling guide, providing the ability to perform compression loading on thin specimens, typical of MMC's of interest.

Strain Controlled Testing

Verilli and Gabb performed fully reversed ($R=-1$), strain controlled, high temperature (260°C and 560°C) in a vacuum, fatigue testing of a tungsten fiber/copper matrix MMC [29]. The fiber-matrix relation of this material differ from the typical SiC/Ti system. The ductile tungsten fiber and the ductile copper matrix provide a ductile-ductile fiber-matrix relation. Conversely, brittle SiC fibers and a ductile Ti matrix produces a brittle-ductile relation. The ductile-ductile relation results in a relatively strong fiber-matrix bond, as compared to SiC/Ti. This difference can be a major factor in propagation of cracks and damage in a composite. A failure criteria of a 25% drop in tensile stress from maximum tensile stress was adopted as a failure criteria, as opposed to specimen separation. Comparisons of test results were made to previous tests run at a stress ratio of $R=0.05$. Both test sets resulted in the matrix failing by formation of cavities at grain boundaries. Fiber cracking was not prevalent, and bridging of matrix cracks occurred. When matrix damage was sufficient, the ductile tungsten fibers carrying most of the load would start necking, as opposed to fiber breakage characteristic of brittle fibers, such as SiC. The necking was much more pronounced in the $R=0.05$ tests than in the $R=-1$ cases.

Lerch and Halford performed fully reversed, strain controlled fatigue tests on a $[\pm 30^\circ]_{8s}$ SiC/Ti-15-3 (32 ply) composite at elevated temperature (427° C) [14]. The relatively thick specimen prevented buckling and allowed the compression loading. The results were compared to load controlled tests run under zero-tension cycling. On either a strain range or a stress range comparison basis, the fully reversed test had much longer lives than the zero tension tests. The R=0 tests revealed much damage due to strain ratchetting, with short matrix cracks, matrix necking, and fiber cracking. The R=-1 tests had damage restricted to long, isolated matrix cracks. Also, for a given strain range, it was found that the R=-1 fatigue lives slightly less than those of the matrix alone.

Sanders performed an extensive tensile fatigue characterization of 0° and 90° unidirectional laminas of the SiC/Ti-15-3 composite system [23]. The tests were performed over a wide range of maximum strains, at elevated temperature (427° C), under the strain control mode, using a hybrid control mode. Microscopy and analytical modeling were conducted to help define and characterize the initiation and progression of deformation and damage. For 0° fibers, initial response was creep deformation, while for the 90° fibers it was fiber-matrix interface debonding. The 0° specimens failed due to fiber fracture if maximum strain

was above 0.73% and had matrix plasticity above 0.55%. Below the 0.73% loading, the dominant failure mode was matrix cracking. The 90° specimens fiber-matrix interfaces debonded above 0.1% maximum strain. Propagation of matrix cracks was the dominant damage mechanism for loading above 0.35%, while between 0.35% and 0.23%, small, nonpropagating interface cracks were evident, along with matrix creep accumulation. Below 0.23% no evidence of matrix cracks was present. The damage evident was a progression of fiber-matrix interface damage. Finally the various specimen dominant failure modes were noted on the fatigue life curve by dividing the curve into regions of dominant failure modes for respective maximum applied fatigue strains.

Summary

This chapter has provided a minimal background regarding MMC fatigue testing, related terminology, and several recent studies related to MMC testing. The information provides a better understanding of the techniques, terms and procedures of the current work, discussed in the following chapters. Although much work has been performed on MMC's under monotonic and fatigue tension testing, none has been performed on the SiC-6/Ti-15-3 [0/90]_{2s} system under elevated temperature, fully reversed, strain controlled mode. Moreover, several studies have been accomplished on other metal matrix composite systems in general. However, when looking at all the specific test

parameters, such as static vs. fatigue loading, temperature loading, R ratio, fiber composition, size, and density, matrix composition, control modes, etc., usually not much, if any work has been performed in one concentrated area.

The knowledge gained from the objectives of the current work will provide a better understanding of SiC/Ti-15-3 fatigue life. The objectives was to investigate the fully reversed fatigue behavior and damage mechanisms in a cross-ply, [0/90]2s, metal matrix composite (SCS-6/Ti-15-3) at elevated temperature (427° C). This was accomplished by using a tension-compression, strain-controlled loading mode, with a strain rate of 0.2%/sec.

From the review of literature of MMC's and the SCS-6/Ti-15-3 system, the following observations can be made:

- 1) The dominant failure mode of a MMC depends on the loading condition and the relative ductility and strength of the fiber and matrix constituents.

- 2) The relative high strength of the Ti-15-3 matrix makes it a significant load carrying component for MMC's.

- 3) Transverse cracking in off-axis plies is a major damage mechanism.

- 4) Exposure to elevated temperature tended to cause age hardening of the Ti-15-3 matrix material.

- 5) Few fully reversed or strain controlled experiments have been reported for the Ti-15-3 composite system and no study is available addressing the current study objectives.

III. Test Equipment and Procedures

This chapter provides a description of the testing materials, equipment, and associated procedures in this study. The fiber reinforced composite material used is described in detail, along with the demanding specimen preparation requirements. The details of the testing procedure--strain-controlled, tension-compression, high temperature--are described. The equipment and associated setup procedure also will be described. Finally, the equipment, preparations, and procedures required to perform a microscopic evaluation is discussed.

Composite Material and Specimen Description and Preparation

Material Description

The material under investigation was an eight (8) ply silicon carbide fiber reinforced titanium metal matrix cross-ply ($[0/90]_{2s}$) composite. The composition of the Titanium alloy is: 15% Vanadium, 3% Chromium, 3% Aluminum, 3% Tin, with the remaining 76% being Titanium. The material designation, in abbreviated form, is SCS-6/Ti-15-3, where:

Matrix: Ti-15V-3Cr-3Al-3Sn

Fibers: SCS-6, silicon-carbide.

The continuous Silicon-Carbide fibers composed approximately 36 percent (by volume) of the composite. The fibers have a nominal diameter of 0.142 mm. These fibers have an inner

carbon core enclosed in a cylinder of bulk SiC with alternating layers of silicon and carbon, the final layer being carbon. Some key properties (at room temperature) of the matrix and of the fibers are shown in Table 3.1.

Table 3.1: Key Properties of Fibers & Matrix

Property	SCS-6	Ti-15-3
E @427°C (GPa)	400	74
α (10E-6mm/mm)	4.9	10
ν	0.25	0.36
σ_{ult} (MPa)	3550	865

Specimen Description and Preparation

Prior to testing, the test specimens must be cut, machined, and polished. This pre-test specimen preparation included: inspecting the as-received plate, cutting specimens from the plate, machining the rectangular specimen into the required dogbone shaped specimen, heat-treating the specimen, and polishing the specimen edges to remove any damage from cutting and to facilitate the taking of edge replicas. The following sections discuss these detailed procedures.

As-Received Plate Description

The material for the test specimens was received in square plate form, with nominal dimensions of 305mm x 305mm x 1.55mm (roughly 1 square foot). The material plate was

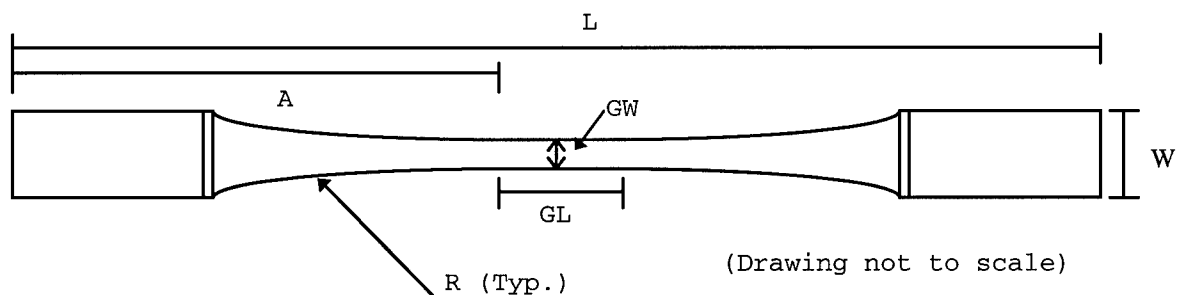
manufactured by Avco Specialty Metal, Textron Corporation, using a hot isostatic pressing (HIP-ing) manufacturing process. The exact procedures used are proprietary, but basically involve alternating layers of fibers and matrix foils and applying high pressure and temperature to bond the materials into the composite.

Specimen Geometry

Specimen geometry is a user defined test variable that should help provide gage length specimen failures and comparability with other tests if applicable. Three specimen designs (rectangular, dogbone rectangular, and hourglass) are the common designs currently in use in MMC research. Gayda and Gabb [7] performed load control test on unidirectional SCS-6/Ti-15-3 MMC at elevated temperature, using both rectangular and dogbone specimen designs. They reported that the fatigue life was not affected by the specimen's design, with all of the rectangular specimens failing in the hot zone. Sanders [23] used rectangular specimens with good results also. Boyum[3], however, in tension-compression work, used the dogbone design to prevent failures outside the heated zone. Since this work was using the same material, temperature, and a R value of -1, the decision was made to go with a dogbone configuration of basically the same design, described in the following paragraph. A diamond embedded saw blade was used to rough cut the rectangular specimens from the plate. Then a

computer programmed milling machine, using a diamond encrusted milling bit, was programmed to cut the exact final dimensions of the dogbone specimen.

The design of the dogbone specimen involved tradeoffs between obtaining a maximum width reduction in the gage length versus a maximum radius of curvature at the specimen shoulder. Dogbone specimens frequently fail at the specimen shoulder because of localized stress concentrations caused by the high shear stress near the end of the transition in the shoulder region [3]. This requires a large shoulder radius to minimize the stresses and chances for failure. However the larger radius increases the specimen length, increasing the compression buckling problem. Figure 3.1 presents the resulting specimen design. The design was the result of tradeoffs among the shoulder radius, gauge length minimal area, and buckling considerations.



$L = 13.65$ cm	$A = 6.83$ cm
$GL = 1.905$ cm	$R = 34.8$ cm
$W = 1.270$ cm	$GW = 0.51$ cm

Figure 3.1: Dogbone Specimen Geometry

Buckling Guide Description

Compressive stresses could cause specimen buckling, invalidating the test. Buckling is a problem with thin MMC materials, which are made thin to keep the manufacturing cost minimized. However, many material applications will be subjected to compressive stresses, thus including the compressive loading in testing would be desirable.

The dogbone specimen design eliminated the temperature gradient failure problem, but a buckling in compression problem remained. Figure 3.2 shows the buckling guide used to overcome buckling of the thin MMC specimen. Again, since Boyum had good results from this design, the same basic design (AFIT Buckling Guide) was used for the current work. Essentially the buckling guide clamps around the specimen at the top and bottom and has a fork/bolt guide slider near the middle to allow for unresisted specimen strain displacement.

A slight modification of the guide (Modified AFIT Buckling Guide) was incorporated to strengthen the bending resistance to withstand the higher strain loadings of this study. An outside of the fork slider surface was added (See Fig 3.2). This addition served to strengthen the guide and prevent out of plane bending at the higher loads.

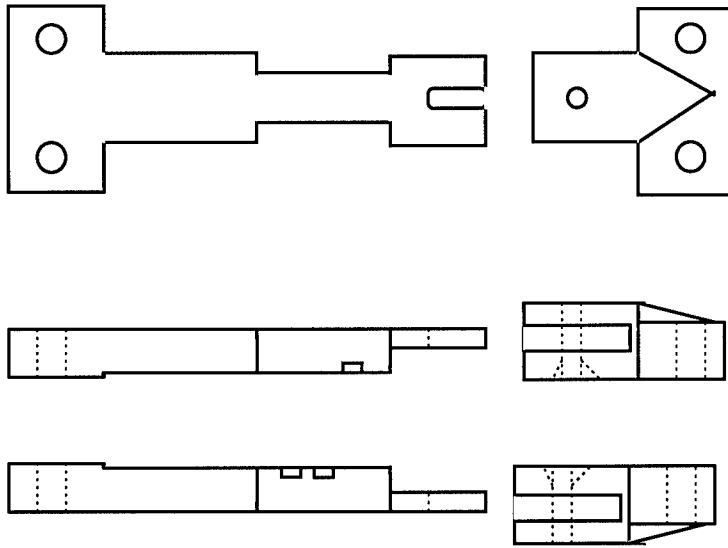


Figure 3.2: Buckling Guide Geometry

Heat Treatment

Mall and Schubbe [18] performed load controlled thermo-mechanical fatigue testing (TMF) on the same cross-ply material. The temperature ranged from 149-427° C. Age hardening of the matrix increased the modulus up to 20% early in the fatigue life. In order to stabilize the microstructure, thus minimizing diffusion induced property changes, the material was heat treated prior to testing.

Lerch and Saltsman [13] investigated the problem of the effect of heat treatment on both the neat matrix and the SCS-6/Ti-15-3 material. The aged samples of both the matrix and the MMC, ranging the temperatures from 300-700° C and the time exposed from 24 to 168 hours. As might be expected, significant changes in some material properties occurred, depending on the time and temperature. Importantly, it was stated that the material must be protected from oxidation at temperatures greater than 550°C. This can be accomplished by heat treating the specimen in an inert environment, such as Argon. Often investigations [3, 23] included a MMC heat treatment at 700°C for 24 hours in an Argon atmosphere for the Ti-15-3 system. The specimens, in the present work, were heat treated in the same manner.

Polishing Procedure

The final specimen preparation before testing was to grind and polish the specimen edges to remove any cutting damage and to provide a surface sufficient for recording edge replicas. For straight-edged specimens, an automated polishing procedure was used in work by others[23]. However since the dogbone specimens have a irregular geometry, this process could not be used. Instead a hand polishing technique was used that has been developed by previous researchers at AFIT[3].

The first stage of the process was the rough grinding. The specimens were ground with a silicon carbide grinding cloth (120 and 180 grit) attached to a specialized grinding/polishing device. The device had a variable speed, 2.54 cm (1 inch) diameter rubber disk in the handset, with the grinding/polishing cloth attached to the disk by adhesive backing. Lapping oil was used to help both remove debris and cool the specimen during grinding. Next, actual grinding by hand was accomplished by application of successively finer grades of silicon carbide (240, 360, and 400 grit), also with lapping oil. The paper was cut to fit around a standard artist type eraser. The grinding was done longitudinally in order to remove larger scratches and to minimize any transverse scratches that could be left by the grinding itself and be possible stress risers.

For the polishing stage, the grinding tool was again used, but with a nylon pad replacing the silicon carbide paper. The specimens were polished with successively finer diamond suspension slurries (45, 15, 6, 3, and 1 μm) along with appropriate diamond paste. Next, a neoprene pad replaced the nylon pad and Mastermet was applied to the water moistened pad and specimen edge. Immediately after completion of this step, the specimen was totally immersed in water and washed thoroughly. This step was critical to keep the Mastermet from drying on the surface and ruining the desired finish. After a successful polishing, the edge

had a mirror like finish, very suitable for edge replication.

The other edge did not require polishing, only the removal of cutting process scratches and imperfections. The above initial grinding process was repeated, but stopping after hand grinding with 240 grit paper. Since this relatively rough side was to be used for the extensometer, further grinding or polishing could be detrimental, facilitating extensometer slippage. This translates to inaccurate data and possibly inadvertent specimen failure.

After polishing, aluminum tabs were epoxied to both side of both specimen tab ends. This helped to protect the specimen from any grip induced impressions or damage. In addition, the aluminum tabs provided the grips an improved surface on which to clamp and eliminate grip slippage.

Experimental Equipment

The test system used in this study consisted of three primary subsystems. They are: a) Mechanical Loading (Loadcell), b) Temperature Controlling (Micricon), and c) Data Acquisition (PC computer with associated software).

Figures 3.3 and 3.4 illustrate the testing setup. The mechanical loading was accomplished on a 22 Kip servo-hydraulic motor test frame (MTS model 823) with water cooled hydraulic grips. A ceramic rod, air cooled, 12.7 mm (0.5 inch) gauge length extensometer (MTS model 632.50004) measured the displacement within the gauge length.

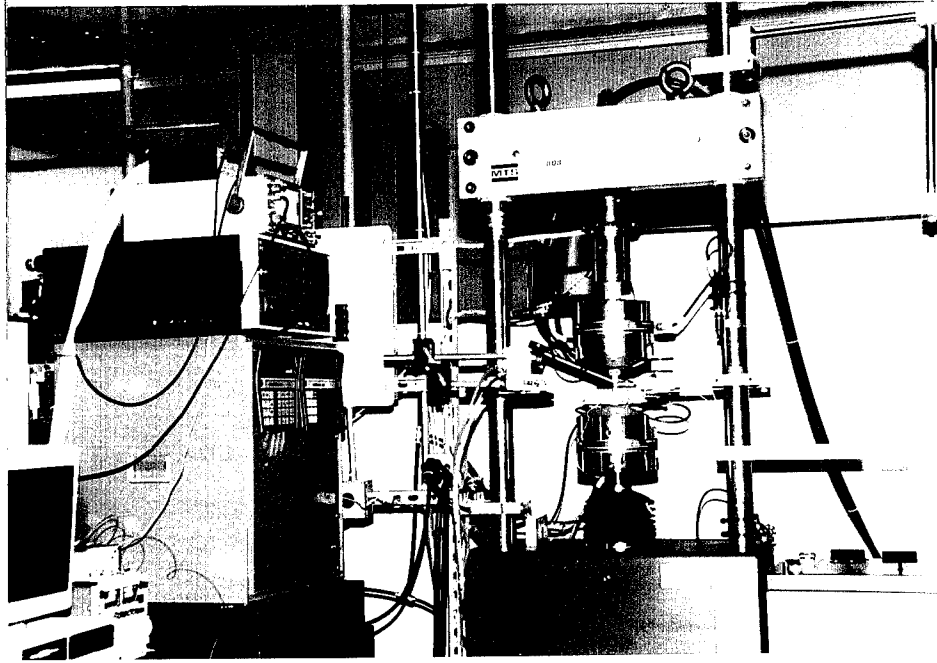


Figure 3.3: Fatigue Testing Apparatus

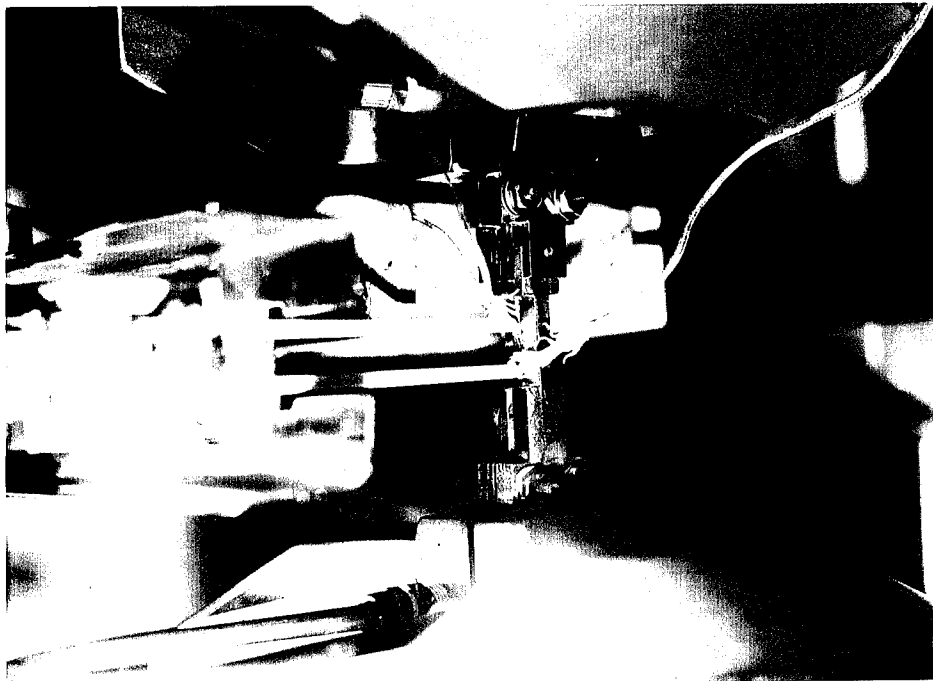


Figure 3.4: Specimen Test Setup

The microprofiler (MTS model 458.91) served as the function generator for the DC controller (MTS model 458.11).

The high temperature test environment was provided and controlled by two 1 kW, tungsten filament, water cooled, parabolic strip heaters. The strip heaters were controlled by a Micricon (model 82322) controller. To minimize thermal gradients in the gauge section, the strip heaters were offset from one another. Three Chromel-Alumel (type K) thermocouples were used as temperature feedback transducers. Two of these were connected to the controller, with one used as part of the data acquisition subsystem.

The data acquisition system consisted of a 386DX 16 MHz PC computer, Techmar Labmaster analog-to-digital (A/D) converter board, and the data acquisition software written by Sanders[23]. The program prompted the user for required test parameters, automatically programmed the load and temperature controllers, and recorded test data into computer files, as required.

Experimental Procedures

Experimental procedures for this investigation included the following: preliminary actions, edge replication, thermocouple welding, buckling guide installation and alignment, extensometer placement, start-up actions, and manual cycling and test stoppage when required.

Additionally, a different loading procedure was required for performing a monotonic tension test.

Preliminary actions included measuring the specimen gauge length cross-sectional area, aligning and mounting the specimen in the loadcell and taking the initial edge replica. Aligning and mounting the specimen was accomplished by using a bubble type level to assure vertical alignment and then gripping the specimen with the top grip. This action held the specimen firmly while the alignment was rechecked and, if aligned, moving the bottom grip into proper position and gripping the specimen bottom. Keeping the load cell under the load controller (at zero load), the initial edge replica was taken, with the replica process discussed below.

Edge replication involved taking a permanent impression of the polished specimen edge at various times during the fatigue life, the first replica being the initial, unloaded specimen replica. The advantage to this method is that specimen edge damage can be recorded as the test progressed, allowing at times to see damage initiation and progression, without removing the specimen from the testframe. Wetting cellulose acetate film with acetone and, with an artist type eraser, pressing the wetted film against the specimen edge for approximately 60 seconds produced the impression of the specimen edge. Replicas were taken on the specimen, cooled to room temperature, at predetermined intervals based on fatigue life and whenever a relatively large drop in modulus

was observed. To provide for better crack replication, the specimen was loaded to approximately 80% of the maximum observed load for that test segment. The replicas were then examined for damage.

Thermocouples attached to the specimen provided for thermal control and data recording of the test temperature. Two type-K chromel-alumel thermocouples were tack welded to the specimen, one on front with the other on back, 6.35 mm (0.25 inch) from the center in opposite vertical directions. These provided the temperature information to the temperature controllers previously discussed, with the third type-K thermocouple, in the specimen center, providing temperature data to the data acquisition system.

After thermocouple installation, the buckling guide was installed and aligned. Before actual installation, the sliding surfaces of the buckling guide were covered in powdered graphite to minimize any friction. During installation, care was taken not to disturb the tack welds since the thermocouples were easily dislodged. The specimen-guide alignment was checked and the 4 main bolts tightened.

Next the extensometer was placed onto the specimen side. The device was required to be balanced in order to provide equivalent top and bottom pressure on the extensometer tips and not slip during the test.

This adjustment was accomplished by adjusting the set screws on the extensometer mounting bracket. When the rods would not easily slip, the extensometer was then zeroed to finish the process.

Testing start up procedures included the bringing the specimen to temperature and taking a initial modulus. First cycle was manually run after the temperature had been slowly elevated to 427° C. The manual controlled first cycle was recorded by running a program named STATIC, written by Mr. Mark Deriso. After the requested testing parameters were entered, the controller was manually operated. With the maximum and minimum strains being precalculated manually, the strain outputs were observed as the specimen was loaded. Upon reaching these strains, the loading was reversed and one cycle completed. After completion of the manual first cycle, the program STRAIN TEST was again invoked for the long-term test control.

Occasionally the testing was stopped. Very important for strain controlled testing is to set maximum and minimum controller safety interlock limits. This helped insure the test specimen was not inadvertently overloaded or failed because of extensometer slippage, etc. The interlocks sometimes stopped a test because of these reasons

Another type of test often performed to characterize MMC material properties is a static, or monotonic, tension test. A static test involves increasing the applied strain

(or load) until specimen failure. This provides information of maximum stress and strain allowed for a given temperature and strain rate. Some material properties found using this method include: elastic modulus, ultimate tensile strength, and the yield stress/proportional limit. The current work used the ultimate tensile strength information to define an upper limit for fatigue loading of the particular composite.

Post-Test Procedures

Post-test procedures included visually examining the specimen after failure and processing data, sectioning, heat treating, mounting sections, lapping and polishing, etching and micrography. Upon specimen failure, the specimen was visually inspected to note the overall condition and fracture surface. Additionally the final recorded data was processed to provide mechanical response trends.

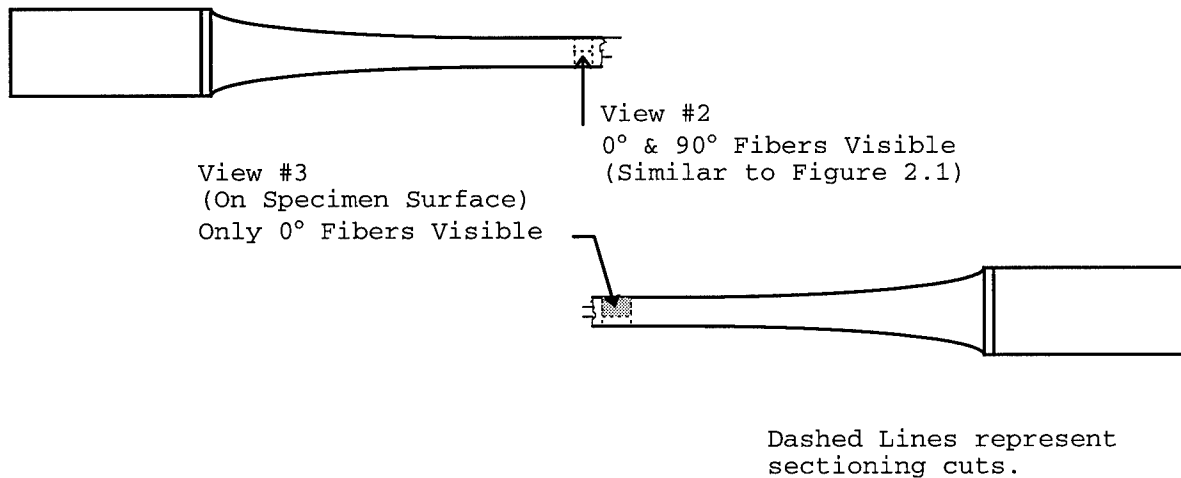
Sectioning Procedures

Sectioning the specimen involved cutting small pieces out of the specimen near the fracture surface, in order to facilitate micrography and failure analysis. Figure 3.5 illustrates the sectioning cuts made in the failed specimens.

Initially, the fracture surfaces were cut, using a low speed diamond wafering saw, from the specimen to study in the scanning electron microscope (SEM). Next a centered longitudinal cut was made, with a transverse cut made at the

end of the longitudinal cut. This provided two sections, not including the fracture surface. One of the sections was to be mounted and observed such that only the first layer of 0° fibers were revealed, while the other section would be positioned to reveal an edge view from the interior center looking outward.

One of the failed specimen halves of each test was heat treated prior to sectioning. This heat treatment allowed the alpha phase of the matrix to precipitate, especially along slip bands. The alpha phase is reported to allow easier observation of slip bands. The heat treatment included wrapping the specimens in Tantalum Foil and placing the specimens in an inert atmosphere at 427°C for 24 hours. The heat treated specimens were sectioned as described above.



(Not to Scale)

Figure 3.5: Typical Failed Specimen Sectioning

Sectioned Specimen Mounting and Polishing

The sectioned specimen samples were mounted in 2.54 cm (1 inch) diameter specimen mounts to allow automated fine polishing. The specimens were mounted in a conducting molding compound (Konductomet). Once mounted, an automated method of grinding, or lapping in this case, was used. A Buehler Maximet with a number 6 platen and successively smaller diamond suspensions (45, 15, 9, 6 and 3 μm) were used to grind the mounted specimen surfaces for preparation of the series of Vibromet polishers.

The three Vibromets used for this work were: 1 μm , 0.5 μm diamond paste and Mastermet polishers. The first polisher contained a solution of 1 μm diamond paste, a perforated Texmet cloth and Hyperex OS lubricant. The second polisher contained a solution of 0.5 μm diamond paste, a nylon cloth over a perforated Texmet cloth and Hyperex OS lubricant. The final polishing Vibromet contained 0.06 μm Colloidal Silica Neutral Solution (MasterMet) with a micron cloth. The specimens were polished in the 1 μm , 0.5 μm and MasterMet Vibromets for approximately 12 hours, 12 hours and 45 minutes, respectively. Again care was taken to keep the MasterMet from drying by immediately immersing the specimens in water

and accomplishing an ultrasonic cleaning process. Upon completion of polishing, the specimens were either observed microscopically or acid etched.

Etching

To emphasize different features, such as slip bands, grain boundaries, or damage, the samples were etched in an acid based solution, or etchant. Two etchants were used in this research. Kroll's etchant was used to highlight the microstructure and damage mechanisms, while a solution of 3% ammonium bifluoride and 97% distilled water was used to locate slip bands. Only the post-failure heat treated specimens were etched, since the heat treatment precipitates the alpha phase which contrasts with the matrix when etched with the ammonium bifluoride solution[5].

Micrography

The specimens were now ready for microscopy. All polished specimens were examined using the optical microscopes at various magnifications to record the microstructure changes and damage mechanisms. Because of focal length problems with the fracture surfaces irregular nature, the SEM was used to investigate these surfaces. Once the desired image was obtained from a specimen, a 101.6 x 127.0 mm (4 x 5 inch) microphotograph (Poloroid) was taken of the image.

IV. Experimental Results and Discussion

The focus of this chapter is to discuss the experimental results from testing, and the subsequent microscopic examinations. Also furnished are the results from a monotonic tension, elevated temperature test. The mechanical responses of the fatigue specimens are presented, including stress vs. strain (σ - ϵ) curves, maximum and minimum stress (σ_{\max} & σ_{\min}) vs. cycles curves, and modulus (E) vs. cycles curves. Micrographs examining the microstructure, damage mechanisms, and fracture surfaces of the specimens are discussed afterwards.

Monotonic Tension Test - Strain Controlled

Figure 4.1 shows the monotonic tension stress-strain response of the $[0/90]_{2s}$ composite when tested under strain controlled mode, at a strain rate of 0.2%/sec. This test was performed at 427° C up to tensile failure, providing the maximum strain limit of the material. The curve shows the three stage stress strain response characteristic of crossply laminates. In the first stage, the linear-elastic response region extends to the first knee at approximately 0.06% strain (80 MPa). Boyum [3] reported a knee at the same load level and temperature. This stage is characteristic of undamaged material (no cracks or debonds). At the 0.06% knee, 90° fiber debonding initiates[23].

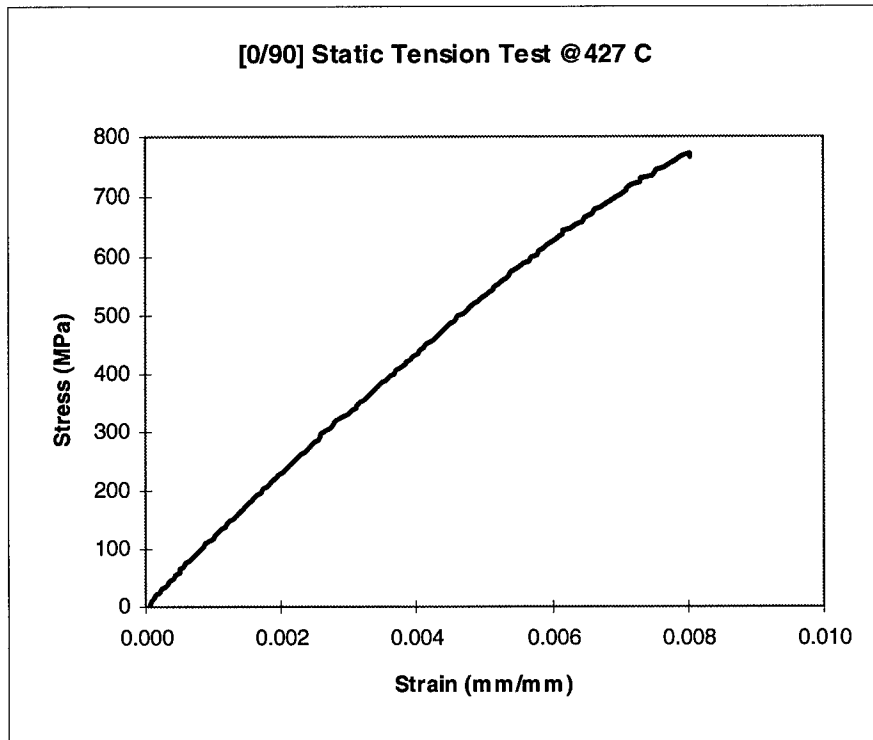


Figure 4.1: Monotonic Tension Test (0.2%/sec Strain Rate)

This debonding decreases the stiffness of the material, illustrated by slight decrease in slope of the stress-strain response, from 126.4 GPa to 103.5 GPa. After the debonding, the response is fairly linear until 0.55% strain, where a slight nonlinear response initiates. At this point, Sanders[23] reported that, for unidirectional Ti-15-3 composite, plastic deformation of the matrix initiates. This suggests matrix plasticity initiates at this strain.

The initial and secondary moduli of the static test compare well with the average initial and secondary moduli reported by Boyum[3]. Boyum reported an $E_1=129.24$ GPa and an $E_2=109.5$ GPa, while the current test provided an $E_1=126.4$ GPa and an $E_2=103.5$ GPa, less than 6% of difference between the two studies.

Fatigue Testing Results and Discussion - Strain Controlled
Mechanical Response

A total of seven fatigue tests were conducted on the SCS-6/Ti-15-3, $[0/90]_{2s}$ composite. The maximum applied strain levels were: 0.73%, 0.6%, 0.5%, 0.4%, 0.3%, 0.25%, and 0.2%. These strain levels fell into regions IIa and IIb of the fatigue curve regions presented in Table 4.1. Figure 4.2 overlays the static test curve and the dominant failure mode regions, allowing a visual comparison of ultimate strength and fatigue failure modes. This section presents the fatigue mechanical responses and trends observed from the testing, divided into dominant failure mode regions. These regions are summarized in Table 4.1. As shown, the resulting failure mode categories illustrated by this experimental work consisted of three regions: I (Fiber dominated failure region), IIa (Mixed fiber and matrix failure mode), and IIb (Matrix dominated mode). Fatigue responses for the failure modes differed, as discussed next.

Table 4.1: Summary of Failure Modes

<u>Max ϵ (%)</u>	<u>Failure Mode</u>	<u>Region of Fatigue Curve</u>
$\epsilon < 0.45$	Matrix Failure	IIb
$0.75 > \epsilon > 0.45$	Mixed Fiber and Matrix Failure	IIa
$\epsilon > 0.75$	Fiber Fracture	I

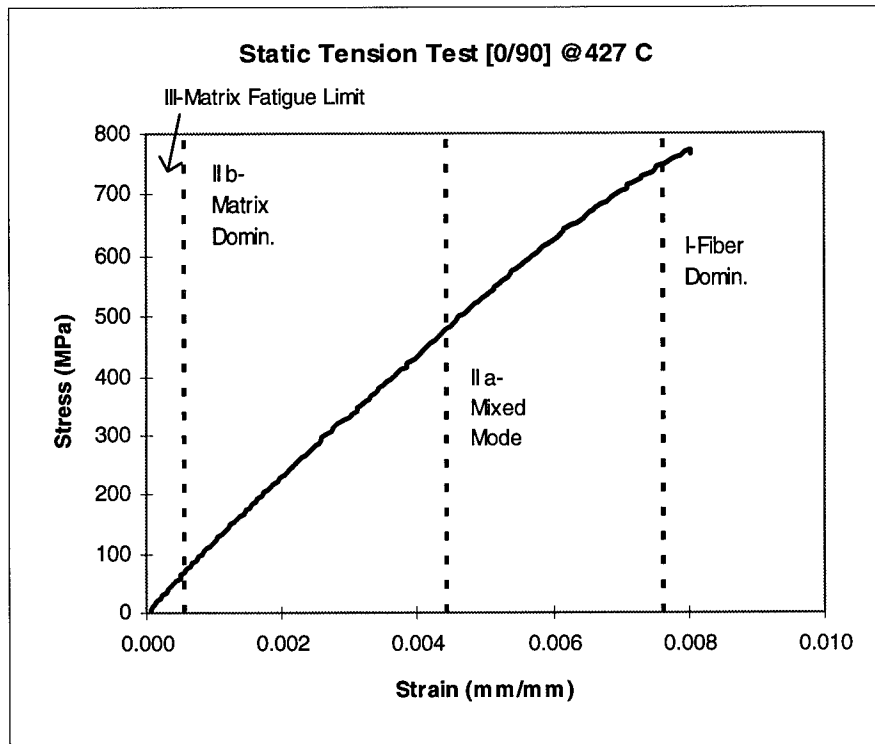


Figure 4.2: Monotonic Stress-Strain Curve/Fatigue Failure Mode Region Overlay

Region I - Fiber Dominated Failure Mode

Region I was not represented by any fatigue test of this study. No specimen demonstrated solid evidence of the requirements to belong to this category. The 0.73% test was very close to being a totally fiber dominated failure, but demonstrated some minor matrix cracks. An argument could be made to include the monotonic tension test (0.8%) in this category, but this test was not a fatigue specimen. However, the 0.8% experiment possessed all the microscopic evidence characteristic of a fiber dominated failure and has been used as a upper bound for the fiber dominated region failure surface and micrography evidence.

Previous studies[23] have found slip bands at strain levels in the Regions I and IIa. For the present work, no slip bands were found, although a published procedure for finding the slip bands was followed[15]. Boyum, in similar elevated temperature load controlled work, did not find any elevated temperature specimen slip bands. However, it was reported that diffuse slip was present for the specimens. Perhaps this form of slip was present in the current work, but did not provide enough contrast to detect with the method used.

This static test will be elaborated further in the Region I failure mode discussion in the Microscopy, Fractography, and Damage Mechanisms section. The mechanical response from the Region IIa 0.73% test will be presented next.

Region IIa - Mixed Fiber and Matrix Failure Modes

0.73% Modulus and Stress Responses

Figure 4.3 illustrates the variations in the unloading modulus, or stiffness response over the fatigue life of the specimen tested at a maximum strain level of 0.73%. The unloading modulus was found to be the most consistent modulus measurement for this work. The unloading modulus is the modulus measured from the portion of the stress-strain

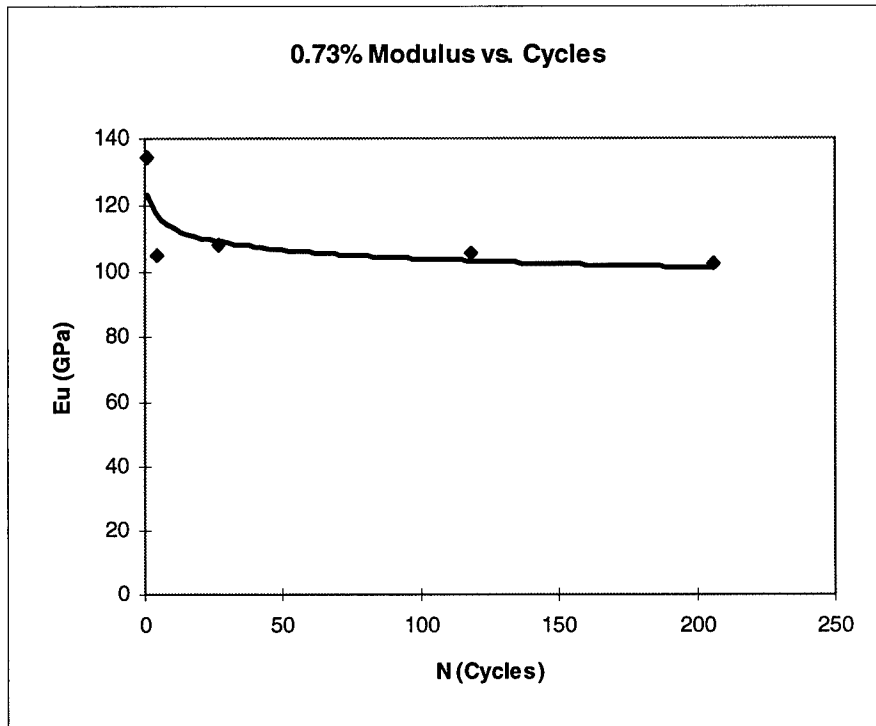


Figure 4.3: Modulus History, 0.73% Test

response that starts at the maximum load and ends at zero load. An initial drop in stiffness can be observed after the first cycle due to debonding of fiber matrix interfaces in the 90° plies. The modulus then remained relatively constant over the entire fatigue life. This is one of the characteristics of fiber dominated failure. As will be discussed further in the fractography section, the evidence indicated that the failure was rapid and thus was fiber dominated. Figure 4.4 illustrates maximum and minimum stress response over the fatigue life of the same specimen. The maximum and minimum stress remained relatively constant,

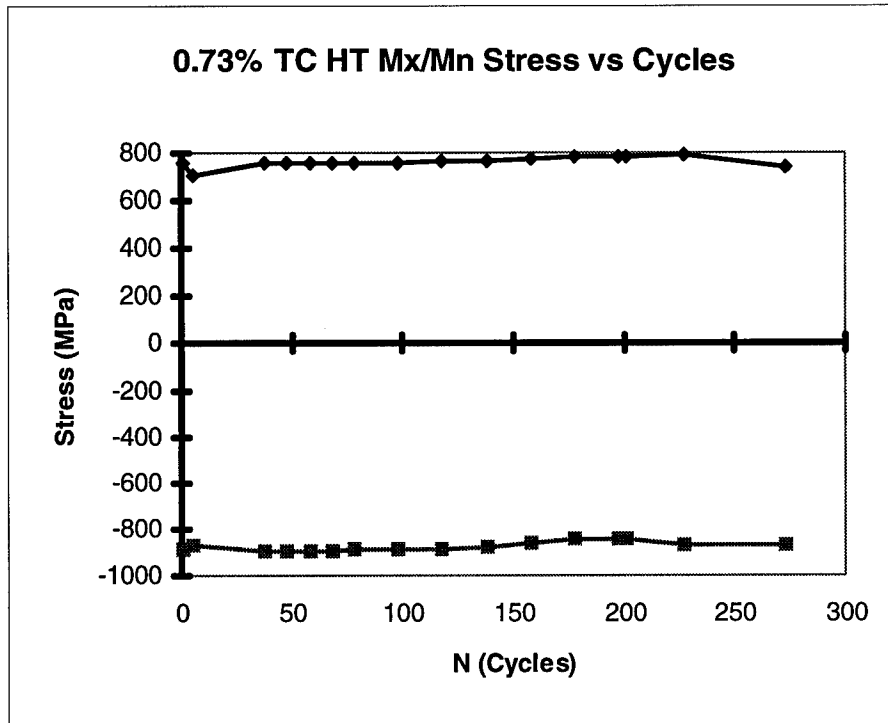


Figure 4.4: Maximum/Minimum Stress History, 0.73%.

following the same trend as the modulus response. It will be shown that the specimen micrograph showed a small amount of matrix cracking initiating from the 90° fiber interfacial region, thus supporting the mixed mode conclusion.

0.73% Stress-Strain Response

Figure 4.5 illustrates the variation in the stress-strain responses over the life of the same specimen. Initial, intermediate-life and near final stress-strain plots are presented, with the second, third, and fourth curves being offset to facilitate observing differences in the plots. Of note on the first cycle plot is the relatively large hysteresis and the associated residual

plastic deformation of 0.07%. A non-linear response occurs at approximately 0.55%, the onset of matrix plasticity and of fiber nonlinear response previously discussed. Subsequent cycles illustrate a decaying hysteresis trend, suggesting that plastic deformation and damage occurs in the initial stages of the fatigue life at this strain level. The stiffness in compression was observed to be that of the undamaged composite. The transition is likely the result of the force required for closure of the transverse fiber-matrix debonding.

The cycle 178 (N=178) plot has the decrease in hysteresis discussed and the variation of compression and tension stiffnesses. The N=242 plot does not show much change from the N=178 plot, with little hysteresis and no noticeable change in stiffness.

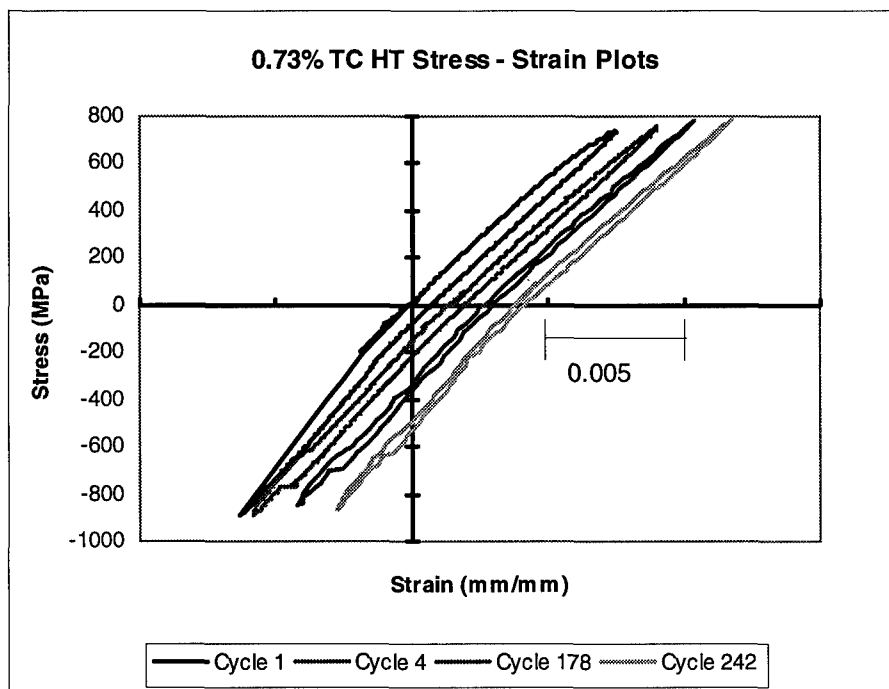


Figure 4.5: Stress-Strain Plots, 0.73% (Offset)

0.6% Modulus and Stress Responses

Figures 4.6 and 4.7 show the typical history of the modulus and maximum/minimum stresses for another specimen whose dominant failure mode was also mixed fiber failure and matrix cracking. The particular case shown is for a specimen loaded in fatigue at a maximum strain of 0.6%. Like the 0.73% test, the characteristics of this specimen were closer to that of a fiber dominated failure than of a matrix dominated failure, but the matrix cracking had increased. Figure 4.8 shows evidence of this observation. The presence of several 0° fiber cracks and of non severe matrix cracking was observed. It will be seen that since evidence of both damage types was seen, the Region IIa classification could be confidently made. The maximum and minimum stresses demonstrated a slight decrease in stress while the modulus slowly decreased also. The initiation of matrix cracking was a contributing factor to this decline. Even though the modulus did decrease slightly, the final failure was relatively rapid, happening over a few cycles.

As mentioned earlier, the failure was evidently rapid near the end, not showing a large change of modulus nor stress near the end. This response also supports the deduction that although the failure was mixed mode, a larger share of the failure was fiber dominated.

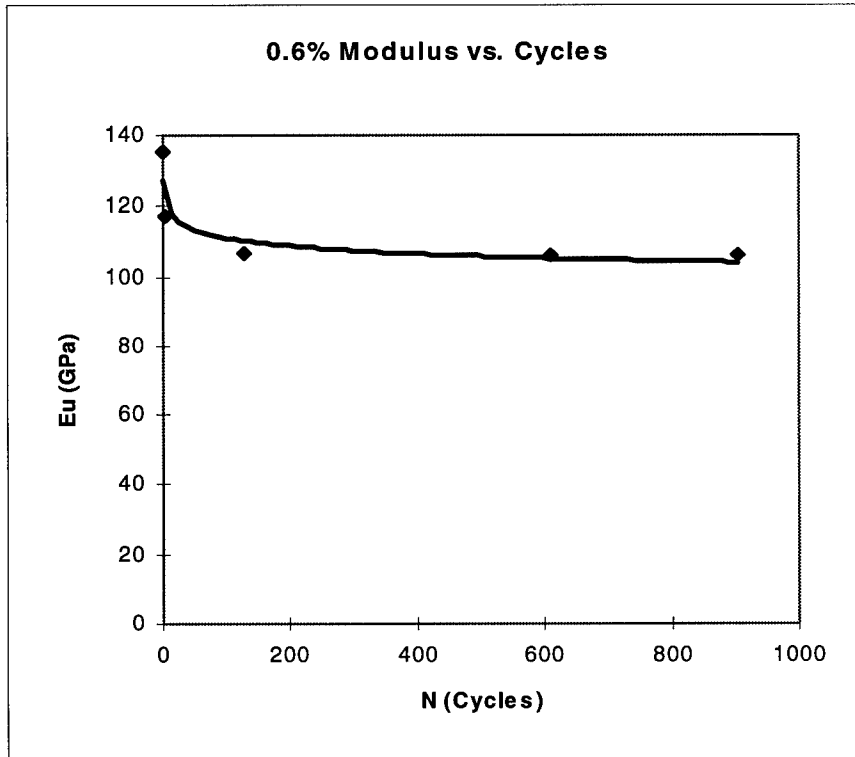


Figure 4.6: Modulus History, 0.6%

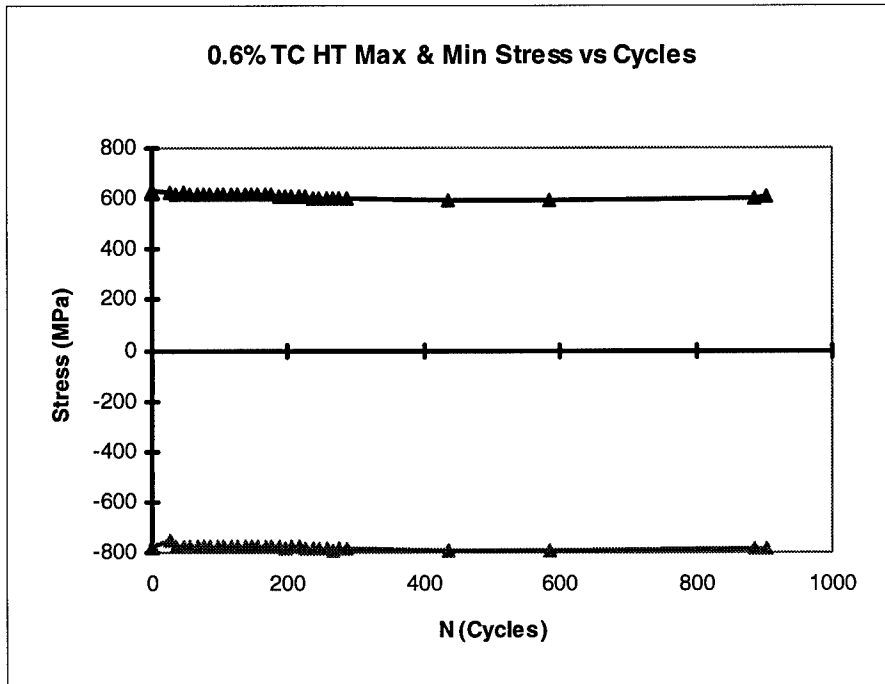
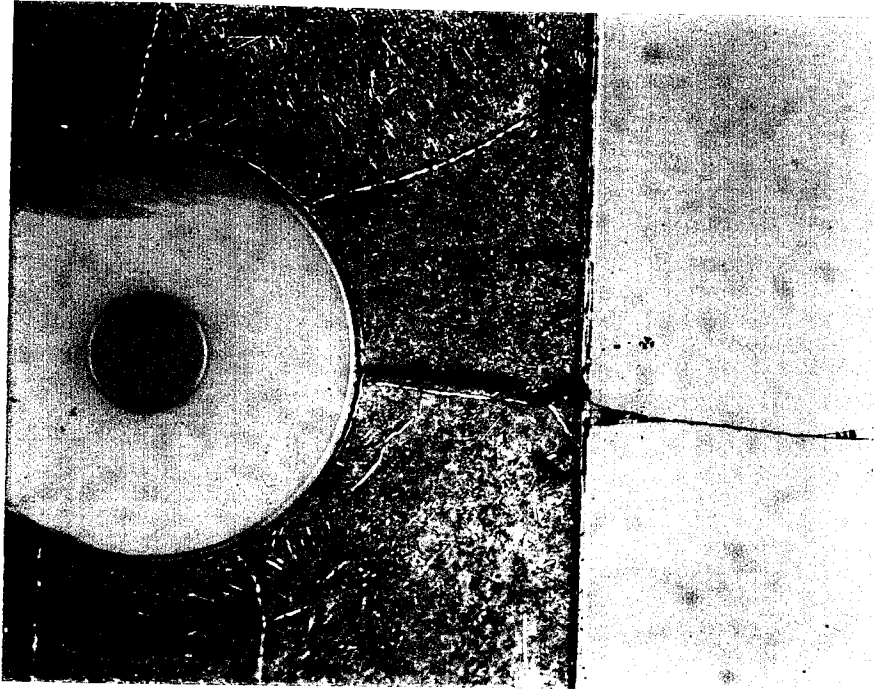


Figure 4.7: Maximum/Minimum Stress History, 0.6%



Loading Direction: \updownarrow

Figure 4.8: Fiber and Matrix Cracking, 0.6% (500X)

0.6% Stress - Strain Response

Figure 4.9 shows the typical stress-strain history for the same case. As with the 0.73% test discussion, the first, half-life, and near final cycles are presented. As can be observed, the degradation was not severe, as previously indicated in Figure 4.6, the 0.6% modulus response history. The first cycle had a larger hysteresis compared to subsequent stress-strain responses, which is typical for the higher level applied strains. However,

hysteresis was evident in the plots throughout the life of the specimen. This can be attributed to any or all of the following mechanisms: creep, plasticity, initial cracking and progression, and fiber matrix debonding. The tensile stiffness decreased as evidenced by the progression of the plots. This decrease differs from the 0.73% test which had a constant stiffness until failure.

Also of note is the stiffening of the material in compression. This happened consistently for most of the experiments. One possible explanation is that cracks and debonds that formed compressed back together, effectively stiffening the material. The ratio of the compression

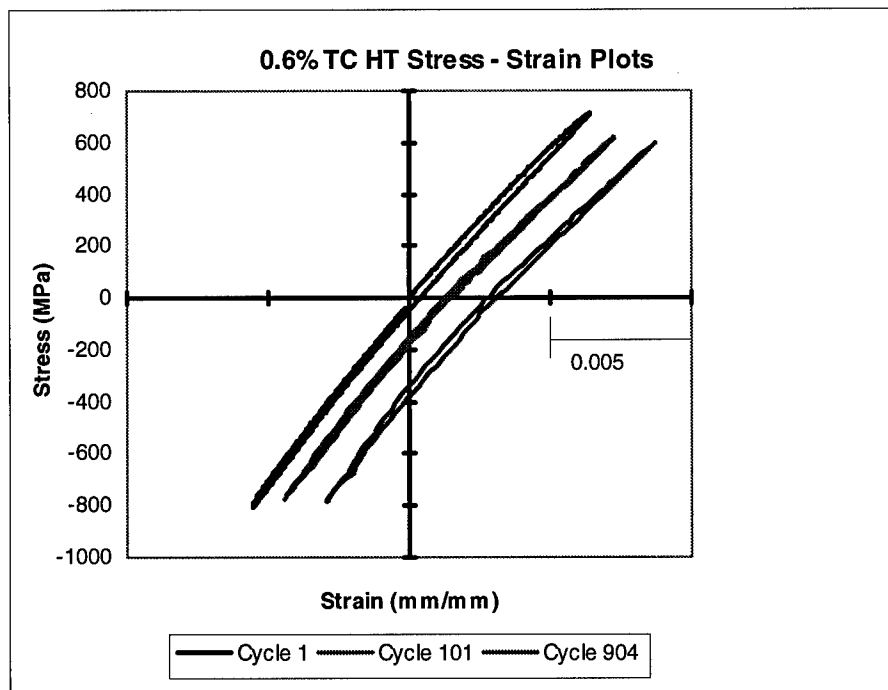


Figure 4.9: Stress-Strain Plots, 0.6% (Offset)

modulus to the unloading modulus at the fatigue half-life was approximately 1.22 for the tests, or a 22% stiffness increase in compression. For example, the 0.73% test $E_c/E_u = 122.2/105.8 = 1.155$, the 0.6% test $E_c/E_u = 134.6/106.1 = 1.2686$, and the 0.4% test $E_c/E_u = 142.9/113.2 = 1.2624$.

Region IIb - Matrix Dominated Failure Mode

Modulus and Stress Responses

Figure 4.10 shows the typical history of modulus for a specimen whose dominant failure mode was matrix cracking. The case shown is a fatigue loaded specimen at a maximum strain of 0.4%. This specimen showed a significant increase in matrix cracking as compared to the specimens discussed thus far, with no fiber cracks, thus indicating a significant change in dominant failure mechanism. This evidence is discussed more in the microscopic evaluation later in this chapter.

The unloading modulus trend supports the damage progression. After the typical first cycle stiffness drop, the modulus slowly and steadily decreased in general. However, a slight increasing trend in the middle of the specimen life was observed, perhaps due to age hardening [23]. Moreover, the modulus started decreasing more rapidly near the failure point, as can be observed.

Figure 4.11 shows the typical histories of the maximum stress and minimum stress for the same test, with the dominant failure mode of matrix cracking. The maximum and

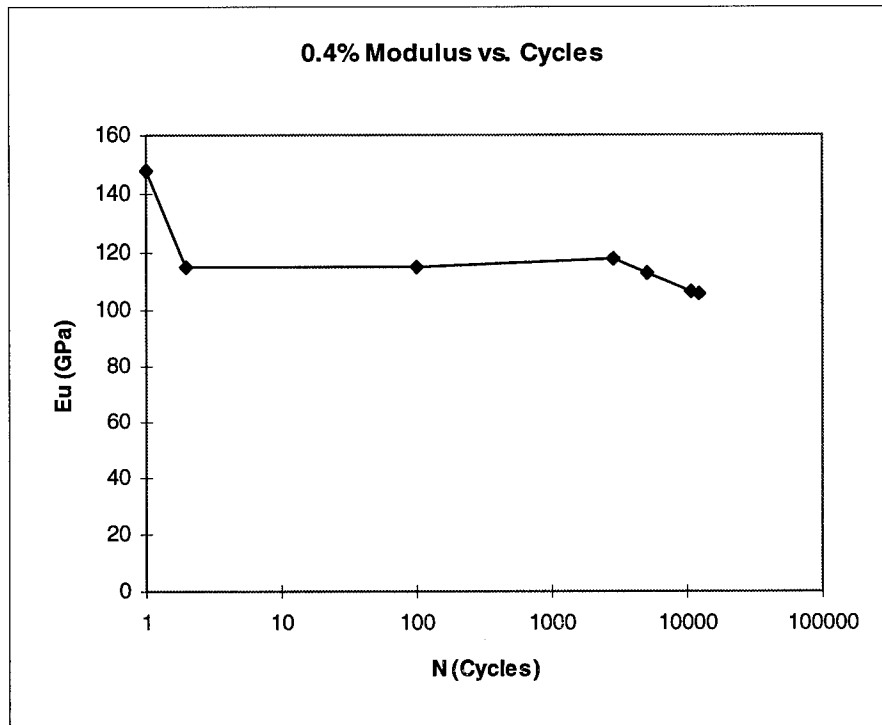


Figure 4.10: Modulus History, 0.4%

minimum stress history plots demonstrate an overall trend of decreasing maximum stress level over the latter half of the specimen life. This trend supports the theory that matrix cracking was the dominant mode of failure, since damage was slowly accumulating and thus the material deformed to a given strain with less stress at higher fatigue cycles.

Stress-Strain Response

Figure 4.12 shows the typical stress-strain history for the same specimen. Similar to the prior discussions, the first, half-life, and near final cycles are presented. The stress-strain plots illustrate that the material degradation was present, but was not severe. This observation is consistent with that in the modulus response history.

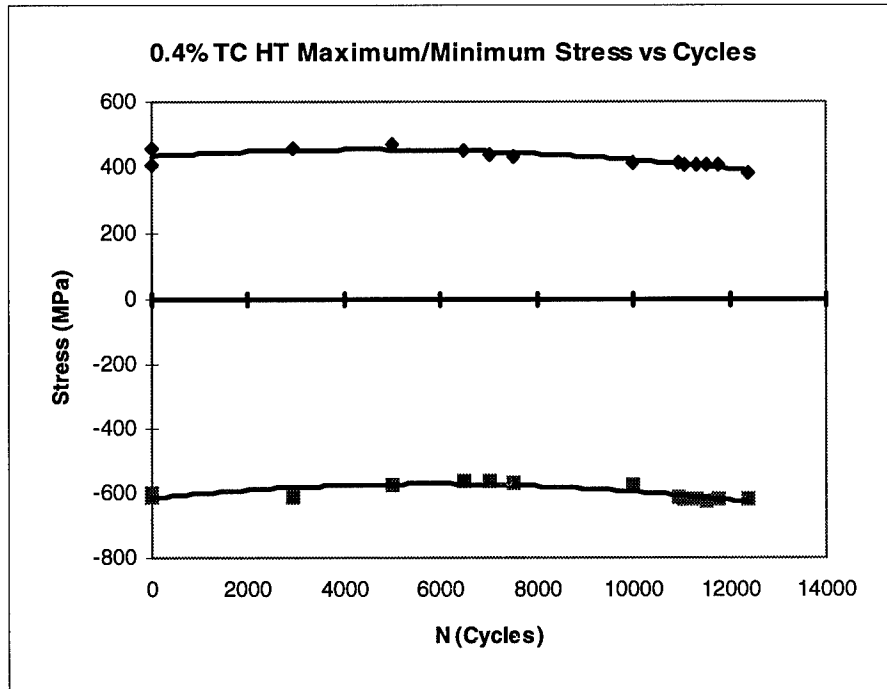


Figure 4.11: Maximum/Minimum Stress History, 0.4%

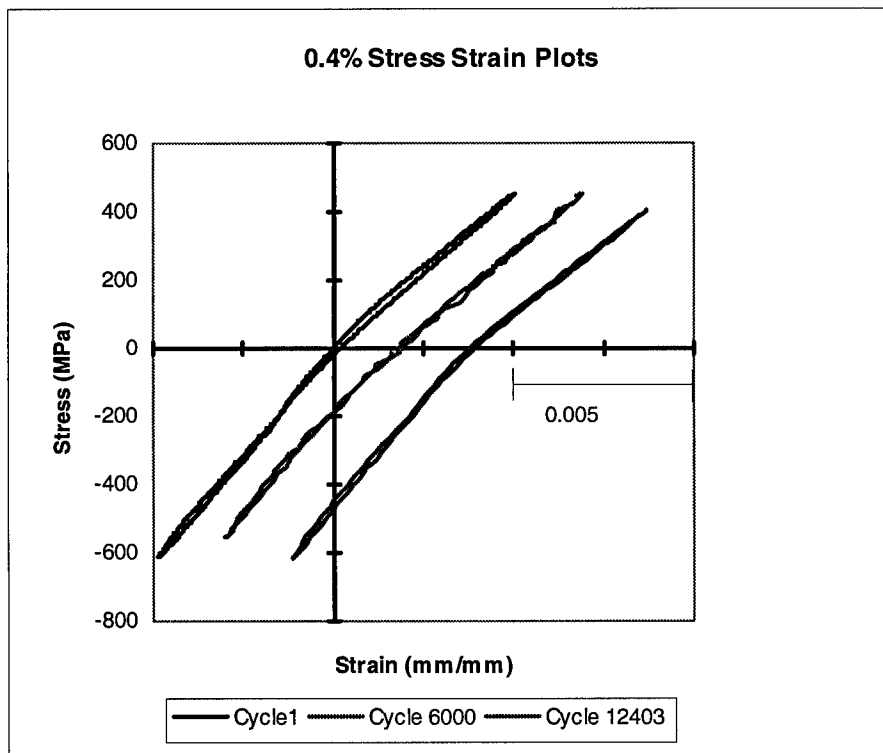


Figure 4.12: Stress-Strain Plots, 0.4% (Offset)

Again, the first cycle had a larger hysteresis, as compared to the rest of the stress-strain responses, as expected. The modulus is indicated by the slope of the stress-strain plots. A stress-strain slope becoming more horizontal indicates a decreasing stiffness, or modulus. This decreasing slope verifies the decreasing modulus trend shown in the modulus history.

Summary - Mechanical (Macromechanical) Response

The preceding discussions have presented the mechanical responses of experiments performed for this work. Failure modes were represented by mechanical response data of representative tests. The mechanical responses presented for each case included modulus histories, maximum and minimum stress histories, and stress-strain plots. The fiber dominated region was not observed in the fatigue tests, but typically has fairly constant maximum stress and modulus history, with failure occurring rapidly upon the initiation of damage. The mixed mode responses had some modulus and maximum stress decrease corresponding to matrix cracking present, but again rapid failure occurred near the end, signifying rapid fiber failure also. Finally, the matrix dominated Region IIb presented response histories of steadily decreasing maximum stress and post half-life modulus, indicating the steady progression of matrix cracks. The notable sharp downturn near the failure point supports a matrix damage dominated failure conclusion.

Fractography, Microscopy, and Damage Mechanisms

This section provides the physical evidence to support the trends and deductions resulting from the mechanical responses. The damage mechanisms are discussed in relation to the dominant failure mode regions. To better understand the progression of damage for the matrix dominated failure mode, an additional test was performed, being interrupted before failure. Fractography will be presented for all test specimen cases, with micrography for the typical cases presented. The following evidence provides support for the mechanical responses to allow confident conclusions regarding dominant failure modes.

Fractography

Figures 4.13 through 4.20 illustrate the fracture surfaces of the 0.8% through the 0.25% tests, respectively. All of these surfaces are presented so that the trends of matrix ductile and/or fatigue failure can be observed. For example, the amount of brittle, relatively flat fracture surface increases with decreasing applied strain levels, as can be seen.

The fracture surface from the monotonic tension static test, Figure 4.13, illustrates the limiting case, allowing for better comparisons with the fatigue tests. As expected, matrix ductile necking exists around virtually every 0° fiber. Evidence of fiber pull-out is supported by the

longitudinal holes in the specimen. This suggests that the failure was due to fiber fractures followed by tensile overload in the matrix. Long protruding fibers from the failure surface are not seen as often as expected. This trend was noted for all the failure specimens. Next, the description of fatigue fracture surfaces follow in order of decreasing maximum strain.

This first group of fatigue fracture specimens had a lack of extensive matrix-fiber crack bridging as a common characteristic. This was determined from internal sectioned micrography, to be discussed later. First the fracture surfaces are discussed to observe trends on the surfaces. Figure 4.14 shows the 0.73% surface which had some evidence of fatigue, but did have much ductile failure/necking. Void-coalescence was evident. Figure 4.15 shows a close-up of the 0.73% fracture surface. This specimen exhibited much ductile matrix failure at the surface, however the close-up shows evidence of fatigue between the middle 90° fibers. As seen, the void coalescence is predominant over the remaining fracture surface. For the 0.6% surface, illustrated by Figure 4.16, a slightly lower percentage of the surface demonstrated necking around the fibers, with some fatigue striations evident. Also, Figure 4.17 indicates that the 0.5% test had decreased the amount of ductile necking present to about 1/3 of the surface, with both void-coalescence and striations present. Striations were evident

between the middle two 90° fibers, a possible nucleation site.

The second group of fatigue fracture surface specimens had extensive matrix cracking and fiber bridging observed in the subsequent micrographic investigation. Figure 4.18, the 0.4% fracture surface, indicated reduced ductile necking to about 1/5 of the surface area. The fracture failure surface had a multi-tiered topography, again with void-coalescence and striations present. The multi-tiered surface perhaps resulted from extensive crack coalescence. For Figure 4.19, the 0.3% test, only a small area had ductile failure with the majority of the failure surface showing brittle failure. Similarly, Figure 4.20 shows, for the 0.25% surface, approximately the same amount of ductile necking around the longitudinal fibers, as compared to Figure 4.19. The majority of the surface in Figure 4.20 indicates a brittle fatigue striation failure. Next, the interior matrix and fiber cracks will be discussed under the microscopy section.

Fiber and Matrix Damage - Microscopy

As described in Chapter III, Figure 3.5 illustrated the two views typical of the micrography of the sectioned samples. As shown, one view is an edge view, looking from inside to outside (view #2), while the other typical view (view #3) shows a layer of the longitudinal fibers obtained by removing the material covering the fibers. View #2

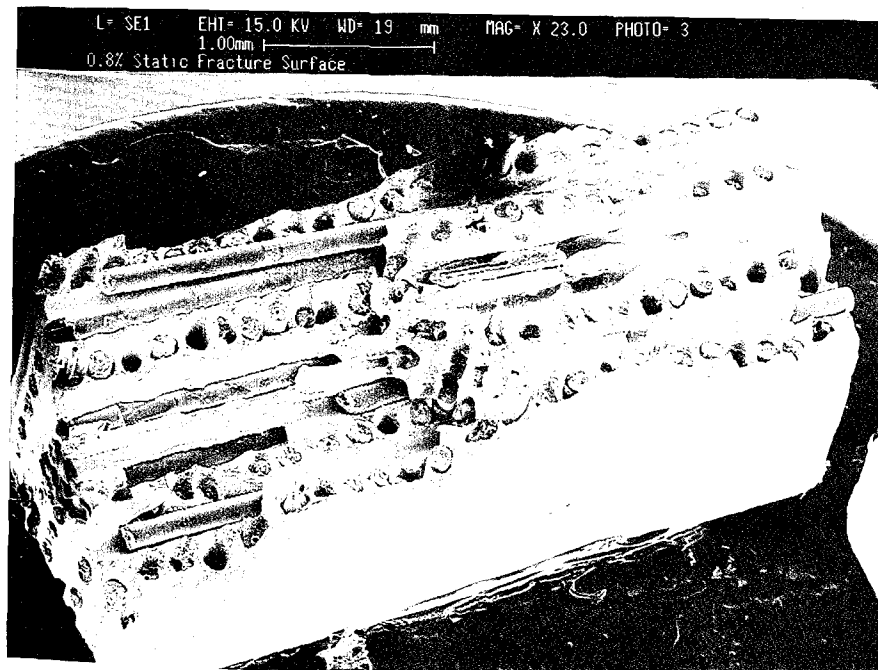
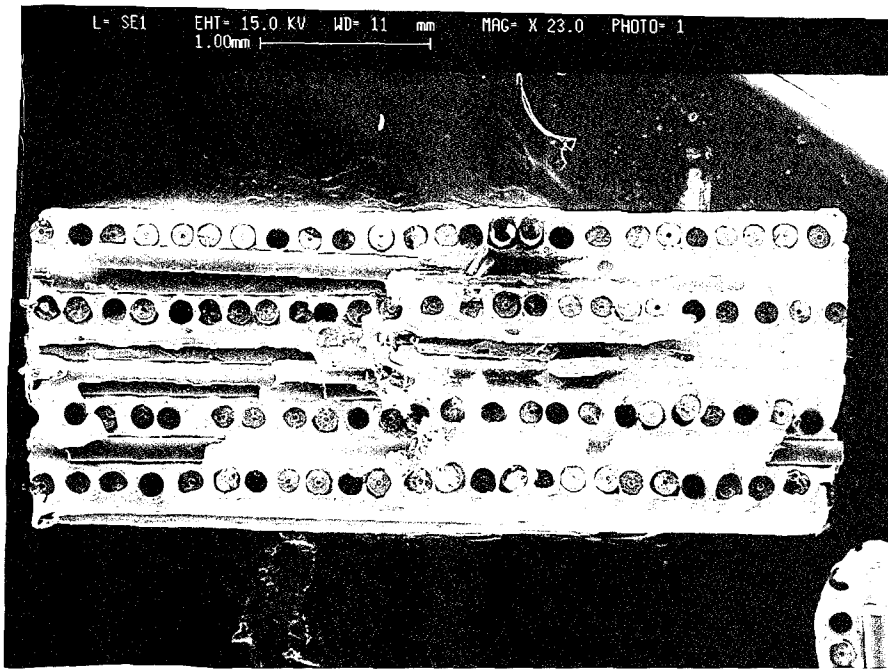


Figure 4.13: Fracture Surface, 0.8%

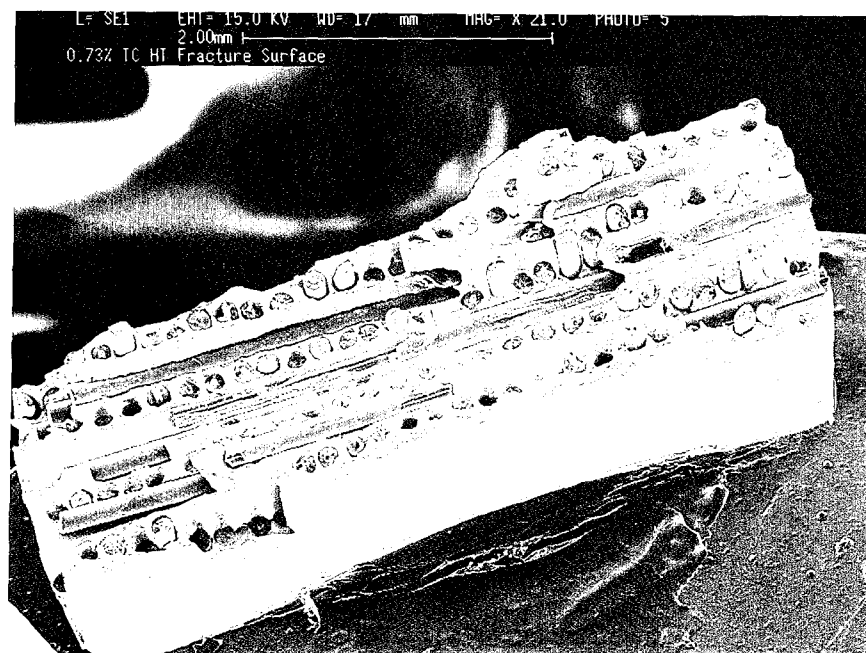
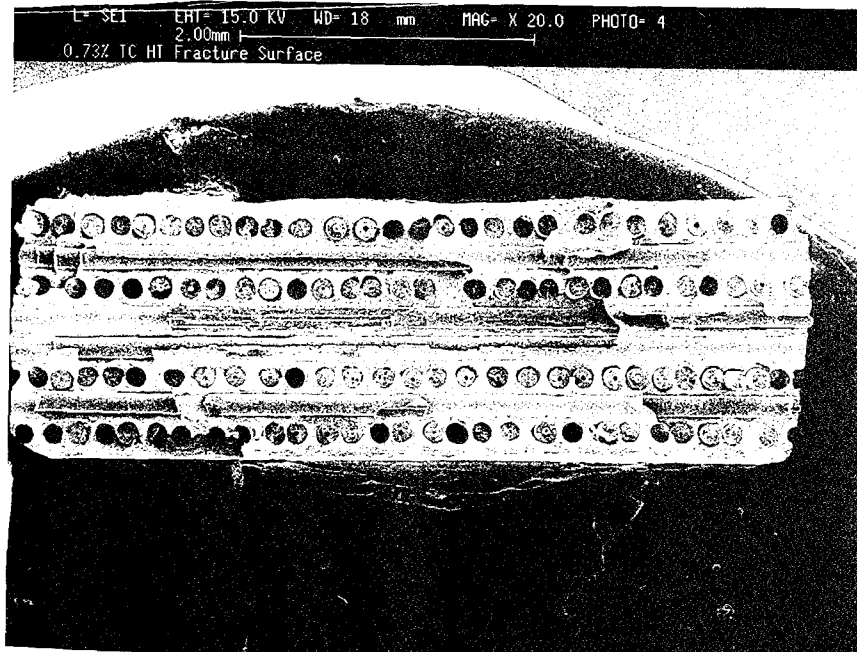


Figure 4.14: Fracture Surface, 0.73%

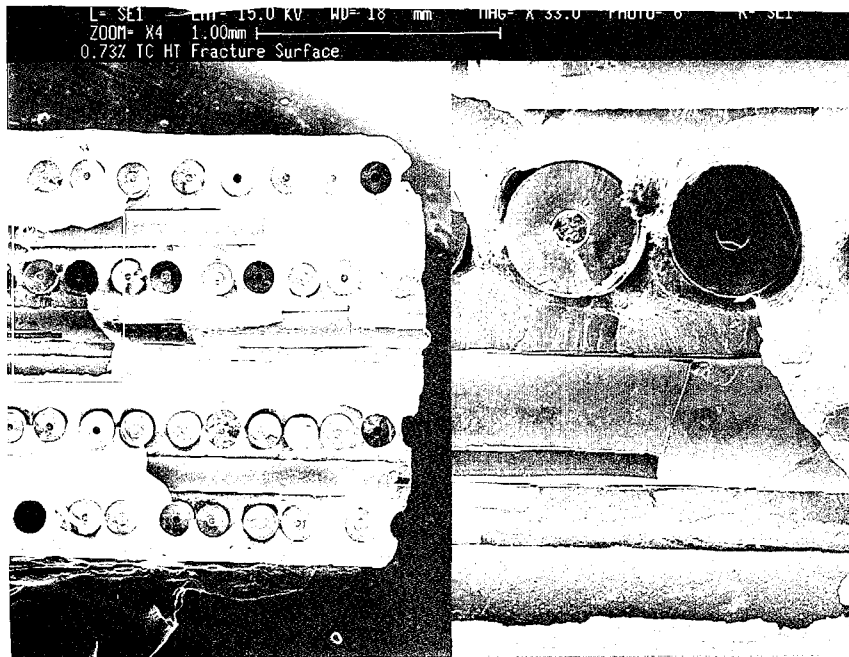


Figure 4.15: Fracture Surface Close-up, Mixed Mode (0.73%)

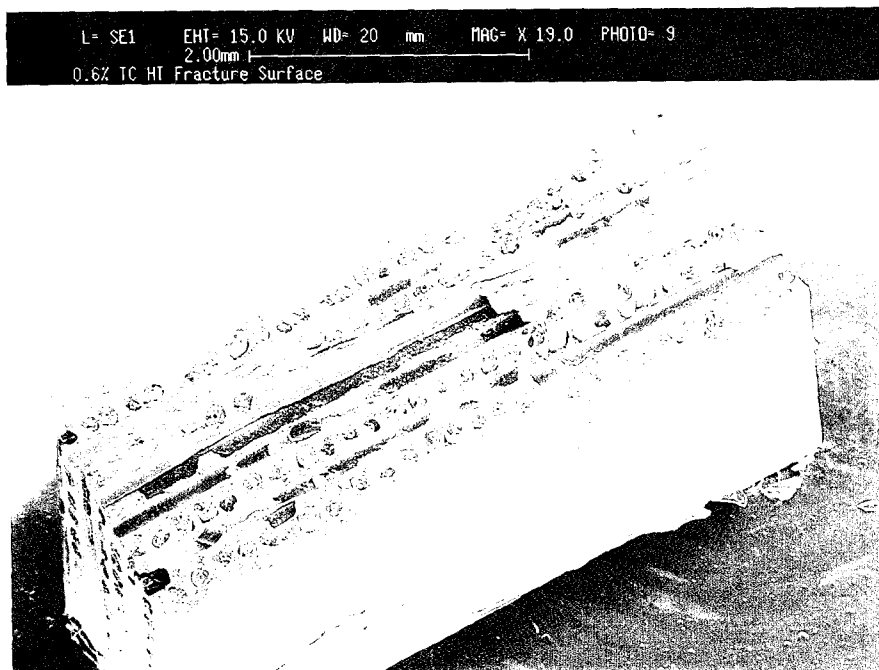
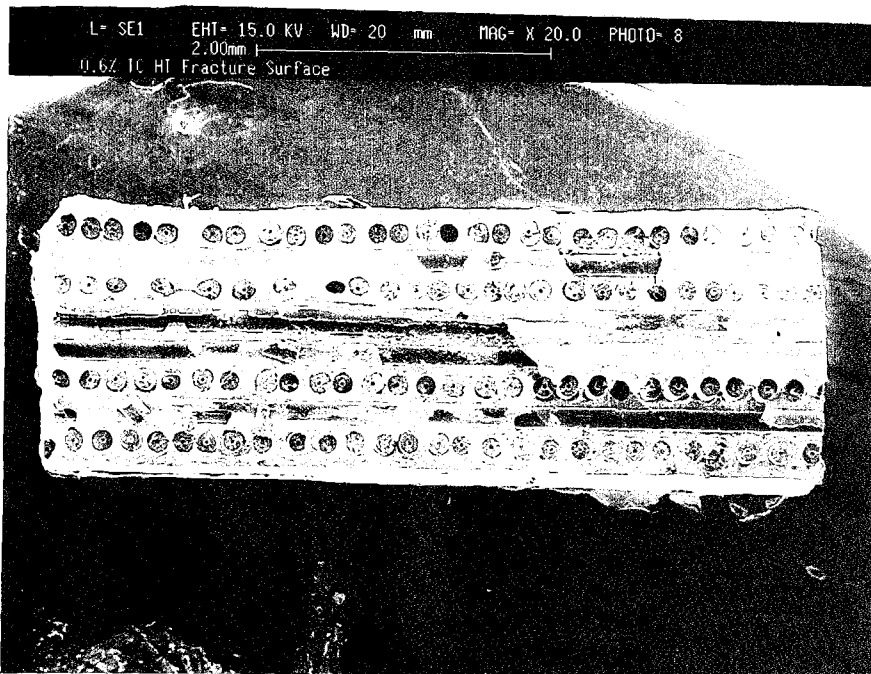


Figure 4.16: Fracture Surface, 0.6%

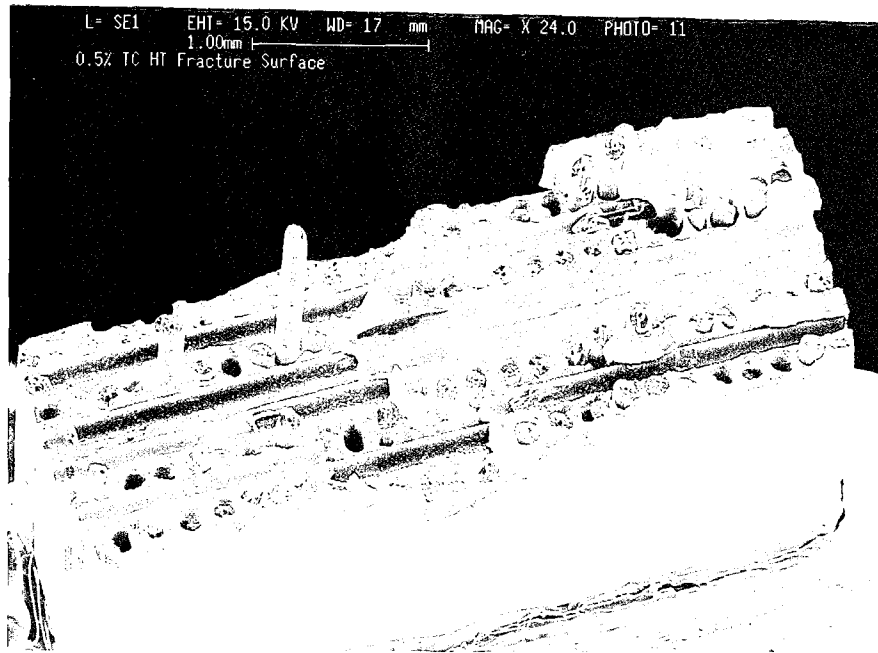
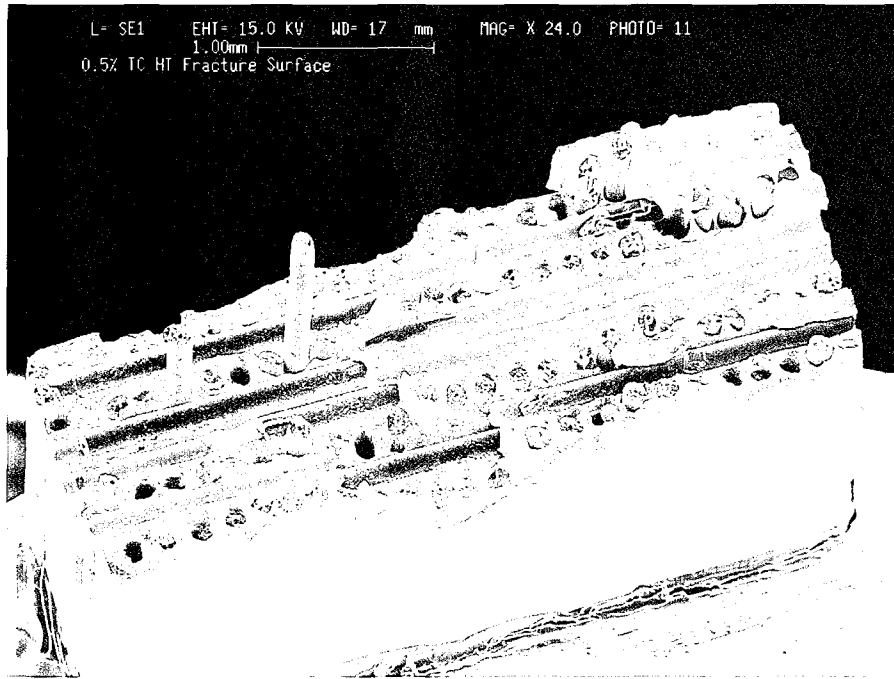
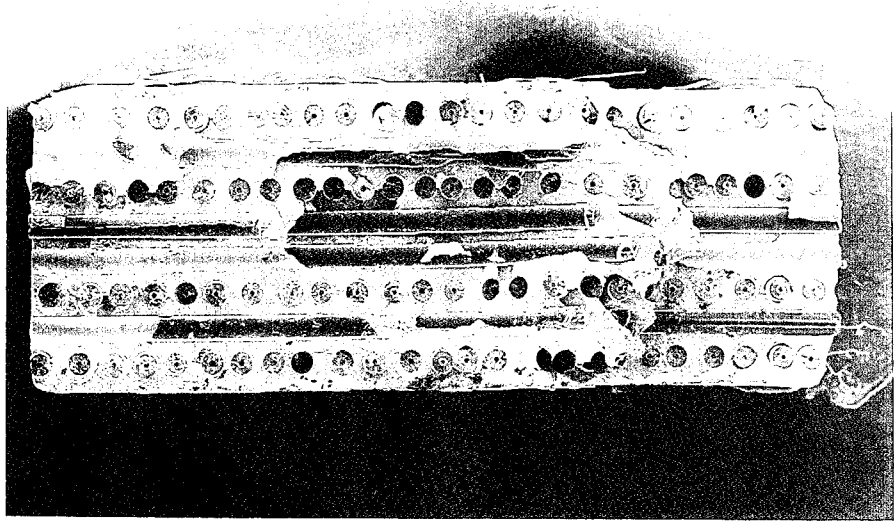


Figure 4.17: Fracture Surface, 0.5%

L= SE1 EHT= 15.0 KV WD= 17 mm MAG= X 22.0 PHOTO= 13
1.00mm
0.4% TC HT Fracture Surface



L= SE1 EHT= 15.0 KV WD= 18 mm MAG= X 20.0 PHOTO= 14
2.00mm
0.4% TC HT Fracture Surface

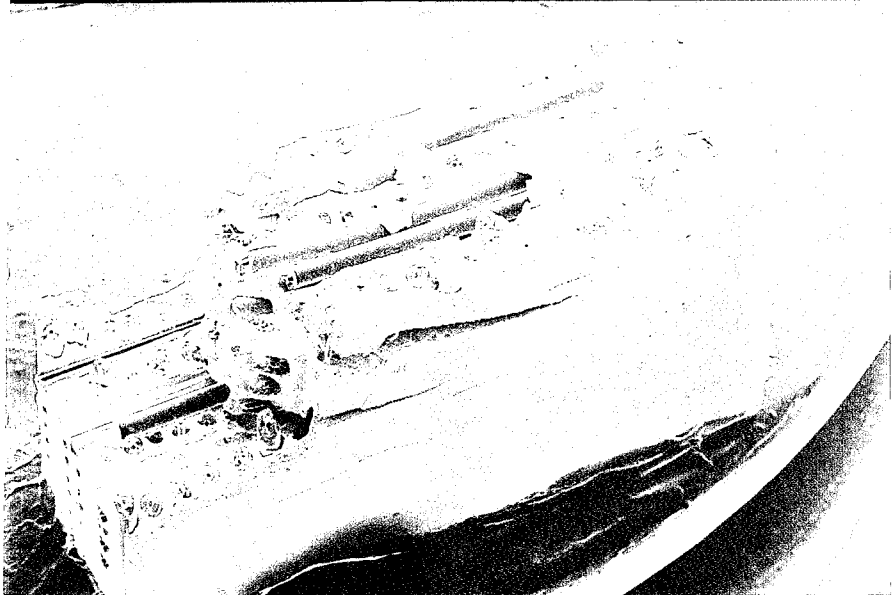


Figure 4.18: Fracture Surface, 0.4%

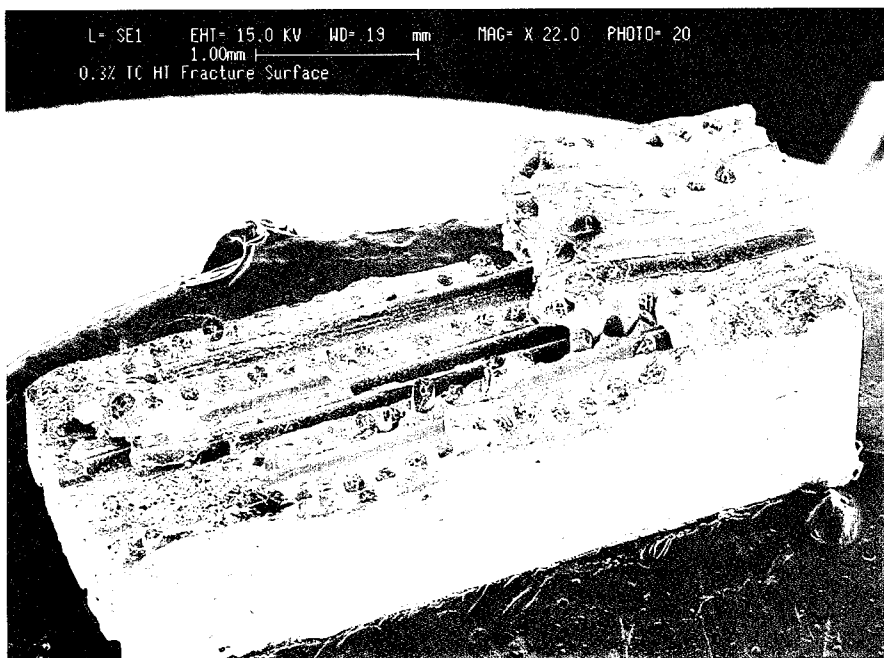
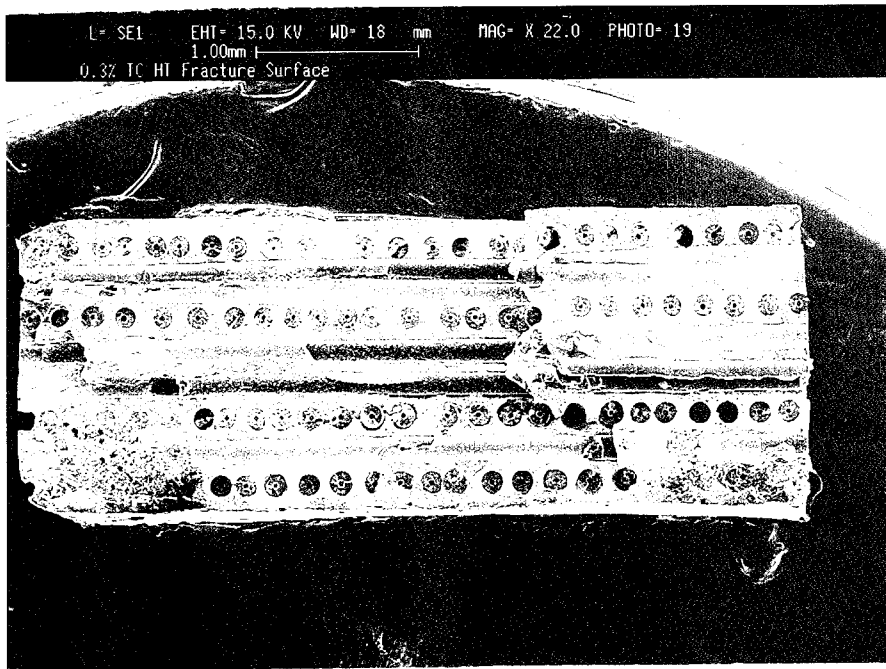


Figure 4.19: Fracture Surface, 0.3%

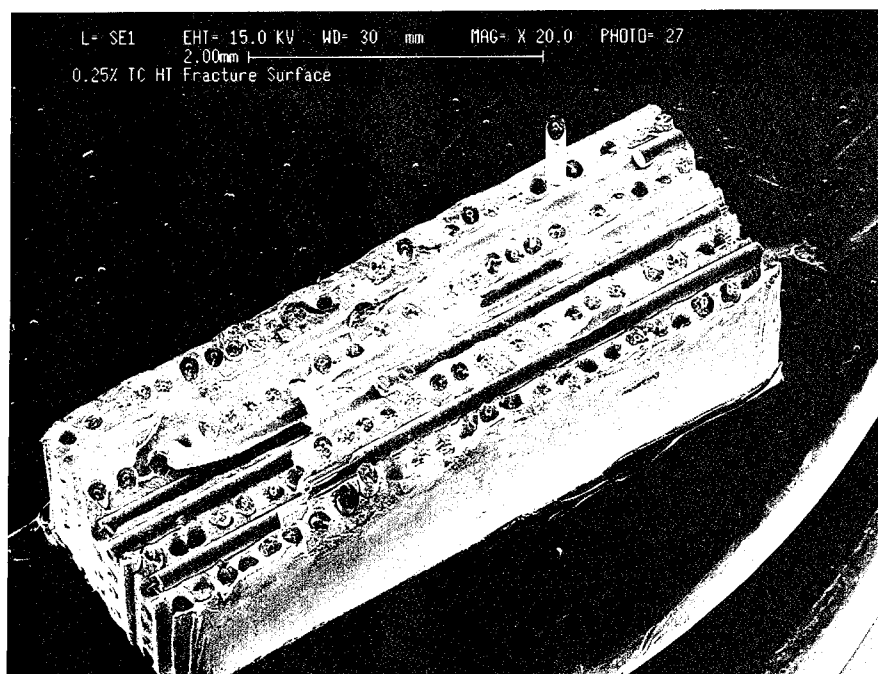
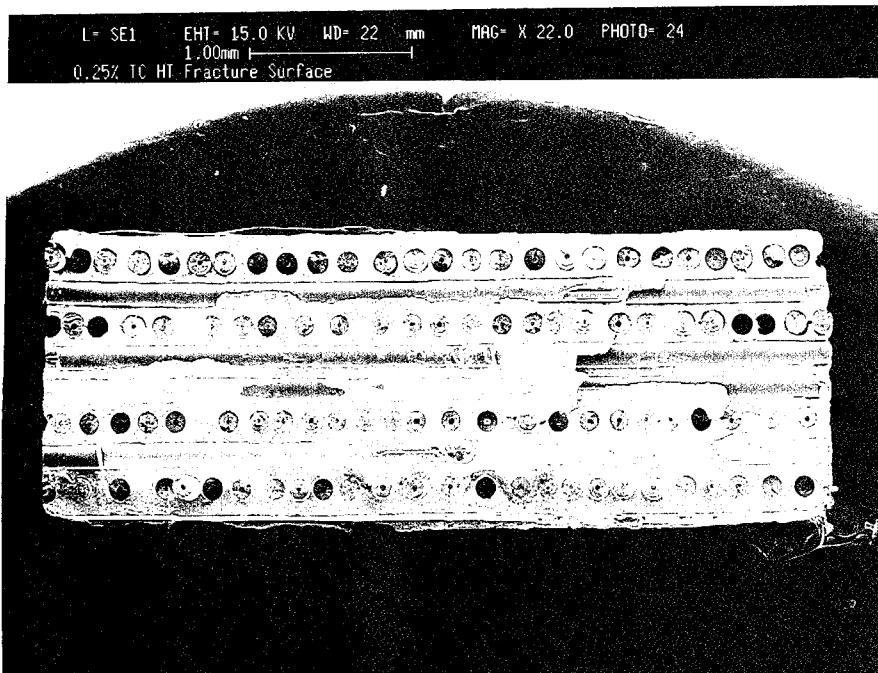


Figure 4.20: Fracture Surface, 0.25%

permits simultaneous observation of the longitudinal and transverse fibers, with their interactions, while view #3 shows longitudinal fiber and matrix damage and interaction.

Region I - Fiber Dominated Failure Mode

For comparison, the monotonic tension test (0.8%) was sectioned and examined. Figure 4.21 shows that longitudinal fibers were cracked and no matrix cracking was evident, although longitudinal and transverse debonding was observed. The above evidence follows fiber dominated failure characteristics.

Region IIa - Mixed Fiber and Matrix Failure Modes

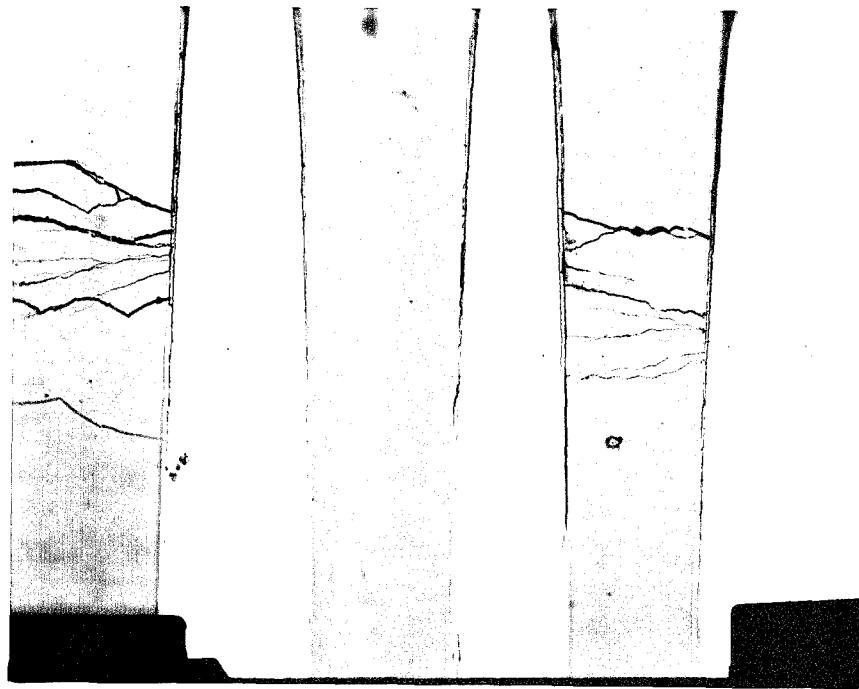
The presence of matrix cracks, along with longitudinal fiber crack evidence, defined the transition to the Region IIa subregion. Figure 4.15 showed a typical fracture surface close-up for a specimen that exhibited a mixed mode, but close to a fiber dominated failure mode. This particular case was for a specimen subjected to fatigue with a maximum strain of 0.73%. The void coalescence is predominant over the fracture surface. A close-up of view #2, Figure 4.22, demonstrates 90° fiber radial cracks typical of many such fibers in the subject view. Figure 4.23, with view #3, did not show the amount of fiber cracking expected to be revealed, although evidence of a longitudinal fiber with a crack was present. Noteworthy is the very small amount of matrix cracking. It is deduced

that the sections of view #2 simply did not capture the extensive fiber break region. Evidently significant fiber breaks were not present in this particular specimen.

Figures 4.24 shows the 0.6% test view #3, illustrating the longitudinal fiber cracks present. Additionally, Figures 4.25 and 4.26 reveal view #2 with both matrix and fiber cracking. This physical evidence supports the mechanical response trends as previously noted. The matrix cracking present, although not significant, played a role in reducing the modulus response.

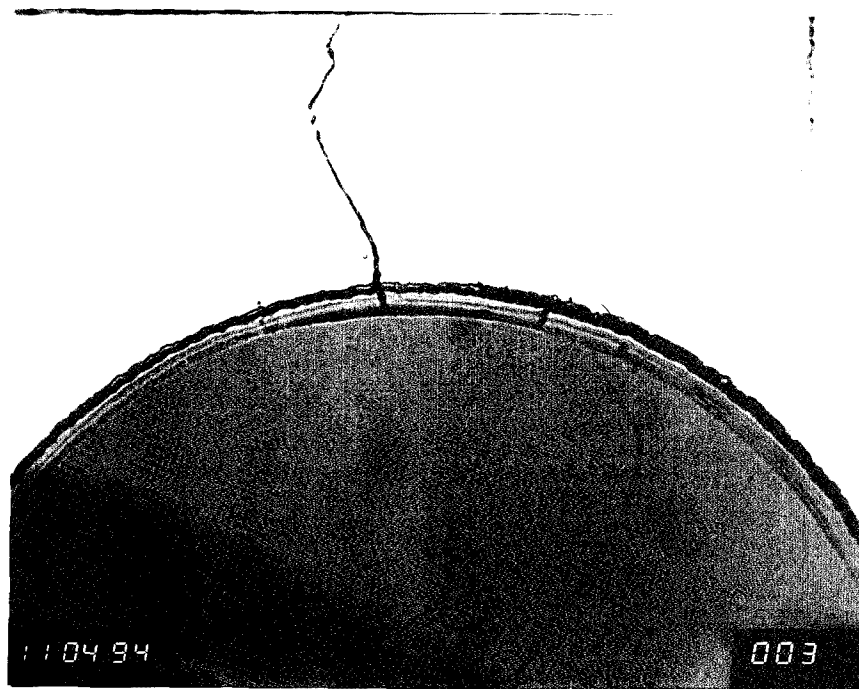
Region IIb - Matrix Dominated Failure Mode

The distinguishing characteristic separating Region IIa from IIb was the transition from mixed failure modes to the matrix damage dominated failure mode. Additionally, no 0° fiber cracks were observed, while the matrix crack density increased substantially as compared to the Region IIa specimen micrography. Figure 4.27 provides the close-up of fracture surface fractography illustrating the fatigue striations. Earlier, Figure 4.18 showed the multi-level fracture surface of the 0.4% specimen; as discussed, the multiple levels perhaps were the result of extensive matrix crack coalescence. Additionally, Figure 4.28 shows view #2 revealing a high matrix crack density and no longitudinal fiber cracks. Supporting this is Figure 4.29, also disclosing numerous matrix cracks with no 0° fiber breaks.



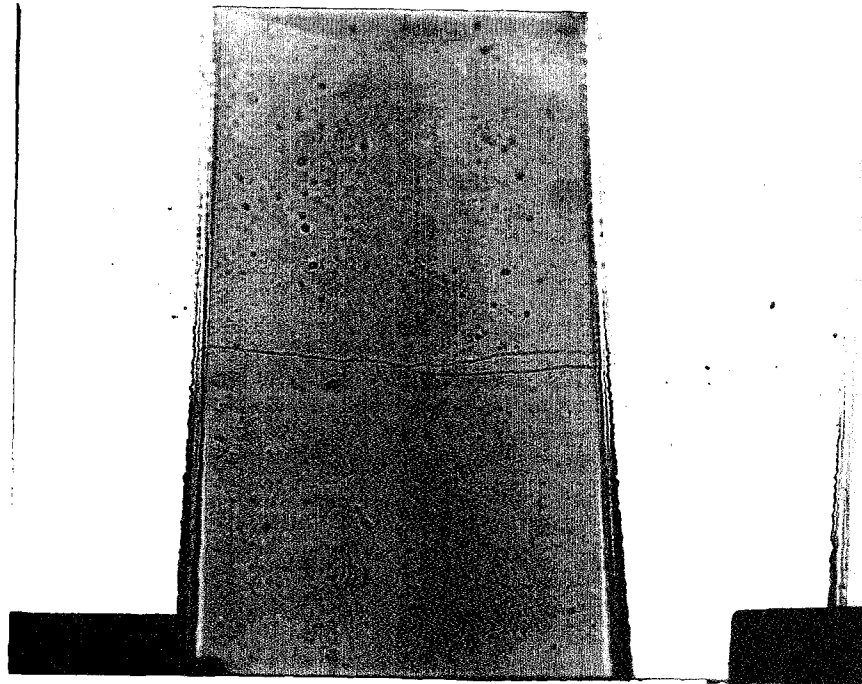
Loading Direction: \updownarrow

Figure 4.21: Longitudinal Fiber Cracks, 0.8% (200X)



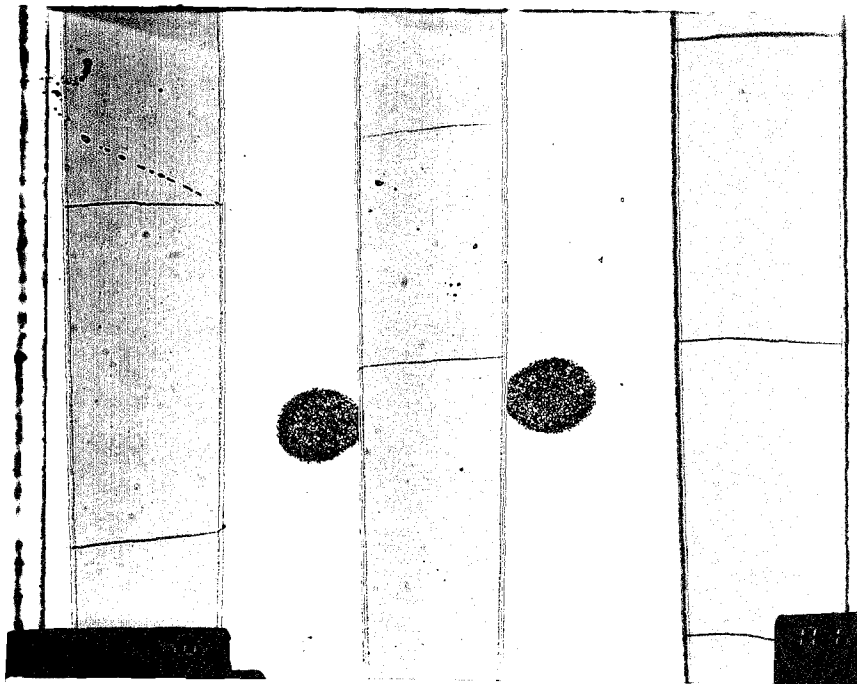
Loading Direction: \longleftrightarrow

Figure 4.22: 90° Radial Crack, View #2, 0.73% (1000X)



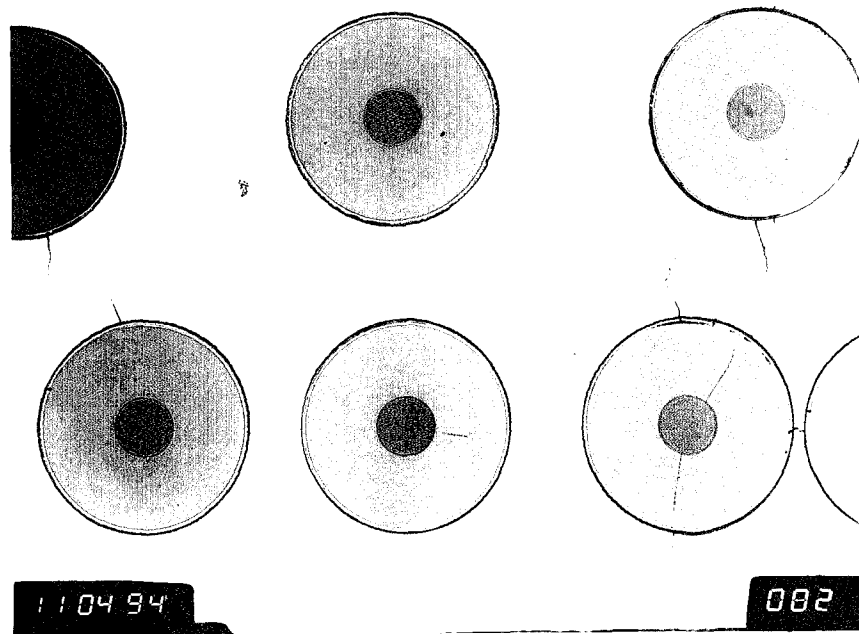
Loading Direction: \updownarrow

Figure 4.23: 0° Fibers, View #3, 0.73% (500X)



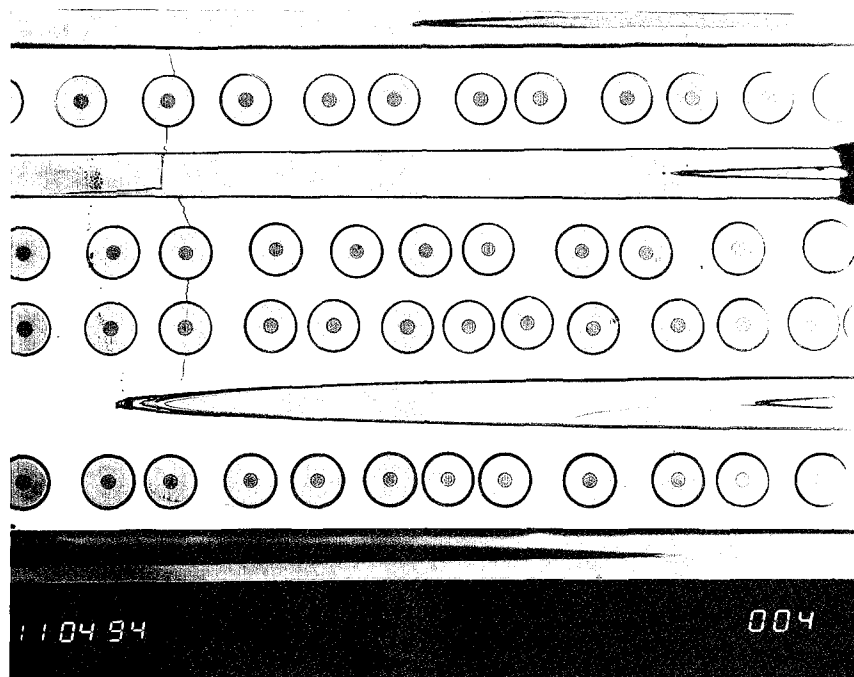
Loading Direction: \updownarrow

Figure 4.24: 0° Fibers, View #3, 0.6% (200X)



Loading Direction: \longleftrightarrow

Figure 4.25: Fiber & Matrix Cracks, View #2, 0.6% (200X)



Loading Direction: \longleftrightarrow

Figure 4.26: Matrix and Fiber Cracks, View #2, 0.6% (50X)

This evidence corresponds to the mechanical response trends discussed earlier for this specimen. To better understand the matrix dominated failures, an interrupted test at the 0.4% maximum strain level was performed, and is discussed next.

0.4% Interrupted Experiment

The primary reason to run an interrupted test was to obtain a better understanding of when substantial matrix cracking begins to propagate throughout the specimen. An interrupted test means that the test was stopped before specimen failure. In this case, the test was stopped at 4000 cycles, at the onset of a modulus decrease. This allows the examination of the sectioned specimen to determine how much matrix cracking had accumulated by that point. Figure 4.30 shows a few layer to layer bridged cracks, the worst damage observed in the interrupted specimen micrography. Figures 4.31 and 4.32 show a few fiber-matrix reaction zone cracks and two minor matrix cracks, but no other damage. Other sections reveal damage less than mentioned above. Again, no longitudinal fibers were observed to be broken, reverifying the matrix dominated region conclusion.

The information from both the 0.4% and 0.4% interrupted tests can provide an insight and support conclusions about crack initiation and progression for the matrix dominated failure. The history of the damage progression is as

follows. As Figure 4.30 shows, the damage initiated at the 90° fiber-matrix interfaces. The cracks then grew in number and length, progressing to the 0° fibers. This provided a pathway for oxygen to the 0° fibers. Additionally during this time some surface cracks may have developed, progressed, and provided even more direct oxygen to the fibers. The 0° fibers began oxidizing near the cracks, thus weakening the fibers, setting up the final fiber failure. Figure 4.18 showed this extensive cracking state after the specimen failure.

Summary - Fractography and Micromechanical Results

The previous fractography and micrographical results provide the physical evidence supporting the damage mechanisms which were deduced from the typical mechanical responses. First, overall fracture surfaces were shown to observe the trend of decreasing ductile failure and necking corresponding to decreasing maximum applied strain. Then the monotonic tension test micrography was observed for a limiting case comparison. Next, typical specimen micrography of the three failure mode regions I, IIa, and IIb were presented and discussed. Finally, the micrography results of the interrupted test (0.4%) were presented, showing that the matrix cracking was not extensive up to 4000 cycles.

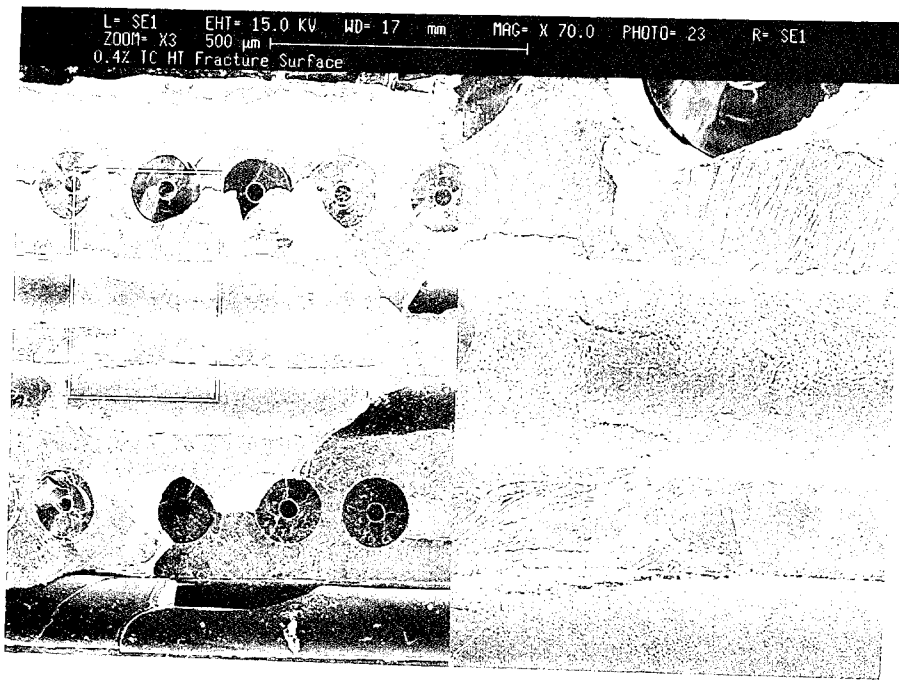
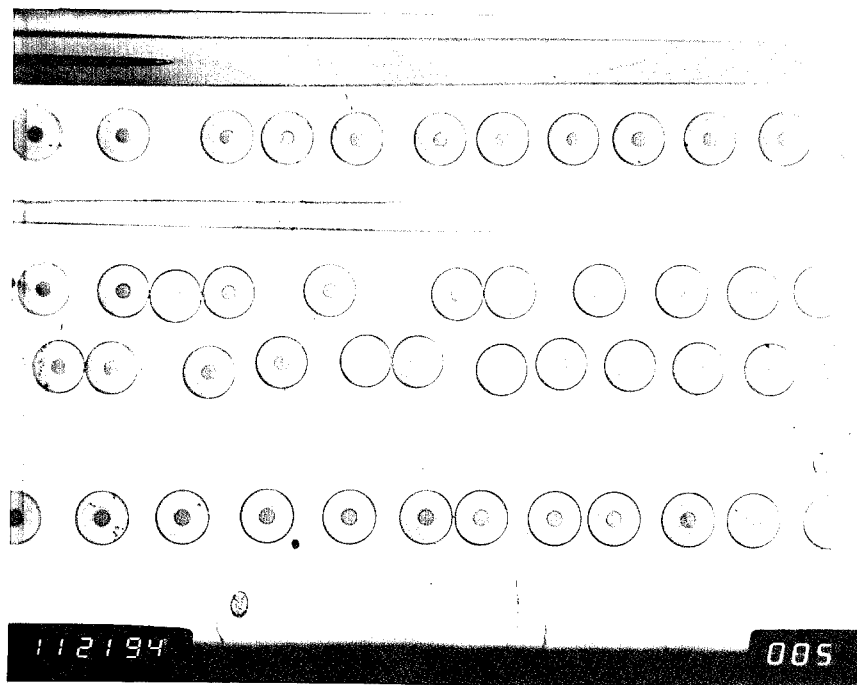
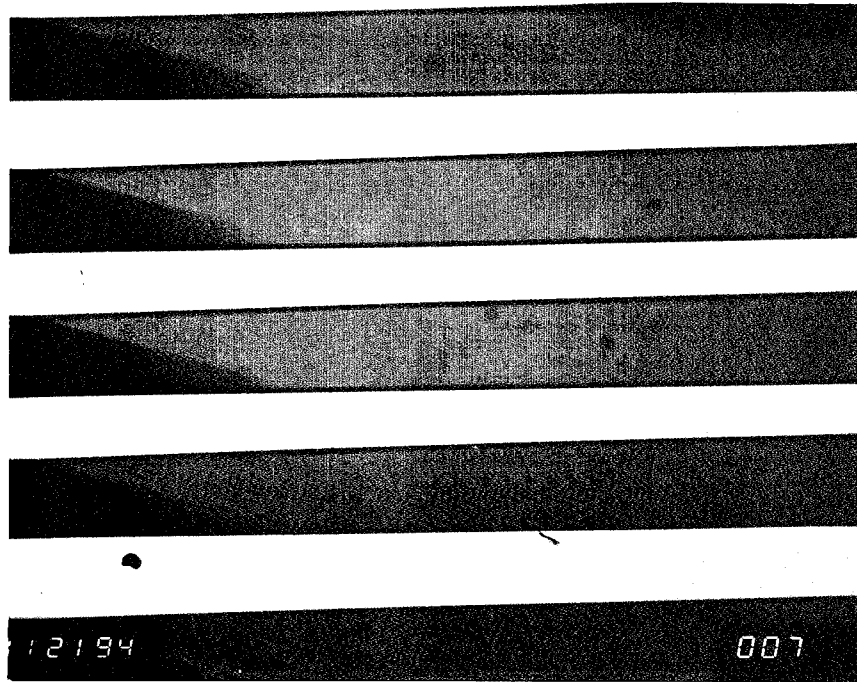


Figure 4.27: Striations, Fracture Surface Close-up, 0.4%



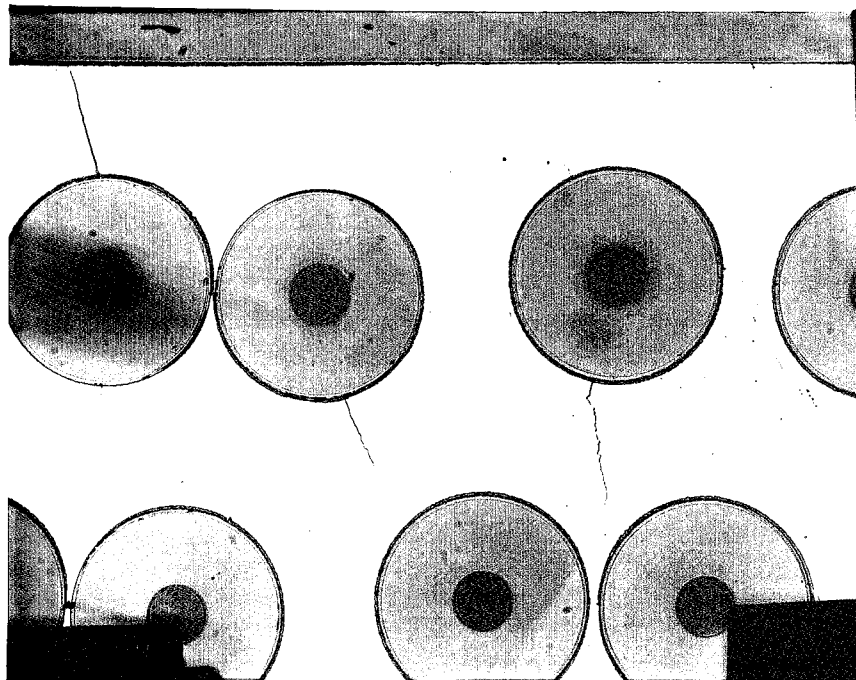
Loading Direction: \longleftrightarrow

Figure 4.28: Numerous Cracks, View #2, 0.4% (50X)



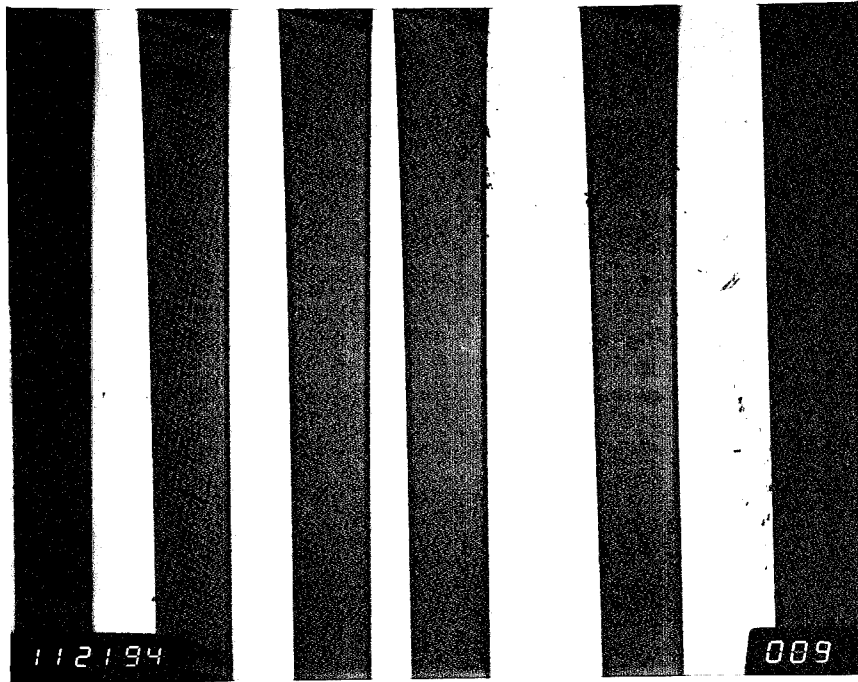
Loading Direction: \longleftrightarrow

Figure 4.29: Numerous Cracks, View #3, 0.4% (100X)



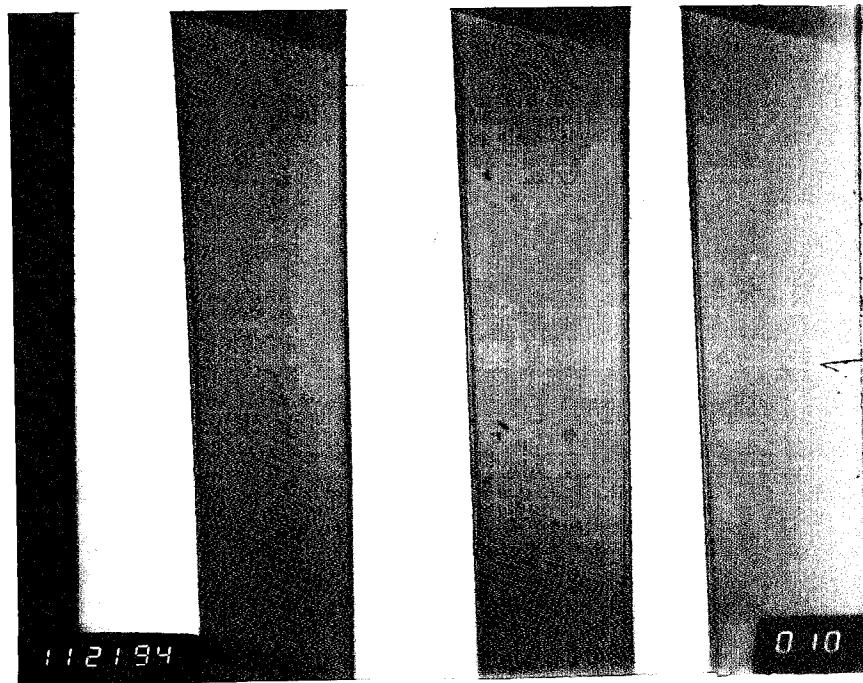
Loading Direction: \longleftrightarrow

Figure 4.30: Matrix Cracks, View #2, 0.4%I (200X)



Loading Direction: \updownarrow

Figure 4.31: 0° Fibers, View #3, 0.4%I (100X)



Loading Direction: \updownarrow

Figure 4.32: 0° Fibers, View #3, 0.4%I (200X)

V. Fatigue Life Analysis and Comparisons

The previous chapters focused on discussing the background, procedure, and results from the fatigue tests. In this chapter, discussion and analysis of the fatigue life measured from the experiments will be presented, along with comparisons to previous investigations. Maximum applied stress or strain are typical variables for comparison of fatigue data, but not the only ones used.

Direct comparisons of fatigue data are not always possible because test variables of experiments often differ. Varying the R ratios or control modes complicates proper comparisons. For example, the best comparison basis between a tension-tension fatigue test ($R=0.1$) with a tension compression case ($R=-1$) is not well defined. If both tests have the same maximum applied load/strain, then comparing on a maximum stress or strain basis would effectively ignore the compressive portions of the fatigue.

The control mode of a test also influences the data gathered. Under the load control mode, maximum and minimum strain, and strain range are monitored, while maximum and minimum stresses are held constant. Conversely, under strain control mode, the variables are reversed with the maximum and minimum stress being monitored, with maximum and minimum strain being held constant. This study primarily will make comparisons of fatigue data utilizing the

effective strain basis. Other fatigue data variables will be also used. For example, presentation of fatigue data utilizing maximum applied strain vs. cycles is discussed.

To circumvent previous comparison problems, some studies present data and make comparisons using various criteria. Utilizing the range of stress or strain provides a method of comparing experimental results from tests with different R ratios. The benefit is that the applied stress/strain range indirectly includes the compression loading, if present, in the data compared. As can be seen, no definitive comparison method has been found. Thus, the comparison base must be used with caution and good judgment.

Also of interest is the effective strain range versus fatigue life. The effective strain range is defined as 1/2 of the strain range for fully reversed loading, or the maximum strain for tension loading only. For strain controlled case with $R=-1$, the effective strain range is the same as the maximum or minimum applied strain. For work under the load controlled mode, this is not the case. Boyum [3] used this fatigue comparison basis with good results. But, before making comparisons of fatigue data, the fatigue life curve resulting from the current work will be presented. Then dominant failure modes from the study will be discussed in more detail.

Fatigue Life Curves - Current Work

Seven fully reversed fatigue tests were accomplished in this investigation. Figures 5.1 and 5.2 show the fatigue life based on a maximum strain and a maximum stress respectively. The maximum stress was measured near the mid-life of the specimen where a relatively steady response of stresses was observed. The abscissa is typical of fatigue plots, representing the number of fatigue cycles plotted on a logarithmic scale.

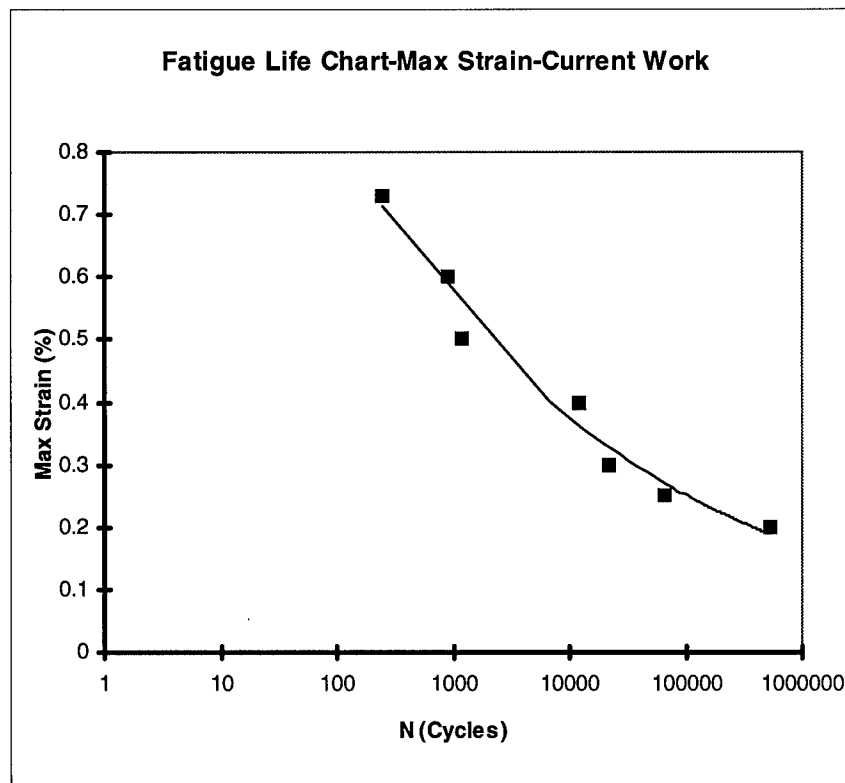


Figure 5.1: Fatigue Life Curve - Max Strain

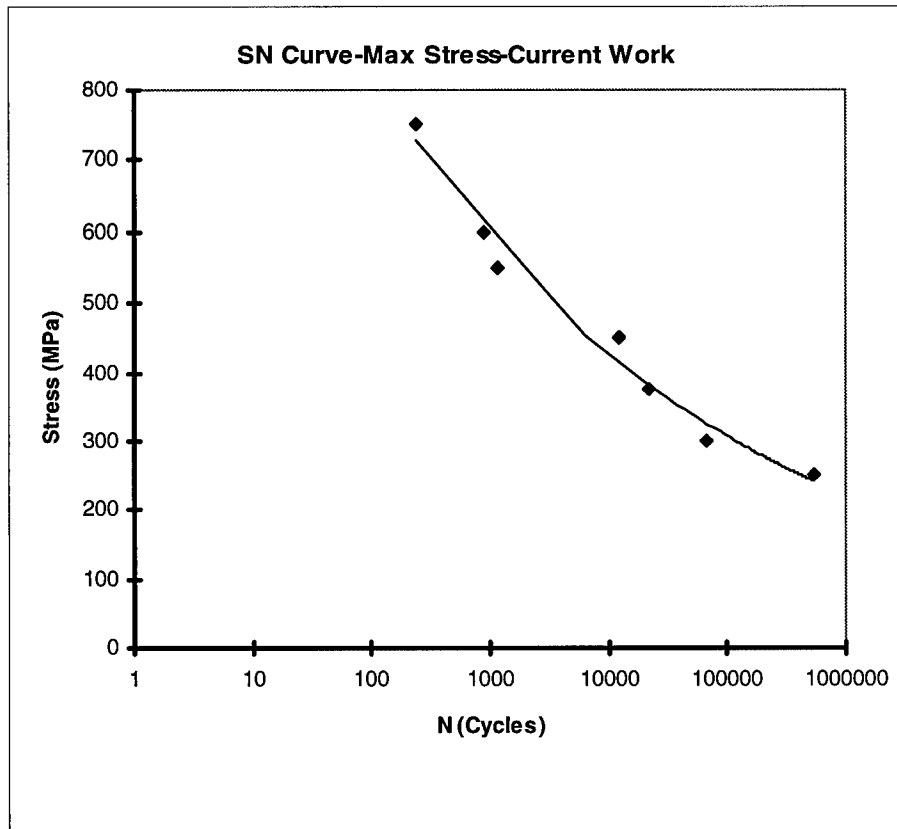


Figure 5.2: Fatigue Life Curve - Max Stress

The ordinate is the maximum strain or stress on a linear scale. The trend is also typical with its general negative slope, indicating that an increase in maximum loading results in a decrease in fatigue life.

Figures 5.3 and 5.4 present the fatigue life results in terms of different variables, strain range and steady state stress range, respectively. The plots are again somewhat typical of MMC's in their general trend. The data follows a relatively smooth decreasing trend with good correlation. Thus it appears that the fatigue data of the current work

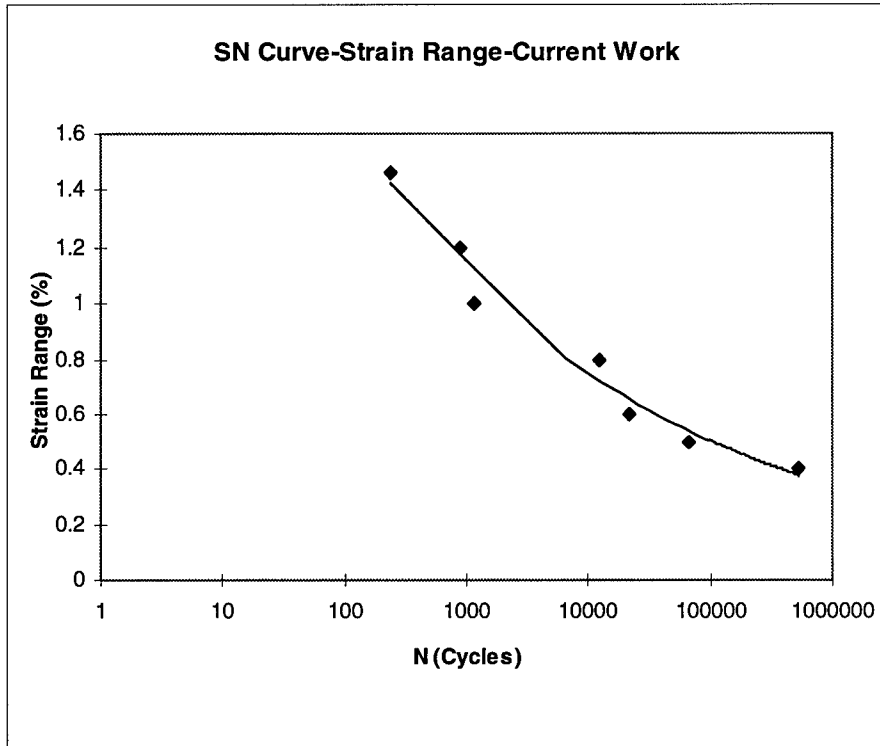


Figure 5.3: Fatigue Life Curve - Strain Range

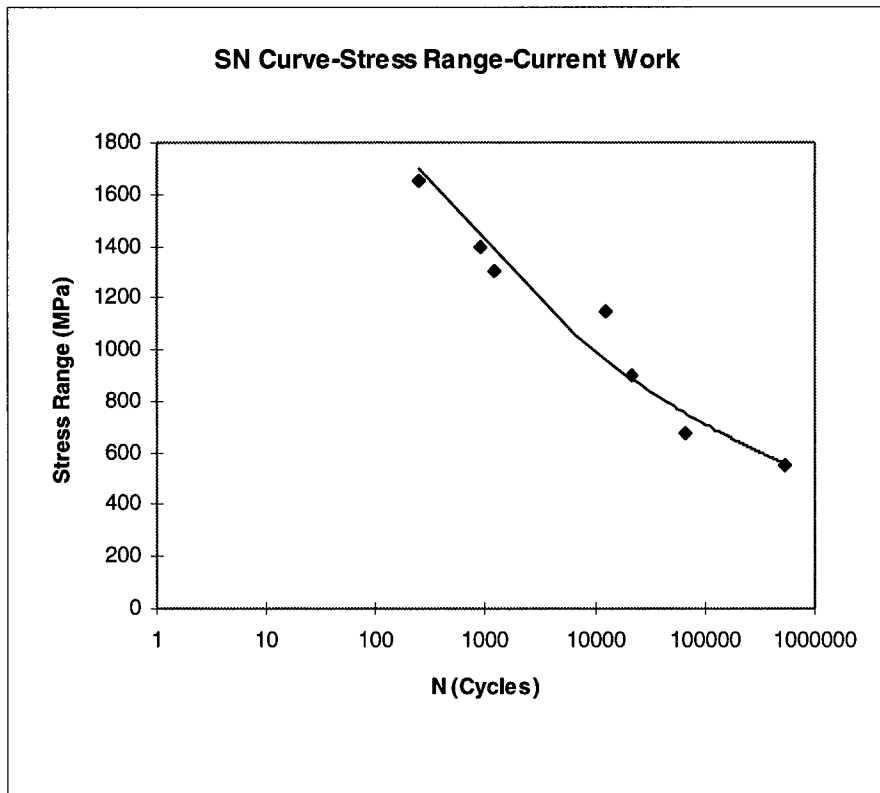


Figure 5.4: Fatigue Life Curve - Stress Range

may be adequately represented on any of the above mentioned basis. It has been observed that this is not true in general, as will be shown on the maximum strain basis comparisons.

Discussion of Dominant Failure Modes

The idea of grouping composite fatigue specimens into fatigue life curve (S-N) regions corresponding to dominant failure mode was suggested by Talreja[27]. This technique shows the relationship between the dominant failure mode of a material and the maximum stress or maximum strain. Previous MMC studies divided the S-N curve into 3 regions[9]: 1) Region I - Fiber Dominated; 2) Region II - Matrix Dominated; and 3) Region III - Matrix Fatigue Limit. The same partitioning can be used in this study. Further, the evidence observed from the current work indicated a need for a subdivision of Region II into Region IIa - Mixed Mode Dominated Failure, and Region IIb - Matrix Dominated. A similar need to subdivide Region II into subregions was presented in the $[0/90]_{2s}$ work by Boyum [3]. The monotonic tension test showing a maximum $\epsilon=0.8\%$ was discussed in Chapter IV as a upper limit or boundary for fiber dominated failure.

Figures 5.5 and 5.6 show the same information as Figs 5.1 and 5.2 but dividing the graphs into the regions of

dominant failure modes. The divisions were determined both by macroscopic response and by microscopic evidence. The previously stated criteria of dominant failure modes was applied. The Region III matrix fatigue limit was estimated because all current specimens failed. Sanders [23] estimated the maximum strain of Region III for the unidirectional 90° layup to be 0.05%. This appears to be a reasonable and conservative estimate because the crossply composite has the relatively stronger 0° layers present.

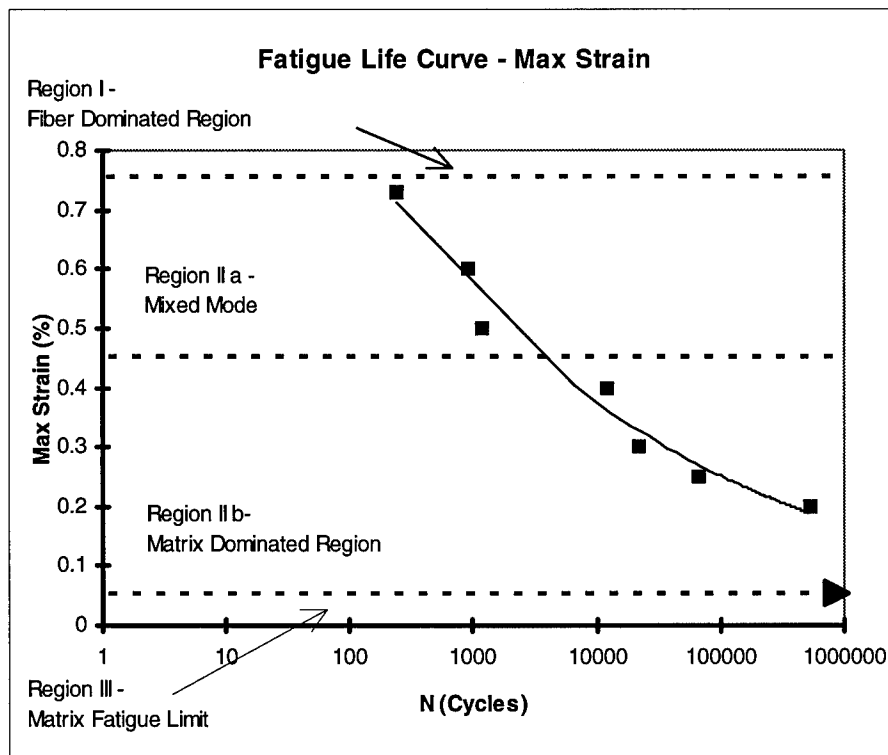


Figure 5.5: Partitioned Maximum Strain Fatigue Curve

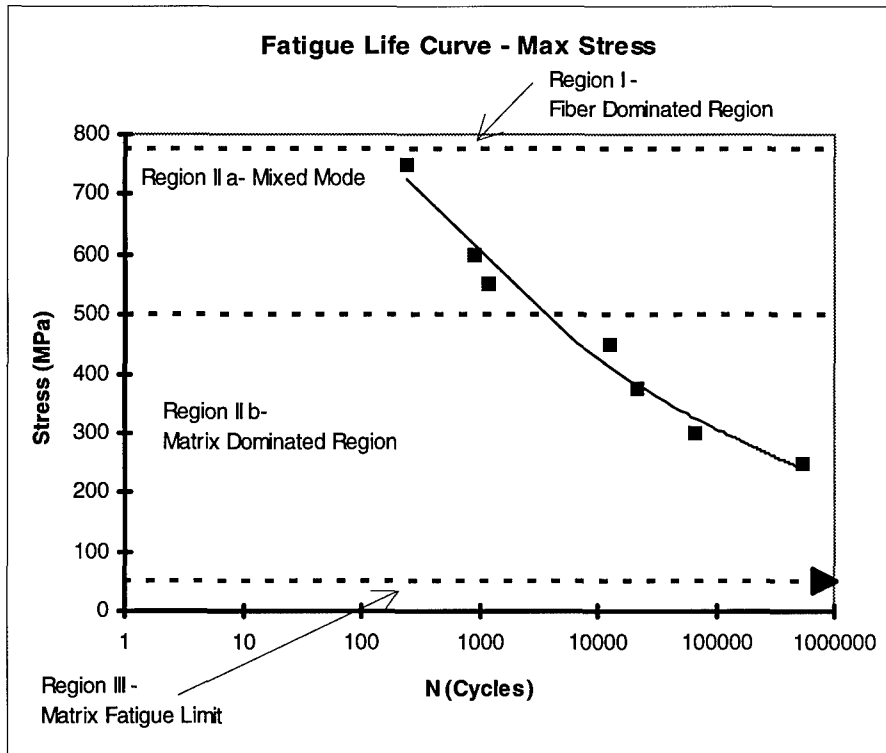


Figure 5.6: Partitioned Maximum Stress Fatigue Curve

Region II was further divided into Regions IIa and IIb. Region IIa is a region where longitudinal fiber breakage and matrix cracking were both observed, thus implying that the failure mode was mixed since both modes were present. Region IIb, where fiber bridging was observed, is the matrix dominated failure region. No broken longitudinal fibers were present, and matrix cracking had increased substantially. The number and length of matrix cracks in this region had increased from the Region IIa tests, as can be observed from Figures 4.26 and 4.28.

Comparisons To Previous MMC Fatigue Work

To this point, the fatigue life results of only this work have been presented. Next, this work will be compared to the results of other studies, including Boyum, Gabb and Gayda, Lerch and Halford, and Sanders[3, 7, 14, 23]. As stated before, differing test conditions present a comparison challenge, but methods discussed earlier will be used to present the results.

The first figure, Fig 5.7, compares, utilizing a maximum strain basis, the current work with the previous works that used the same composite materials, layup, and fully reversed loading. The other tests[3] differed by having been accomplished utilizing the load control mode, instead of the strain control mode. Additionally, one of the fatigue data sets was performed at room temperature. As can be noted, the load control mode tests provide good comparison data sets since almost all test variables are the same, except for control mode and temperature. The data for the current study behaves as expected, following a well correlated trend. As can be seen, there exists a low correlation for some of the maximum strain data reported for the load control tests. Thus, the need for a better comparison basis is evident.

The next basis considered to compare the same data was to use the effective strain range basis as discussed earlier. Figure 5.8 plots the same tests as seen in

Fig 5.7, but using the new basis. Again the current data has a well correlated trend. However the data that was scattered in the last comparison is now well correlated and follows the same general trend as the current test data. Therefore, the effective strain range basis method appears to be a good method for comparing fully reversed strain controlled results with fully reversed load controlled results, all other variables being constant.

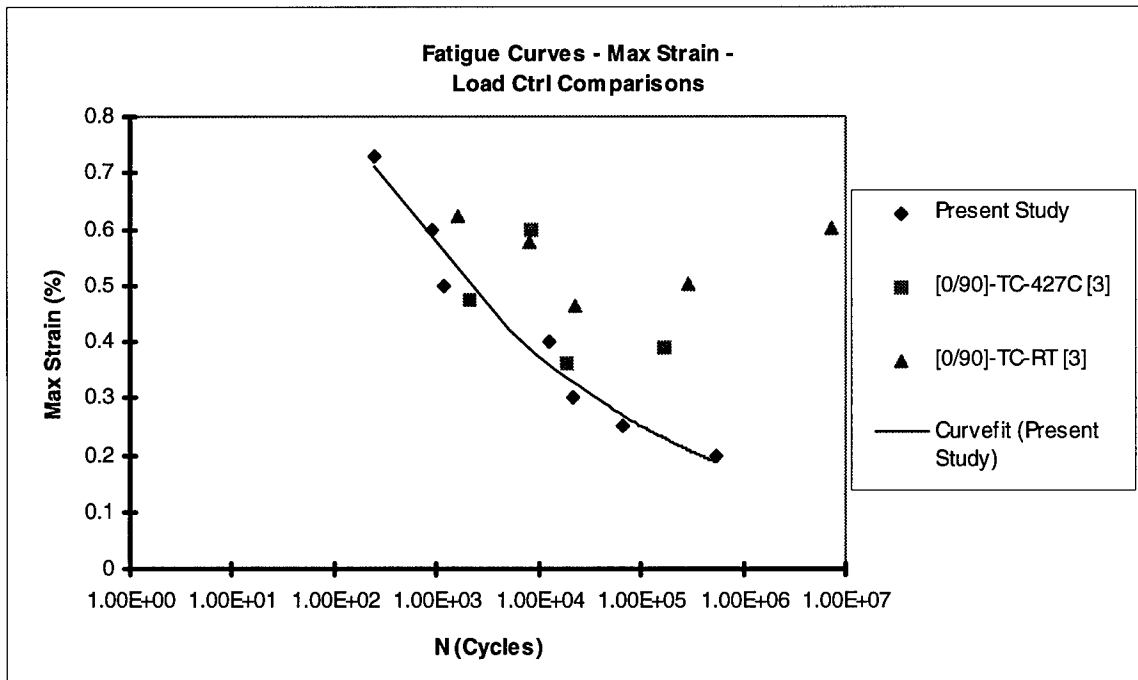


Figure 5.7: Maximum Strain Fatigue Curve - Strain Versus Load Control Comparison

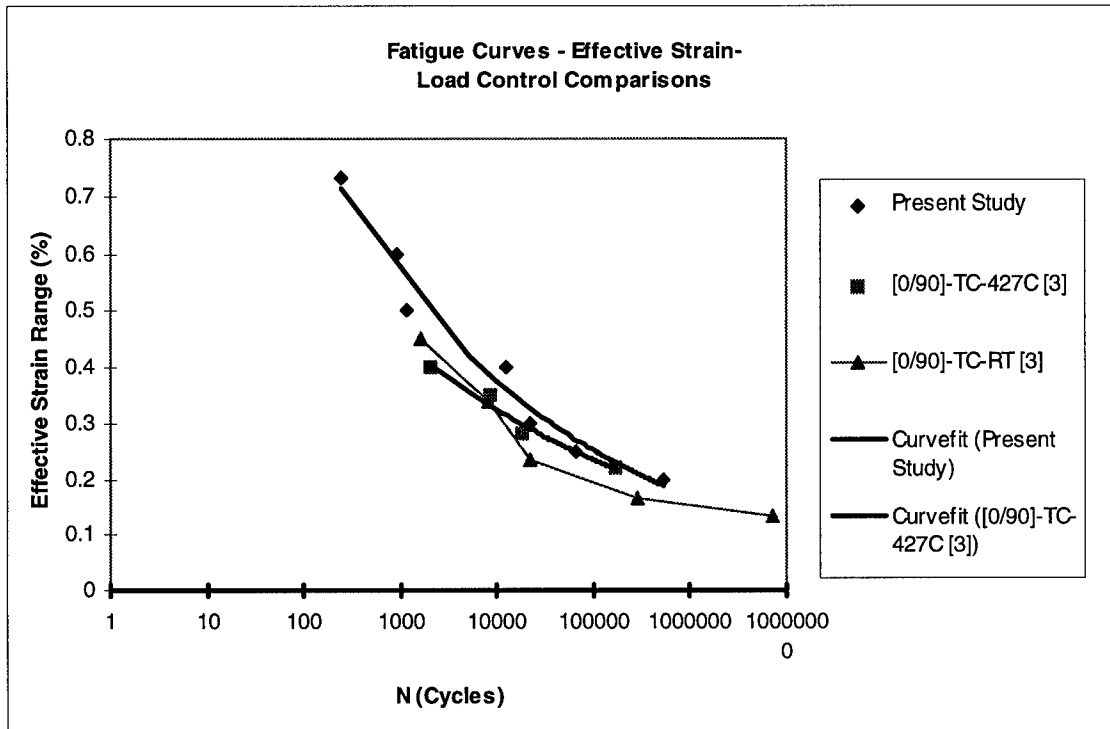


Figure 5.8: Effective Strain Range Fatigue Curve - Strain versus Load Control Comparison

A possible explanation for this behavior is as follows. For common strain controlled tests that utilize an $R=0$, 1, or -1, the effective strain range is the same as the maximum strain. However, for load controlled experiments this is not necessarily the situation. For example, notice the correlation change in the data for the load controlled tests in the two figures just discussed. For typical load controlled testing, maximum and minimum strain may increase much more than the strain range over the fatigue life. Creep and plasticity may account for a maximum strain shift without affecting the strain range (modulus). Therefore,

the maximum strain may not be indicative of the material fatigue characteristic, but the effective strain range may be. Thus as stated above, the effective strain range basis may be a good criteria for comparing load controlled fatigue results to strain controlled. Also of note is the trend of convergence with increasing fatigue cycles of the current work data and that of the [0/90] under load controlled mode. This suggests that in the matrix dominant failure regions, both load and strain control modes begin to provide similar fatigue lives for given effective strain loadings.

Fig 5.9 compares, utilizing an effective strain basis, the current work to other work using the same matrix material, but different layups components. A major change of parameter for the tests being compared in this figure was their all being run under the strain control mode as opposed to some tests being run under the load control mode in previous figures. The data for the current study again behaved as before, following a well correlated trend. Instead of all the tests being fully reversed as previously discussed, the R ratios vary among data sets for these comparisons. This figure shows that the current [0/90]_{2s} layup had a shorter fatigue life than for the room temperature fatigue life of the matrix alone, the 0° unidirectional composite, or the [±30] layups. However, the current crossply had a longer fatigue life than the 90°

unidirectional layup or the high temperature fatigue life of the matrix alone at lower strain values.

The effective strain range basis was used since most MMC strain controlled tests use typical R ratios of 0, 1, or -1, thus maximum strain and effective strain are the same. Although this basis was used, not all the data followed the same trend, but defined trends were observed for individual data sets. Since material composition, test temperature, R ratio, and other variables were not the uniform for all the studies, it is not surprising that all trends may not be correlated along the same curve.

Several factors may affect the differences. For example, the 90° composite has a very different fatigue response than the 0°, [\pm 30], or matrix specimens. This can be attributed to many factors, such as: stress concentrations from the fibers, damage occurring from compression loadings, or cracks and damage occurring and propagating from high stress or weak zones in the materials. Generally cross ply materials have shorter fatigue lives than unidirectional or monolithic materials. Angle ply materials fatigue lives usually fall in between the unidirectional 0° and 90° fatigue lives, and this trend can be observed in the comparison plot.

Another observation from the graph is the comparison of fatigue lives between the matrix alloy (high and room temperature) and the [0/90] crossply. For the 427° C matrix

data, the S-N curves from these cross each other. This states that for low cycle, high strain, high temperature situations, the matrix has the better fatigue resistance. Conversely, for low strain, high cycle situations the currently investigated material has the longer fatigue life. This can be attributed to the crack arresting nature of fiber composites and the presence of the strong 0° fibers with the associated high fracture toughness. The matrix material could possibly develop cracks that are not arrested, but allowed to grow to a critical crack length up to failure.

The only other fully reversed strain controlled study on the SiC/Ti-15-3 system was performed on the [± 30] composite. The fatigue life of this laminate was only slightly longer than the crossply, and a downward trend was noted in the higher fatigue cycle portion of the [± 30] curve. Since the fiber angle was closer to the loading direction than the transverse direction, perhaps the composite reacted in a manner more resembling that of a unidirectional composite than a cross ply with 90° fibers present. Because the [± 30] layup has only off-axis plies, there are no fibers to take the load axially. This stresses the weak fiber-matrix interfaces, initiating matrix cracking and further weakening the matrix.

Figure 5.10 presents the data of Figures 5.8 and 5.9 on the same plot in order to compare the two control modes. This allows all the data sets presented thus far to be observed on a single plot. An overall observation from Figure 5.10 is that both the matrix alloy and 0° specimens had longer fatigue lives than the cross ply composites. However, an exception was noted with the high temperature matrix alloy data. As discussed earlier, the trend fell with increasing fatigue. But of note is the fact that the failure criteria for the matrix was a 75% reduction in stress, as opposed to the typical failure definition of the specimen coming apart[23]. In another comparison, both the unidirectional 90° data and the high temperature matrix alloy data show a convergence for higher fatigue lives. This observation suggests that for lower loadings, the off-axis composite approaches the matrix alloy fatigue limit. Thus the presence of off-axis fibers for these cases impacts the higher loading fatigue lives more than lower loadings.

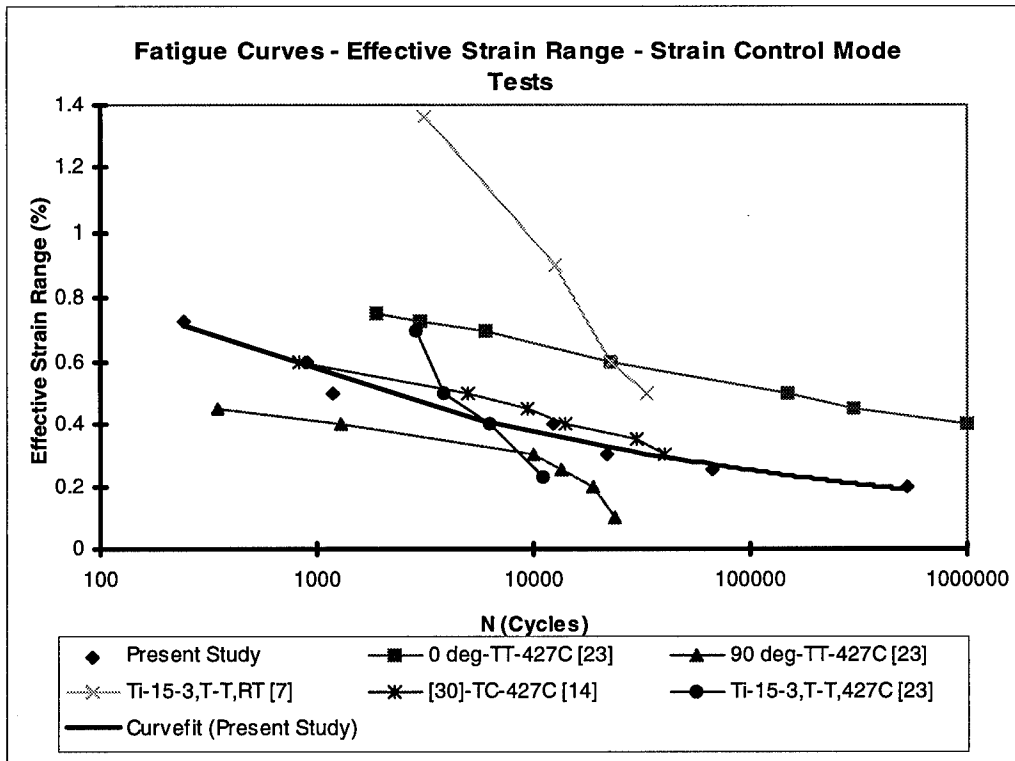


Figure 5.9: Effective Strain Range Fatigue Curve - Strain Control Comparison

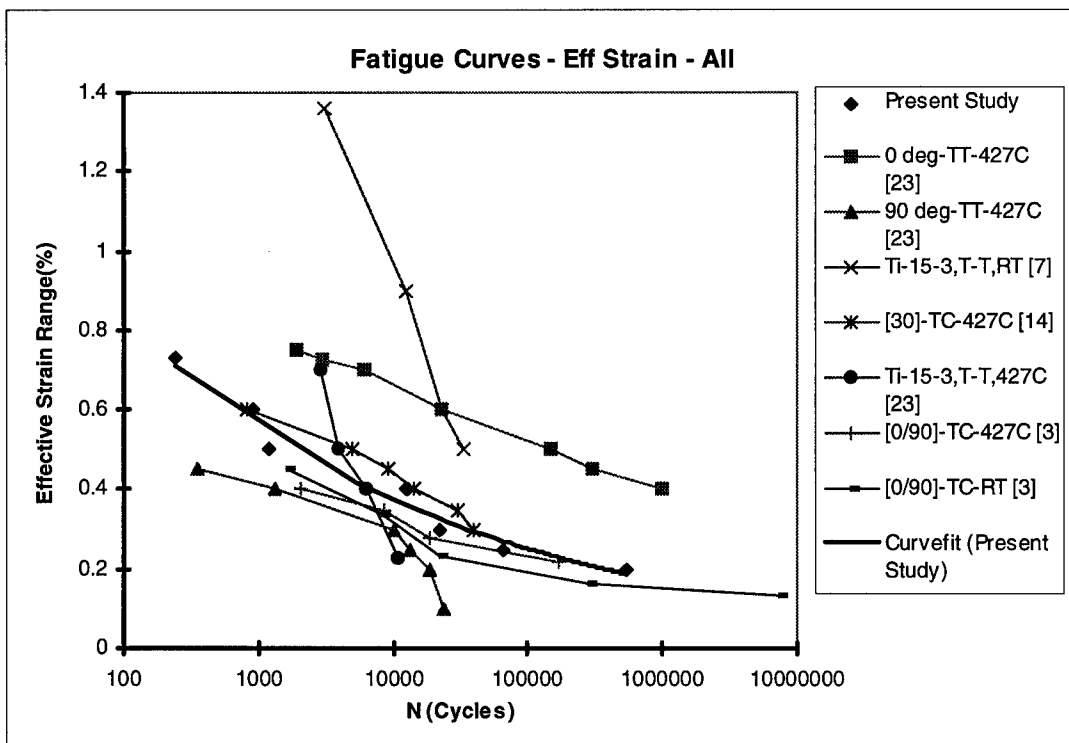


Figure 5.10: Effective Strain Range Fatigue Curve - Overall Comparison

VI. Conclusions and Recommendations

The purpose of this study was to extend the existing knowledge base of the fatigue life and associated damage mechanisms for the SiC/Ti-15-3 composite system. As noted in the literature review, little data has been published for this composite system under the fully reversed fatigue loading, especially for the strain controlled mode.

The effects of elevated temperature (427° C), fully reversed (R=-1), strain controlled fatigue on the SCS-6/Ti-15-3, [0/90]_{2s} was, therefore, investigated in this study. Seven fatigue tests, one monotonic tension, and one interrupted fatigue test were performed to characterize the fatigue life of the material. Results from the fatigue tests indicated various dominant fatigue responses and failure modes were present, dependent on the maximum applied strain.

The monotonic test stress-strain curve showed a three stage response characteristic of crossply laminates: 1) a linear-elastic region extending to approximately 0.06% strain; 2) a decreased stiffness linear range up to approximately 0.55% strain, dominated by fiber-matrix debonding; and 3) nonlinear response above 0.55% until failure at 0.8% strain, dominated by matrix plasticity. The micromechanics showed that this was a fiber dominated failure, as would be expected. This evidence helped define

the Region I fatigue failure, since no fatigue tests, performed in this study, were found to be in that region.

Region I was defined as the fiber dominated fatigue failure mode region, for strains above 0.75%. The highest strain for fatigue testing was 0.73%. The 0.73% test, although categorized in Region IIa, had a mechanical response close to a typical fiber dominated failure response, with plasticity and debonding evident in the hysteresis of the initial cycles. A steady modulus history until failure was evident, indicating minor or no matrix cracking. As mentioned, the static test showed classic fiber dominated failure (no matrix cracking) from microscopic evaluation, while the 0.73% showed some minor matrix cracks, providing for the mixed mode evaluation.

Specimens with maximum fatigue strains between 0.75% and 0.45% were classified as Region IIa, mixed fiber and matrix dominant failure modes. The 0.73% test provided the upper limit for this region, and the 0.6% test was a representative of this region. The modulus history had a fairly steady, slightly decreasing trend, indicating some damage accumulating before a rapid failure. Hysteresis from the stress-strain response was not as large initially as compared to the 0.73% test, indicating less damage and plasticity. Micrography revealed more matrix cracking than the previous test, confirming the trend towards matrix dominated failure.

The tests performed below a strain of 0.45% were categorized into Region IIb, matrix dominated failures. The 0.4% test provided the first example of this failure mode. The mechanical responses had a decreasing trend in the later half of the fatigue life. The initial increasing trend was attributed to age hardening of the material, which had been observed by others[23]. The decreasing trend was due to accumulating damage becoming the dominant in the response. Microscopy revealed no fiber breaks and an increase in matrix cracking, indicating the matrix dominated failure mode.

Region III, the matrix fatigue limit, was not represented by any test in this study, but was estimated from the previous study[23] of the 90° unidirectional specimen. This estimate, 0.05%, is considered conservative for this cross-ply because of the fatigue resistance of 0° plies.

The fatigue life was plotted as maximum strain versus fatigue cycles. As stated, it was found that the fatigue life curve could be divided into three regions representing dominant failure modes of the composite. Region I represented the fiber dominated failure mode for high strain values. Region IIa represented the mixed mode dominant failure area. Region IIb represented the matrix dominated failure mode. Region III represented the fatigue limit of the matrix.

Comparisons were made to previous fatigue life studies. The most direct data comparability was to a study reporting fully reversed, load controlled testing on the same composite system. It was found that the effective strain range basis provided a good basis for comparisons of fully reversed load and strain controlled tests. For higher strain loading, the strain controlled specimens had slightly longer fatigue lives than the load control data. However, the fatigue life curves for the two data sets converged at lower effective strain loadings. This behavior may suggest that the matrix dominated failure mode results in similar fatigue lives for both the load and strain controlled modes.

This study has increased the knowledge base for this MMC material system. However, many areas for this material remain to be investigated. Much testing is required to achieve a complete understanding of the fatigue characteristics of this material system, as with any material. For example, no fully reversed, strain controlled, room temperature fatigue tests have been reported on the $[0/90]_{2s}$ systems. Will the high strain region tests still have a longer fatigue life than that reported for the load controlled counterpart? Additionally, no strain controlled, fully reversed work has been accomplished on the 0° or 90° unidirectional fiber system. What similar or different trends will result from a comparison of these as opposed to the $[0/90]_{2s}$ load and

strain control fatigue life trend comparisons? Thus, much characterization still remains to be accomplished before MMC's are fully understood.

Appendix A

This appendix contains additional raw data not presented in other locations in this document. This information includes data from the following fatigue tests: 0.5%, 0.3%, 0.25%, and 0.2%. Average modulus histories, maximum and minimum stress histories, and stress-strain plots are presented. Curvefit lines in the data plots represent trends, not predictions. Additionally, stress-strain plot offset data are presented for the stress-strain graphs in this document.

0.5% Test

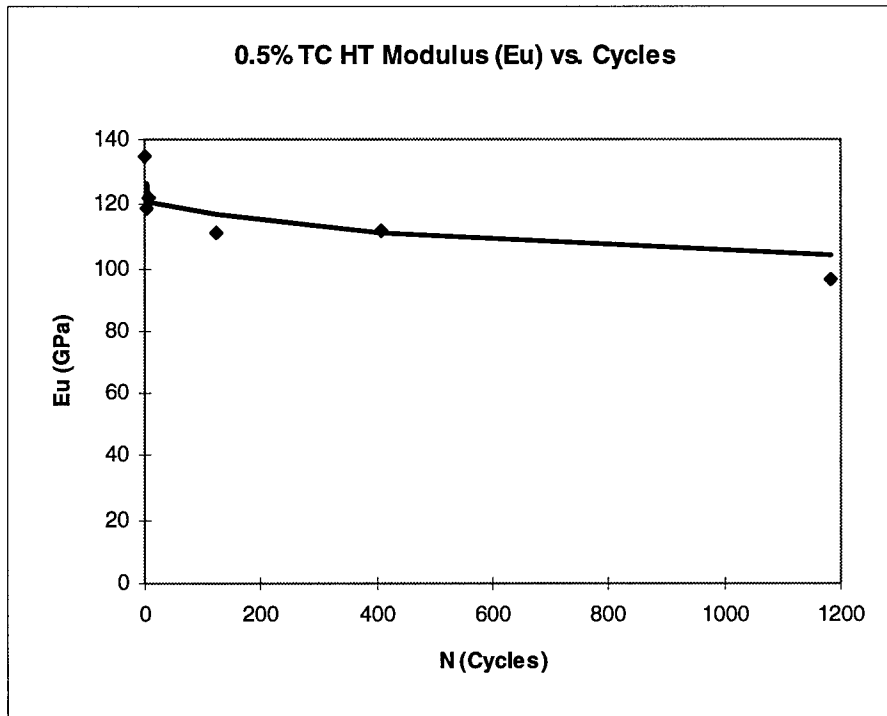


Figure A.1: Modulus History, 0.5% Test

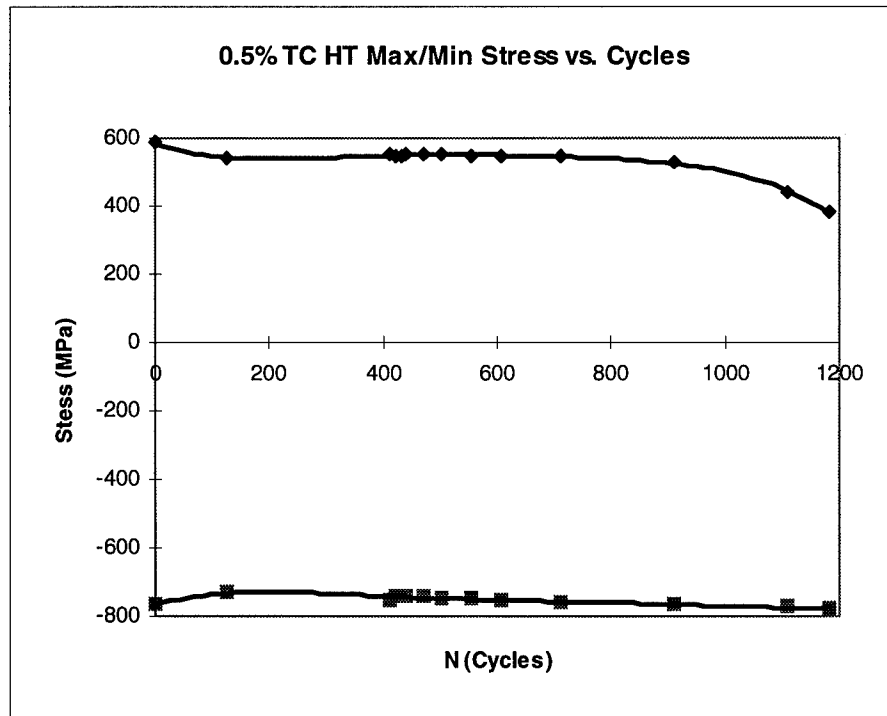


Figure A.2: Max/Min Stress History, 0.5%

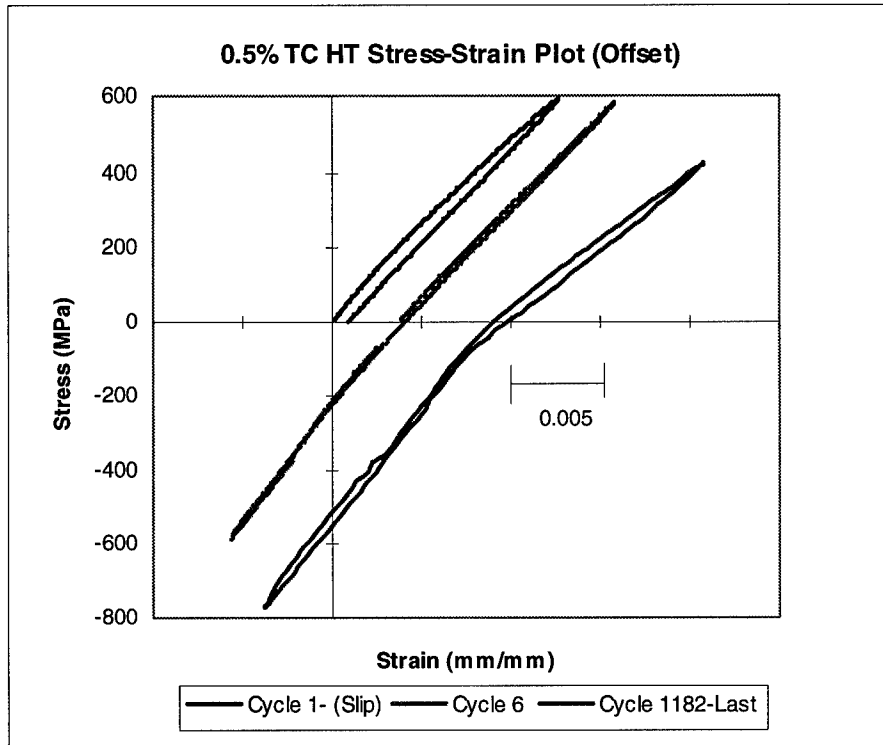


Figure A.3: Stress-Strain Plots, 0.5% (Offset)

0.3% Test

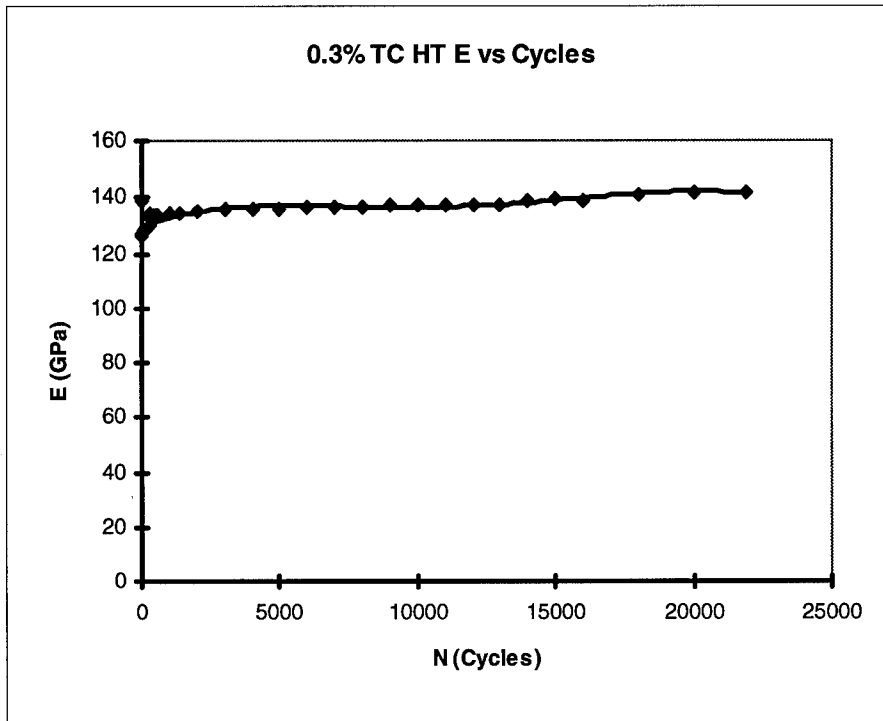


Figure A.4: Modulus History, 0.3% Test

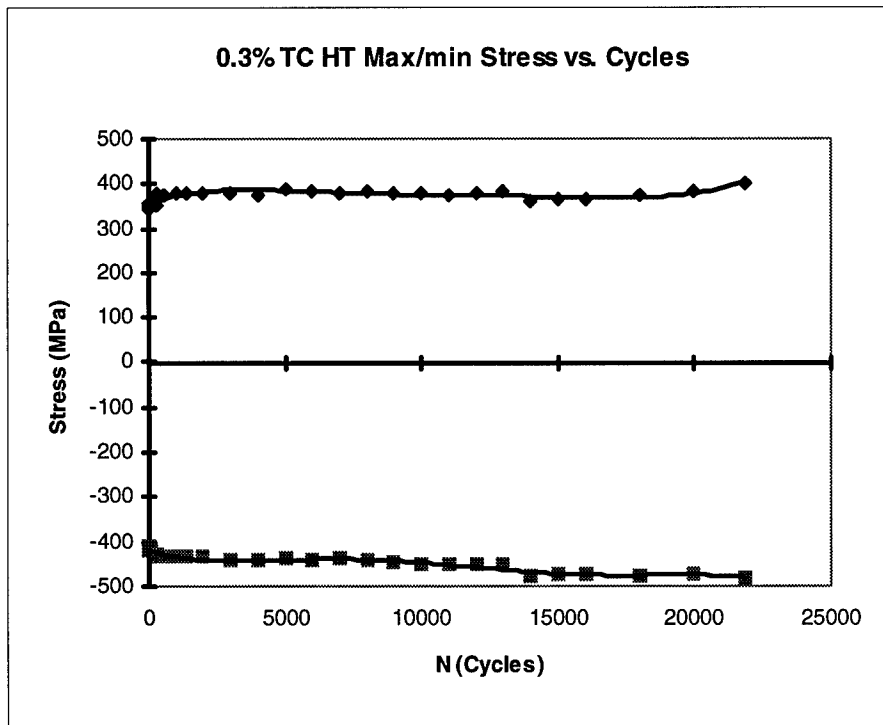


Figure A.5: Max/Min Stress History, 0.3%

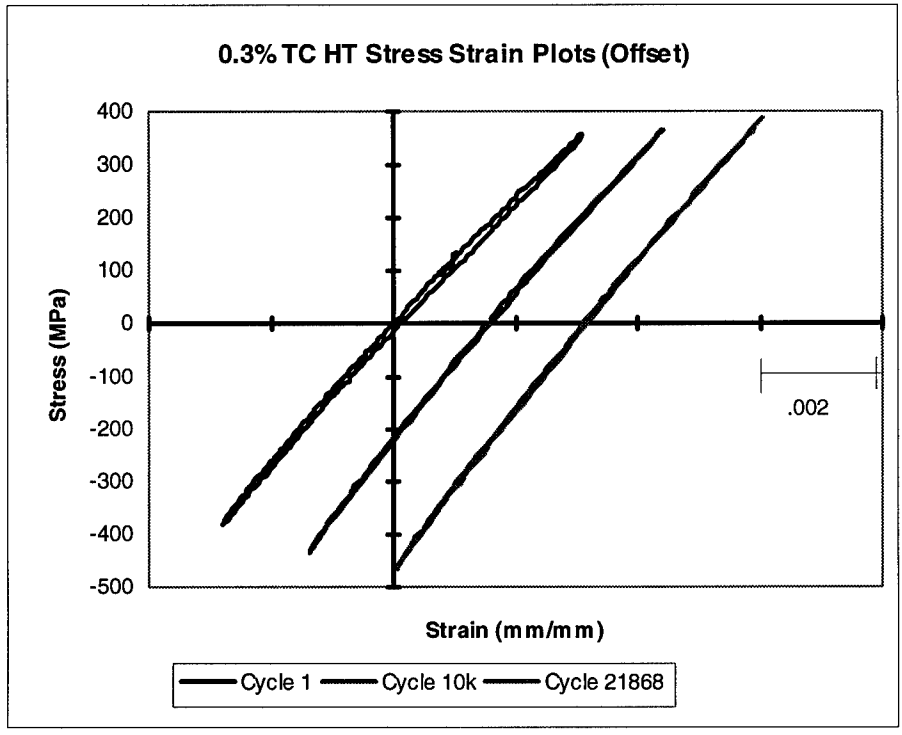


Figure A.6: Stress-Strain Plots, 0.3% (Offset)

0.25% Test

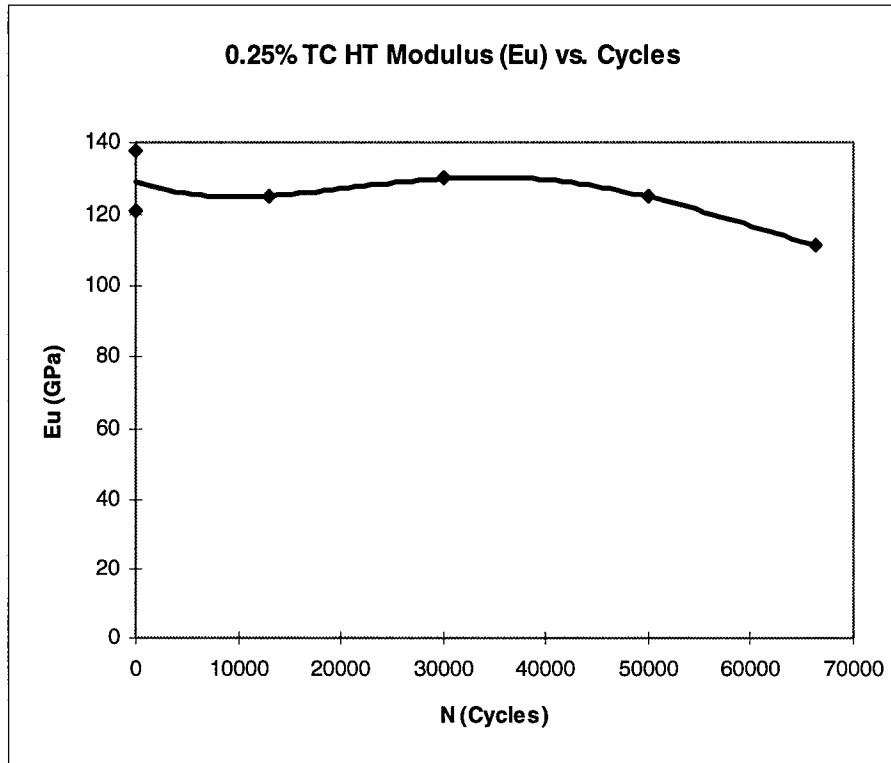


Figure A.7: Modulus History, 0.25% Test

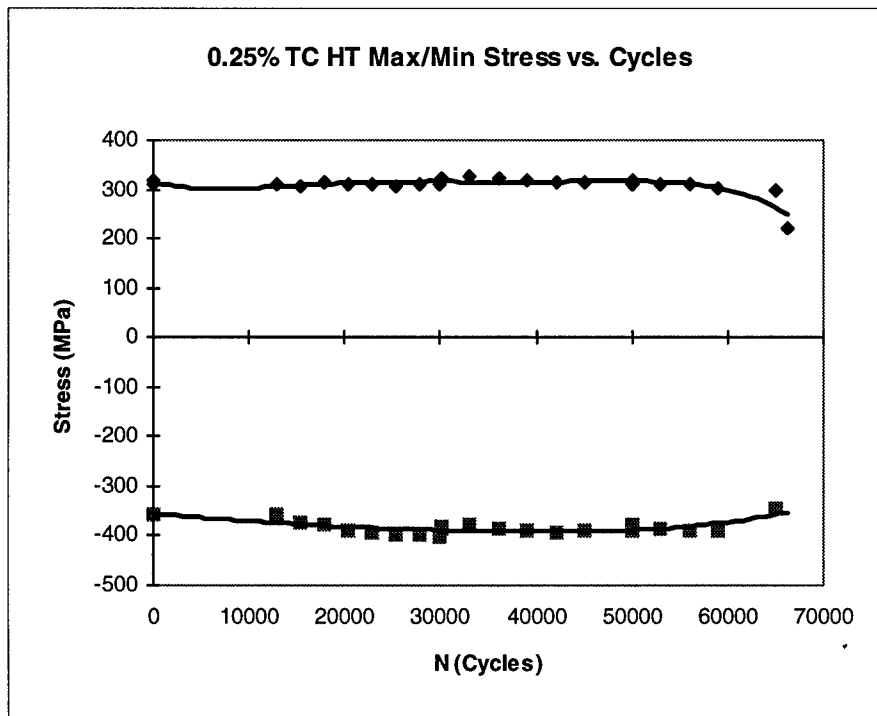


Figure A.8: Max/Min Stress History, 0.25%

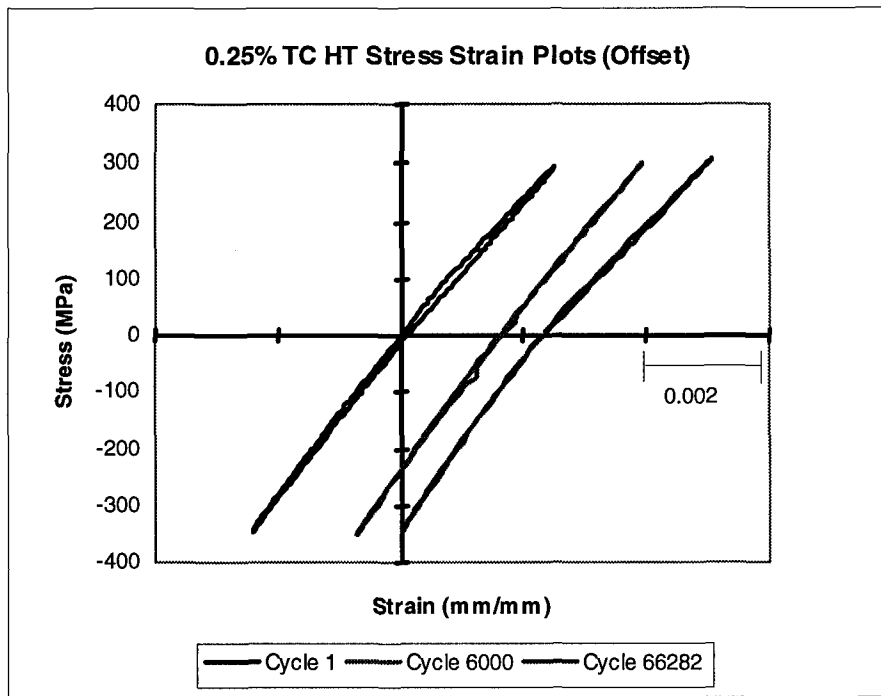


Figure A.9: Stress-Strain Plots, 0.25% (Offset)

0.2% Test

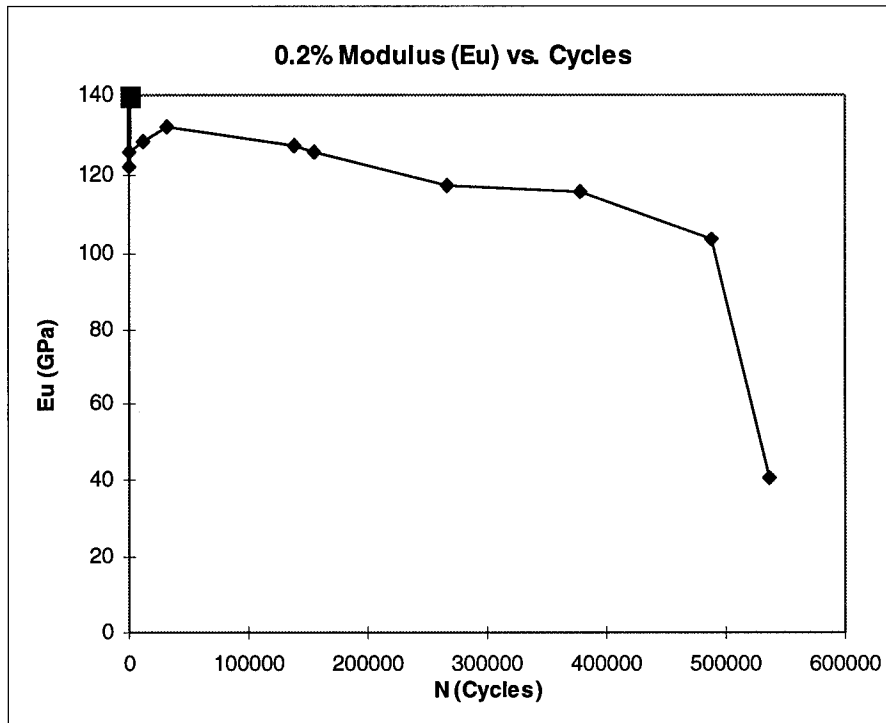


Figure A.10: Modulus History, 0.2% Test

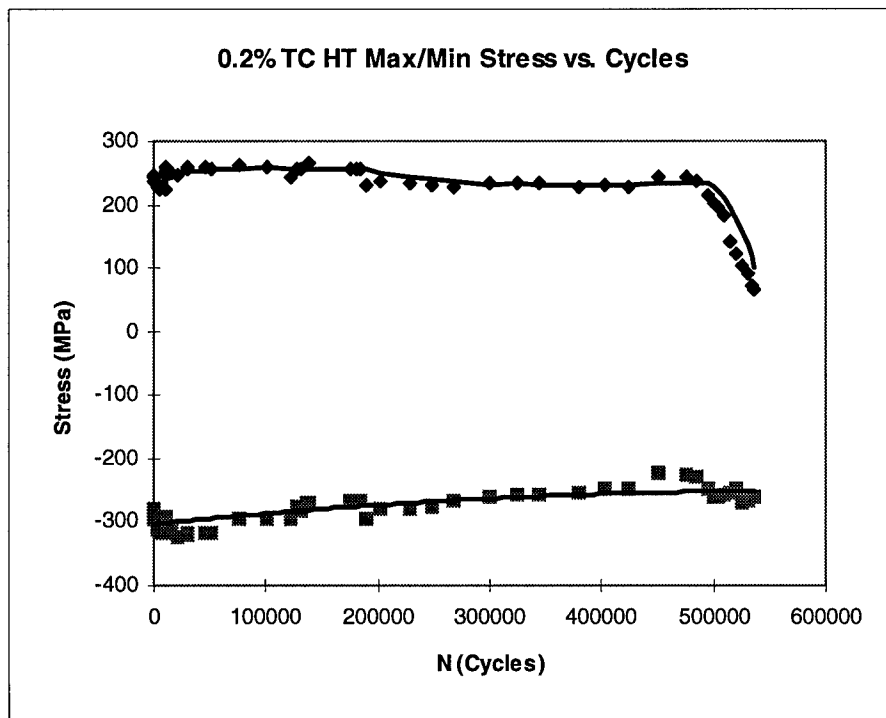


Figure A.11: Max/Min Stress History, 0.2%

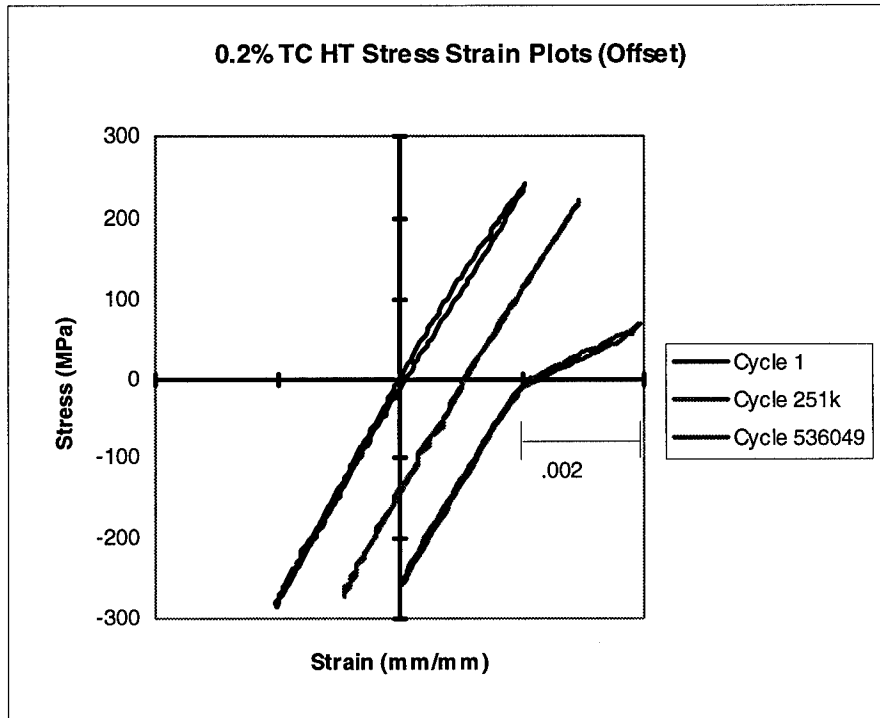


Figure A.12: Stress-Strain Plots, 0.2%(Offset)

Table A.1: Stress-Strain Graph Offset Data*

<u>Test</u>	<u>1st Curve</u>	<u>2nd Curve</u>	<u>3rd Curve</u>	<u>4th Curve</u>
0.73%	1(0)	4(.0015)	178(.003)	242(.0045)
0.6%	1(0)	101(.0015)	904(.003)	
0.5%	1(0)	6(.0015)	1182(.0035)	
0.4%	1(0)	6000(.0015)	12403(.003)	
0.3%	1(0)	10000(.0015)	21868(.003)	
0.25%	1(0)	6000(.0015)	66282(.0025)	
0.2%	1(0)	251000(.001)	536049(.002)	

* Legend: Cycle No.(Offset)

Appendix B

The following appendix contains additional photography not presented in previous sections of this document.

Micrography and a post fracture specimen comparison photograph are included.

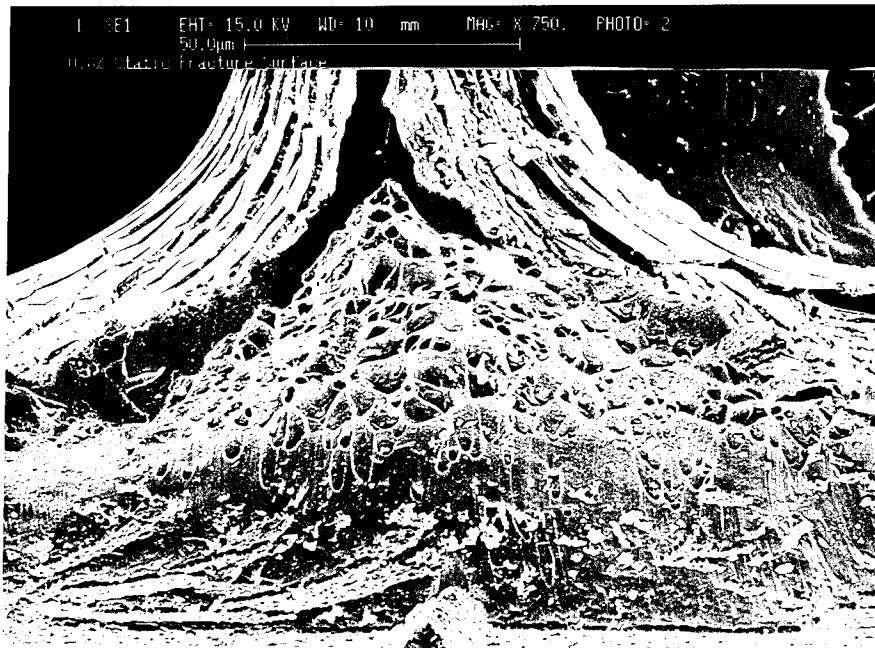


Figure B.1: Ductile Void Coalescence, 0.8% (Static)

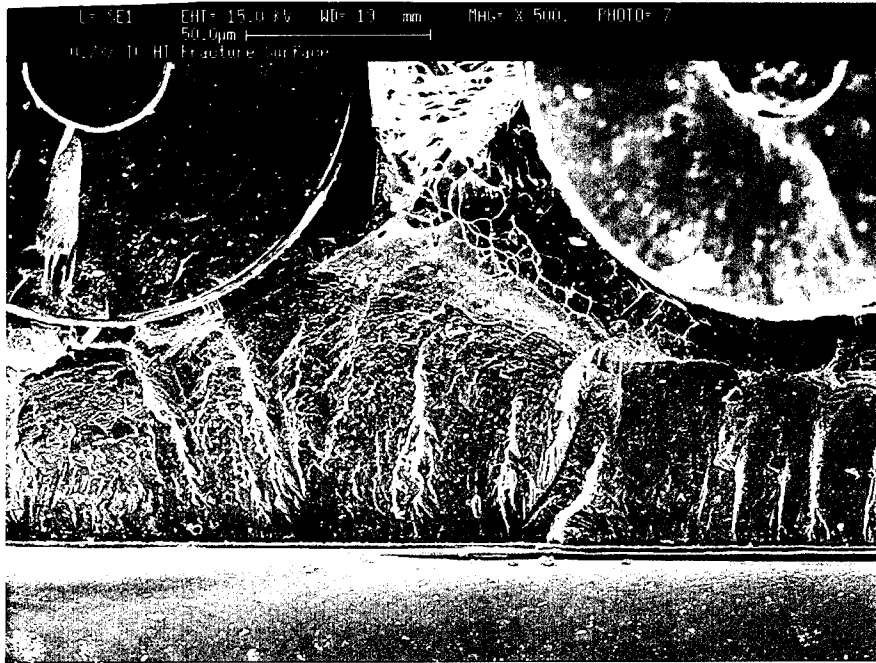


Figure B.2: Ductility and Fatigue Striations, 0.73%

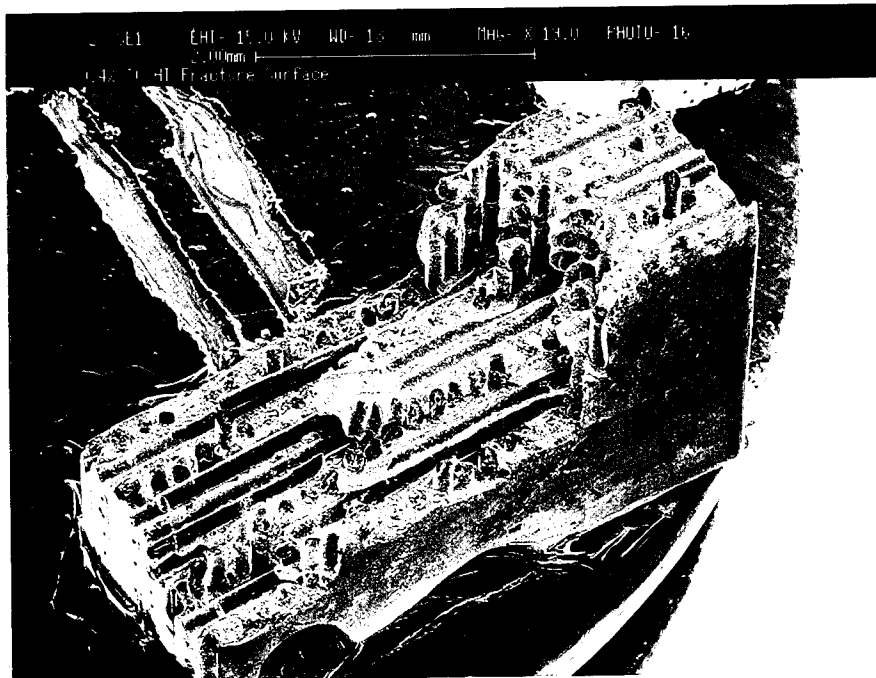


Figure B.3: Fracture Surface , 0.4%

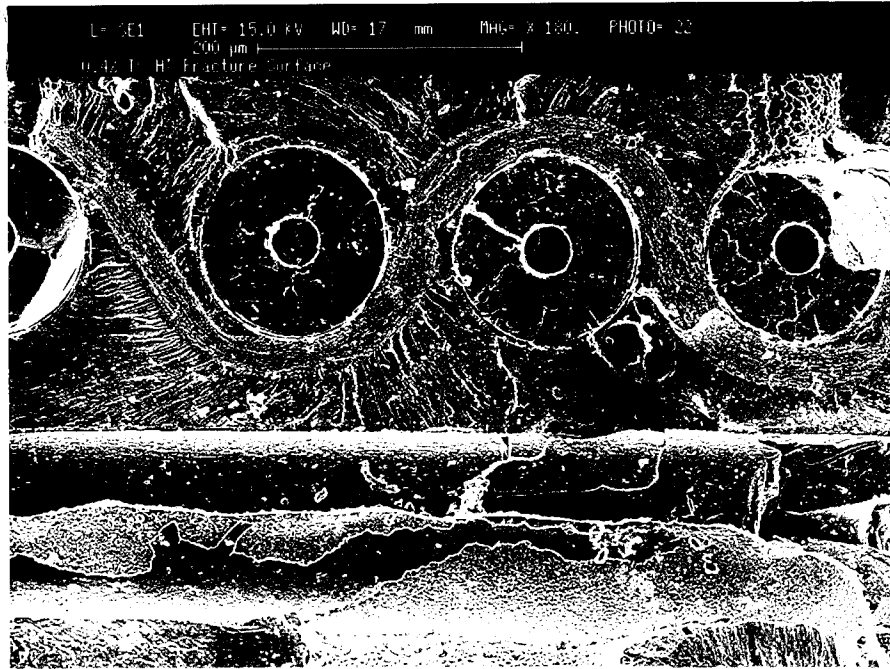


Figure B.4: Molyweave, Fracture Surface, 0.4%

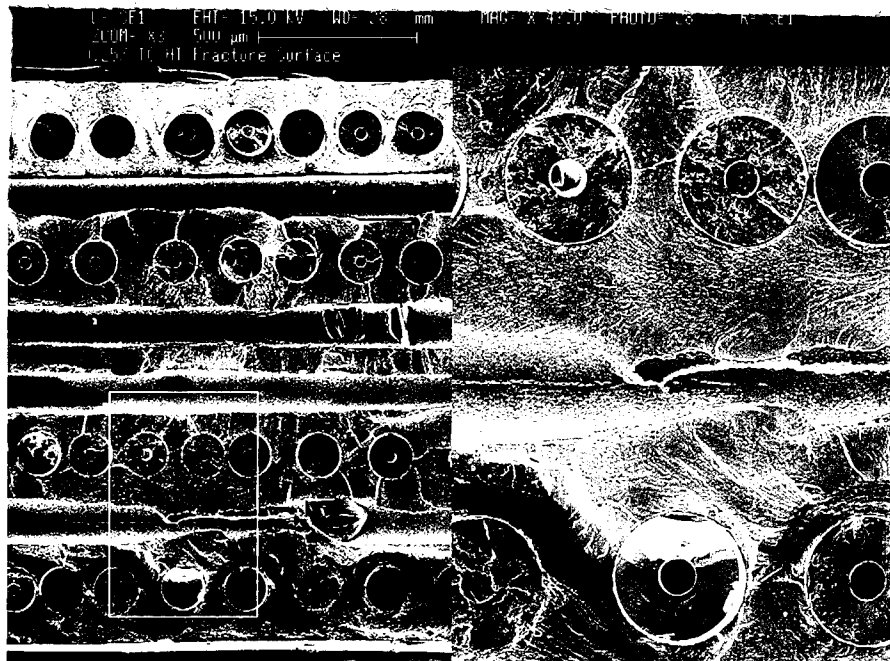


Figure B.5: Extensive Fatigue Striations, 0.25%

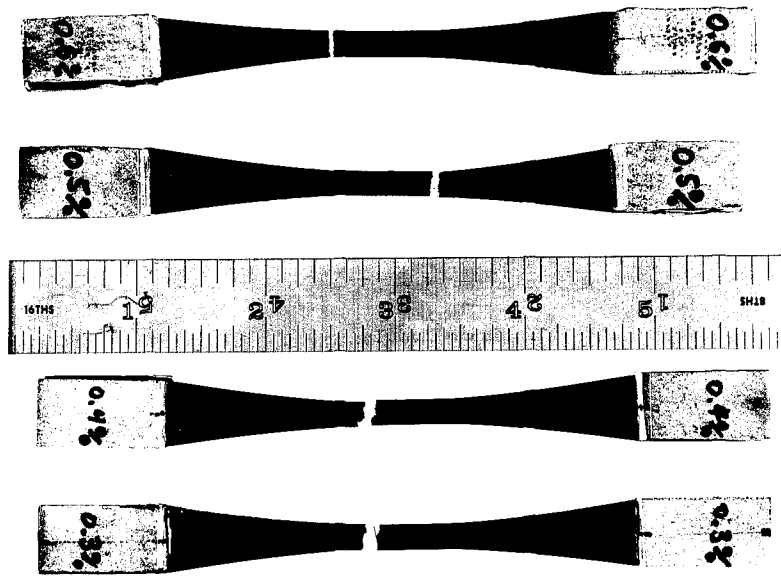
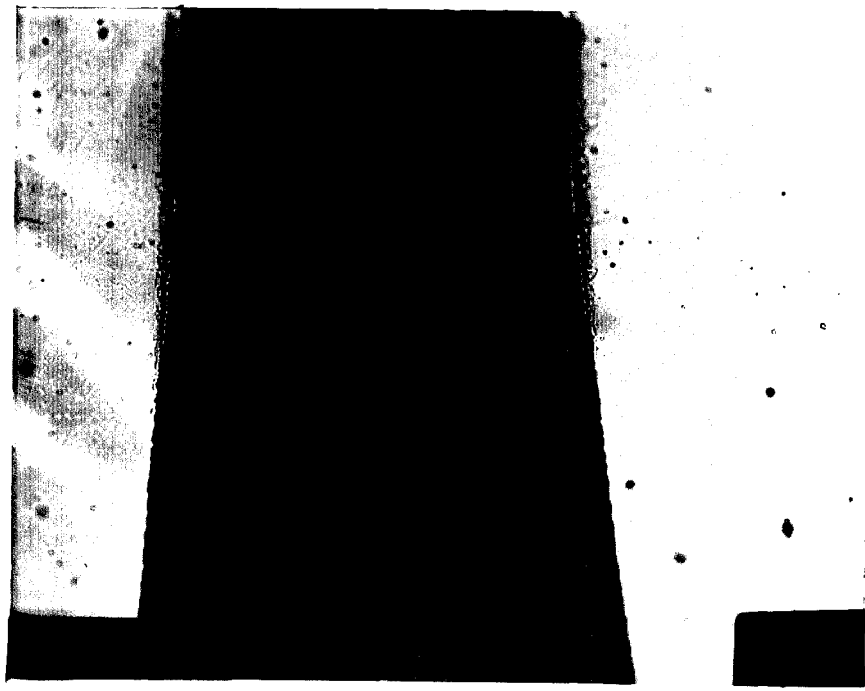


Figure B.6: Post-Fracture Specimen Comparison



Loading Direction: \updownarrow

Figure B.7: 0° Fibers, View #3, 0.73% (500X)

Bibliography

1. Agarwal, B. D. And L. J. Broutman. Analysis and Performance of Fiber Composites (Second Edition). New York: John Wiley and Sons, Inc., 1990.
2. Broek, David. Elementary Engineering Fracture Mechanics (Fourth Revised Edition). Boston: Kluwer Academic Publishers, 1991.
3. Boyum, Elizabeth. Investigation of Tension-Compression Fatigue Behavior of a Cross-Ply Metal Matrix Composite at Room and Elevated Temperature. MS Thesis, AFIT/GAE/ENY/93D-6. School of Engineering, Air Force Institute of Technology, Wright-Patterson, AFB, OH, December 1993.
4. Callister, W. D., Jr. Materials Science and Engineering, An Introduction. New York: John Wiley and Sons, Inc., 1985.
5. Cardova, Barney C. and Bowen. "Micromodeling of Effective Stress Intensities for Bridged Cracks in Fiber-reinforced Titanium Metal Matrix Composites," Composites, 24: #2, 1993.
6. Castelli, Michael. "Thermomechanical and Isothermal Fatigue Behavior of a [90]₂ Titanium Matrix Composite." Contractor Report: NASA CR-191196, NASA Lewis Research Center, Cleveland, OH 44135, October 1993.
7. Gabb, T. P. et al. "The Effect of Matrix Mechanical Properties on [0]₂ Unidirectional SiC/Ti Composite Fatigue Resistance," Scripta Metallurgica et Materialia, 25: 2879-2884, Pergamon Press plc (1991).
8. ----- . "Isothermal and Nonisothermal Fatigue Behavior of a MMC," Journal of Composites and Materials, 24, 667-686, June 1990.
9. Jeng, S. M. et al. "Fracture Mechanisms of Fiber-reinforced Titanium Alloy Matrix Composites: Part IV: Low Cycle Fatigue," Materials Sciences and Engineering, 67-77, 1991.
10. Johnson, W. S. "Damage Development in Titanium Metal-Matrix Composites Subjected to Cyclic Loading," Composites, 24, #3: 187-196, 1993.

11. ----- . "Fatigue Testing and Damage Development in Continuous Fiber Reinforced MMCs," Metal Matrix Composites: Testing, Analysis, and Failure Modes. ASTM, 1989.
12. ----- et al. "Mechanical Characterization of Unnotched SCS₆/Ti-15-3 MMC's at Room Temperature," American Society for Testing and Materials.
13. Lerch, Bradley A. and James F. Saltsman. "Tensile Deformation Damage in SiC Reinforced Ti-15V-3Cr-3Al-3Sn," Report: NASA TM-103620, NASA Lewis Research Center, Cleveland, OH, 44135, April 1991.
14. ----- and Gary R. Halford. "Fully-Reversed Fatigue of a Ti-MMC," Conf. Proceedings of the 17th annual Confer. On Composites, Materials and Structures, Cocoa Beach, Fl, January, 10-15, 1993.
15. ----- . Matrix Plasticity in SiC/Ti-15-3 Composite, Report: NASA TM-103760, NASA Lewis Research Center, Cleveland, OH, 44135, July 1991.
16. Mall, S. and P. G. Ermer. "Thermal Fatigue Behavior of a Unidirectional SCS-6/Ti-15-3 Metal Matrix Composite," Journal of Composite Materials, 25: 1668-1686, December 1991.
17. ----- and B. Portner. "Characterization of Fatigue Behavior in Cross-Ply Laminate of SCS-6/Ti-15-3 Metal M Matrix Composite at Elevated Temperature," Journal of Engineering Materials and Technology, 114: 409-415, October 1992.
18. ----- and J. J. Schubbe. "Thermo-Mechanical Fatigue Behavior of a Cross-Ply SCS-6/Ti-15-3 Metal Matrix Composite," Composites Science and Technology, 50: 49-57
19. Majumdar, Bhaskar S. and Golam M. Newaz. "Inelastic Deformation of Metal Matrix Composites," Proceedings of the 1991 HITEMP Conf, NASA Lewis Research Center, Cleveland, OH, 44135, 1991.
20. ----- . "Inelastic Deformation of MMC's: Compression and Fatigue" Report: Battelle, 505 Ling Avenue, Columbus, OH 43201. (1994).
21. Newaz, G. M. and B. S. Majumdar. "Deformation and Failure Mechanisms in MMC's," ASME Winter Annual Meeting, Atlanta, December 1991.

22. Nimmer, R. P. et al. "Fiber Array Geometry Effects Upon Composite Transverse Tensile Behavior," Titanium Aluminide Composites. February, 1991.
23. Sanders, Brian P. Characterization of Fatigue Damage in a Metal Matrix Composite (SCS-6/Ti-15-3) at Elevated Temperature. PhD dissertation, AFIT/DS/AA/93-4. School of Engineering, Air Force Institute of Technology, Wright-Patterson AFB, OH, December 1993.
24. Saigal, A. et al. "Residual Strains in Titanium Matrix High-Temperature Composites," Material Science and Engineering, A150. 59-66, August 1992.
25. Schulte, K. and K. Minoshima. "Damage Mechanisms Under Tensile and Fatigue Load of Continuous Fibre-reinforced MMC's," Composites, 24, : #3, 197-207, 1993.
26. Sun, C. T. et al. "An Investigation of the Mechanical Behavior of SCS-6/Ti-6-4 Metal Matrix Composite at Elevated Temperatures," Composites and Technology, 49: 183-190 (1993).
27. Talreja, Remesh. Fatigue of Composite Materials. Lancaster: Tecnominc Publishing Company, 1987
28. Telesman, J. and R. McKay. "In Situ Observations and Modeling of the Micro-Mechanics of Interfacial Failure in [90]₂ SCS-6/Ti-15-3 MMC," Report: NASA Lewis Research Center, Cleveland, OH 44135.
29. Verrilli, Michael J., and Timothy P. Gabb. "High Temperature TC Fatigue Behavior of a Tungsten Copper Composite," Fourth Symposium on Composite Materials: Fatigue and Fracture, ASTM Conference Proceedings, March 1991.

Vita

Captain Leon B. Dennis was born January 31, 1964 in Monroe, Louisiana. He graduated from Neville High School in 1982 and entered Louisiana Tech University the following Fall Quarter. In 1987, Captain Dennis graduated with a Bachelor of Science in Mechanical Engineering and was commissioned as a Second Lieutenant in the United States Air Force. His first tour of duty was in the 558th CES at Nellis AFB, NV. There he served in the positions of contract programmer, project manager, and design engineer. He entered the Graduate School of Engineering of the Air Force Institute of Technology in May of 1993.

Permanent Address: 530 Lewis Drive
Fairborn OH 45324